

# POLITECNICO DI TORINO

**Corso di Laurea Magistrale  
in Automotive Engineering**

Tesi di Laurea Magistrale

## **Comparison of electric powertrains with front-, rear- and all-wheel-drive**



### **Relatori**

prof. Andrea Tonoli  
prof. Giovanni Belingardi

*firma dei relatori*

.....

### **Candidato**

Luca Mantovani

*firma del candidato*

.....

A.A. 2018



# Table of Contents

- List of abbreviations..... V
- Symbols..... VII
- 1 Introduction..... 1**
  - 1.1 Motivation..... 1**
  - 1.2 Objective..... 2**
  - 1.3 Thesis overview ..... 2**
  - 1.4 Graphical representation ..... 3**
- 2 State of the Art..... 5**
  - 2.1 Driving cycle simulators for electric vehicles..... 5**
    - 2.1.1 TOTEM ..... 8
    - 2.1.2 WLTP Cycle..... 9
  - 2.2 Double and single track models..... 10**
  - 2.3 Comparison of front, rear, all-wheel drive layouts ..... 12**
    - 2.3.1 Conclusion on the state of the art for the comparison ..... 20
- 3 Reduction of the driving cycle simulation time..... 23**
  - 3.1 Time analysis ..... 23**
  - 3.2 Method..... 25**
  - 3.3 Results..... 30**
- 4 Model improvements and optimizations..... 33**
  - 4.1 Efficient torque allocation strategy..... 33**
    - 4.1.1 Differences with the previous design and reason of changes..... 40
  - 4.2 Powertrain and drivetrain efficiency calculation ..... 41**
- 5 Validation ..... 43**
  - 5.1 Strategy and cycle parameters definition..... 43**
    - 5.1.1 Validation cycle creation ..... 43
    - 5.1.2 Motor parameters definition ..... 46
    - 5.1.3 Validation criteria and validation tool development..... 48
    - 5.1.4 Summary parameters and information on the vehicle ..... 50

Table of Contents

---

- 5.2 Validation result and analysis ..... 50**
- 5.3 Sensitivity analysis..... 58**
- 5.4 Conclusions of the validation..... 60**
- 6 Comparison of front-, rear- and all-wheel-drive topologies ..... 61**
  - 6.1 Comparison maneuvers and parameters ..... 61**
    - 6.1.1 Consumption analysis..... 63
    - 6.1.2 Cost analysis..... 63
    - 6.1.3 Performance analysis ..... 64
    - 6.1.4 Vehicle parameters ..... 65
  - 6.2 Comparison results and analysis ..... 66**
    - 6.2.1 Results with Horlbeck’s motor parameters ..... 66
    - 6.2.2 Results with Tschochner’s motor parameters and analysis..... 70
- 7 Summary and conclusions..... 79**
  - 7.1 Summary ..... 79**
  - 7.2 Conclusions ..... 80**
  - 7.3 Outline ..... 82**
- List of figures ..... i**
- List of tables..... v**
- References ..... vii**
- Appendix ..... xiii**

# List of abbreviations

ICE	Internal Combustion Engines
GUI	Graphical User Interface
DC	Direct Current
SOC	State of Charge
TOTEM	Topology Optimization Tool for Electric Mobility
FTM	Lehrstuhl für Fahrzeugtechnik
WLTP	Worldwide Harmonized Lightweight Vehicle Test Procedure
NEDC	New European Driving Cycle
FWD	Front-wheel Drive
RWD	Rear-wheel Drive
AWD	All-wheel Drive
4WD	Four-wheel Drive
2WD	Two-wheel Drive
PI	Proportional Integral
ASM	Asynchronous motor
PMSM	Permanent Magnet Synchronous Motor
BSM	Battery System Management
ROMO	RoboMobility
AWS	All Wheel Steering
IWM	In Wheel Motors
TVD	Torque Vectoring Differential
ARB	Anti-roll bar
GPS	Global Positioning System
CAN	Controlled Area Network
eTV	Electronic Torque Vectoring



# Symbols

Symbols	Unit	Description
$F_x$	N	Force along local x-axis
$F_y$	N	Force along local y-axis
$l_F$	m	Front wheelbase
$l_R$	m	Rear wheelbase
$l$	m	Wheelbase
$\alpha$	rad	Road inclination, Tire Sideslip angle
$\beta$	rad	Vehicle turning angle
$\delta$	rad	Wheel steering angle
$v$	m/s	Velocity
$g$	m/s <sup>2</sup>	Gravitational acceleration
$F_r$	N	Resistant force
$F_t$	N	Traction force
$F_w, F_{wind}$	N	Aerodynamic force
$m$	Kg	mass
$F_z$	N	Force along local z-axis
$a$	m/s <sup>2</sup>	Acceleration
$I$	Kg m <sup>2</sup>	Inertia
$\theta$	rad	Pitch angle
$h$	m	Altitude



# 1 Introduction

During the last decades, a shift from internal combustion engines equipped vehicle towards electric mobility has been highlighted [1]. The justification to this ascending trend can be explained by the many advantages this new technology brings, in terms of better efficiency and lower consumption. For this reason, it is considered as a possible solution to the always more relevant and actual problem of global pollution and energetic crisis [2, p. 2].

Despite the significantly higher efficiency of an electric vehicle, compared with any predecessor, it still cannot be considered zero-emission mobility. Until the global energy production abandons fossil fuels, such as coal, oil and gas as source to create electricity, a certain amount of pollutants produced and released in the atmosphere could be attributed to any electric consumption. Moreover, while electric motors achieved over the years a minimum level of losses in operation, the storage and delivery media are far from efficient in transmitting and holding electric energy, since up to 70 % is lost during this process [3].

## 1.1 Motivation

In the upcoming world of electric vehicle, the choice among several different powertrain configurations is still possible and, due to the lack of centenary experience when compared to conventional gas-powered automobiles, this decision is still a relevant topic for researches. Neglecting the potential strategies to store the energy, among which it is worth mentioning the most innovative and investigated electrochemical batteries, supercapacitors and fuel cells, the second most relevant and analyzed field concerns, together with the energy management system, the motors layout and vehicle architecture [4, pp. 1-3].

In this category it is possible to distinguish several topologies according to the typology and number of motors per axle, their position, number of gears, kind of gearboxes and differential. But one of the main distinction is carried on according to the driven axles, such as front, rear and all-wheel drive vehicles [5, p. 21].

Already in the actual car market, a general trend of preference of all-wheel drive (AWD) or four-wheel drive (4WD) configuration for the vehicle topology has been reported [6]. The key points of this tendency can be found in the better handling, vehicle dynamics, safety and traction capabilities in poor road conditions [7]. The car industry has seen in this recent gradual shift from combustion engines towards electric motors the opportunity to improve in efficiency, hence reducing the consumption, since the presence of multiple motors does not foresee inevitably the increase of losses and the aggravation of energy utilization which decreases the range of electric vehicles [8, pp. 1-3].

## 1.2 Objective

The aim of this thesis is, first, to create a proper environment for the comparison among front-, rear- and all-wheel drive topologies in electric vehicles, improving the existing one and eliminating bottlenecks and other sources of slowdowns. The current tool permits to simulate certain maneuvers based on some general inputs regarding the characteristics of the drivetrain or the segment of the electric vehicle. The model and the torque distribution controllers are then refined and optimized to always guarantee the correct operation for the required conditions, and subsequently the entire vehicle model is validated to assess the reliability of results when an existing cycle is simulated.

Finally, different vehicle configurations are compared according to different points of view, and the results analyzed to determine which layout is not only the most efficient, but better overall, considering different power levels to widen the analysis and follow the car maker tendency which consists in offering always more than one motorization for the same vehicle model. Moreover, a detailed investigation is to be conducted to identify the most efficient power bias of electric motors between front and rear axle in case of a multi driven axle, once again for different power levels.

## 1.3 Thesis overview

The structure of the following thesis is divided in seven chapters.

The first chapter has already been analyzed and clarifies the motivation, objective and structure of the following document.

The second chapter consists in the state of the art, which investigates the available literature and the experiments already conducted on topics which are discussed during the thesis. Different strategies for torque vectoring, regenerative braking and torque bias are compared and distinctions are highlighted. In addition, a general overview on the concepts of single track and double track models used is given, and the basic principles of the model adopted for this research explained.

The third chapter contains the method used for the time optimization and simplification of the model, from double to single track, the reasons, all the assumptions and approximations needed for this process.

The fourth chapter introduces the modifications and optimization work which has been conducted on the model to correct or improve the operation, ensuring accurate activity and results.

The fifth chapter handles the validation of the model for a custom driving cycle. The process through which the input parameters were found is discussed, as well as the presentation and analysis of the results. Additionally, to further strengthen the validation, a sensitivity analysis is conducted on the topologies which are matter of investigation in the further chapters.

The sixth chapter presents the comparison between the three topologies (front-, rear- and all-wheel drive), as well as the preparation for the test and the discussion of the results. Two different models for the motors are adopted, and the problems and differences explained, as well as the motivation to the adoption of both.

The seventh and last chapter gives a summary of the work done, the explanations, together with the limits and criticalities encountered. Moreover, a proposal for the future development of this study is presented.

## 1.4 Graphical representation

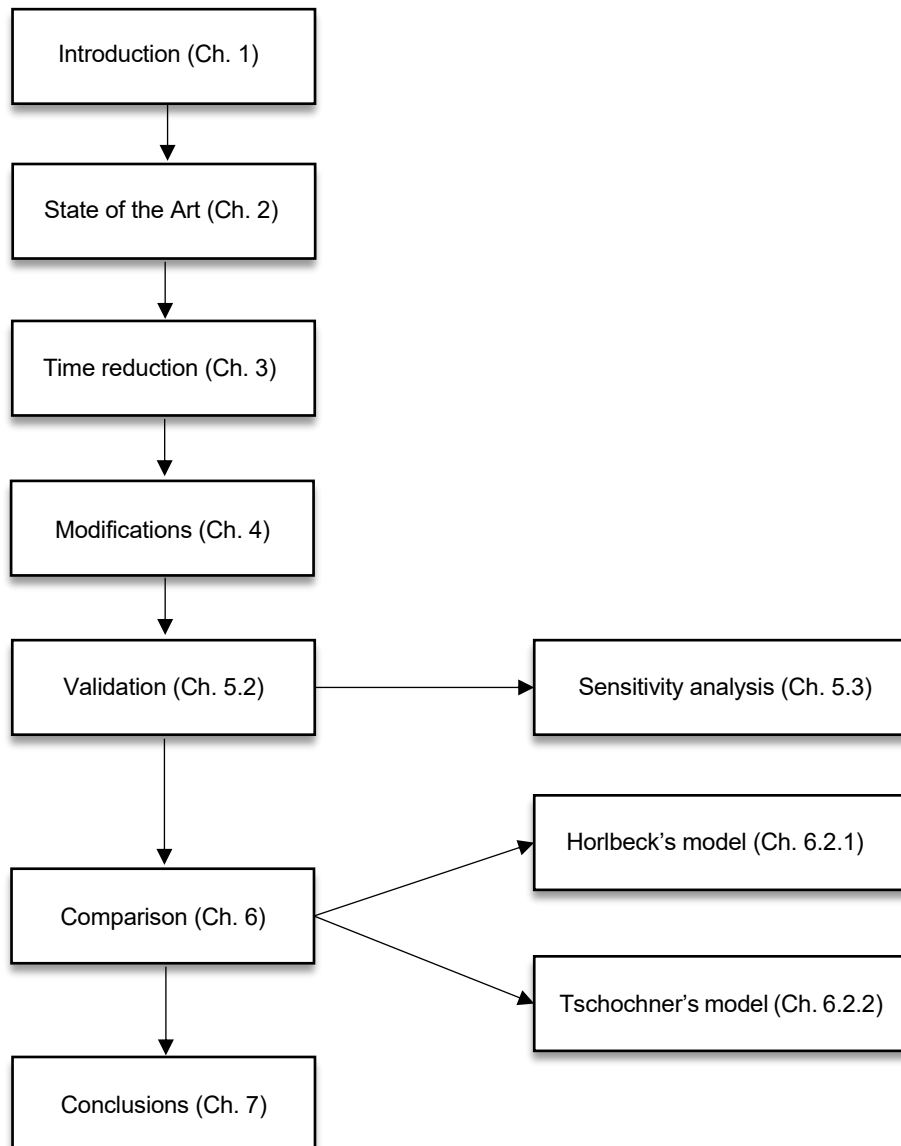


Figure 1.1: Thesis diagram



## 2 State of the Art

In this chapter all the literature research which has been conducted with the aim of deepening the knowledge on the topic of the thesis is presented. The first subchapter (2.1) presents the description of few driving cycle simulators, to give a general overview, and then the one used for this study is introduced and explained. The second subchapter (2.2) clarifies the theory behind the single and double track car model for dual axle vehicles, since is later necessary to make some assumptions. The last one (2.3) is the research on the state of the art for comparison between front, rear and all-wheel drive (AWD) vehicles, with particular focus on the consumption.

### 2.1 Driving cycle simulators for electric vehicles

Due to ever stricter regulations for consumption and always more realistic driving cycles, several studies converged their energy in the creation of “ad hoc” tools for simulation of specific vehicles behavior in relevant driving cycles. As a matter of fact, simulations can help to reduce the cost of development and prototyping and allow a more efficient collection of data. A few examples are here presented with the aim of giving an overview of those capable instruments.

At Texas A&M University, in 1999, a Matlab based simulation and modelling tool has been developed to study the influence of the vehicle configuration on fuel economy, efficiency and emissions [9]. It does not only allow to configure of electric vehicles, but also hybrid and conventional internal combustion engine (ICE) ones. The user is able set the vehicle characteristics according to his exigency, and arrange parameters such as size and weight, gear ratios, and dimensions of the components of the drivetrain. Moreover, it is offered the possibility to create a personalized configuration or even a new component from blank as well as to pick the desired ones from an existing library. The package adopts Simulink as programming method through visual connection among the different ports, mainly for the user-friendly Graphical User Interface (GUI). Subsequently, the driving cycle can be selected among the offered ones (FTP-75, Federal Highway drive cycle, Commuter drive cycle) or a new one can be created.

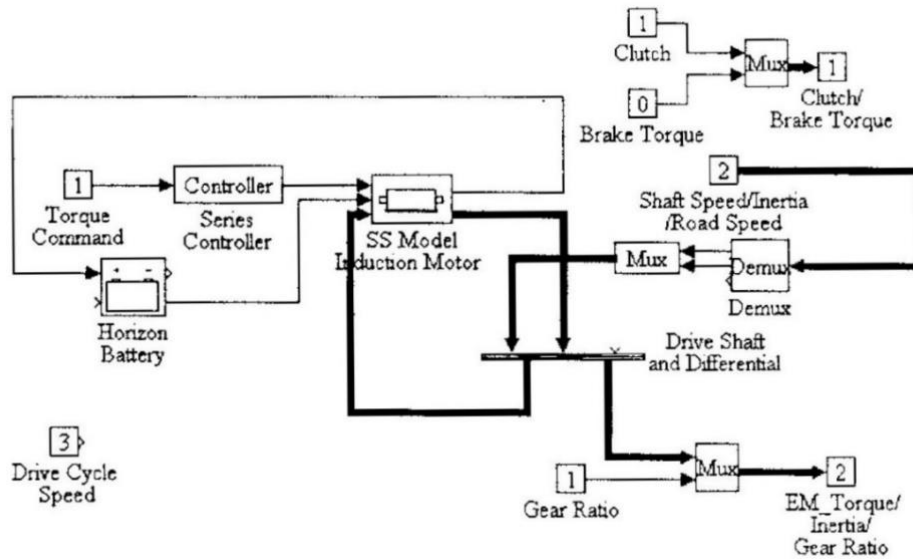


Figure 2.1 Model scheme for electric vehicles [9, p. 1771]

In the design of the purely electric vehicle, the only possibility is to simulate an induction motor, powered by a DC battery pack of 240V. Positive or negative torque are requested by the motor according to the requirements of acceleration or deceleration of the vehicle.

Similar approach has been adopted by the research conducted by the G. H. Raisoni Institute of Engineering and Technology of Pune, India, where a solar power small electric vehicle model was designed adopting Matlab and analyzed through the simulation of different driving cycles [10]. In this experiment a 1000 W solar panel is responsible for charging a 48V 400 Ah battery which powered the vehicle through a brushless DC motor. Several driving environments are simulated, such as city driving, highway and slop surface. Through the balance of the forces applied to a simplified vehicle model the traction power is evaluated and consumption is obtained.

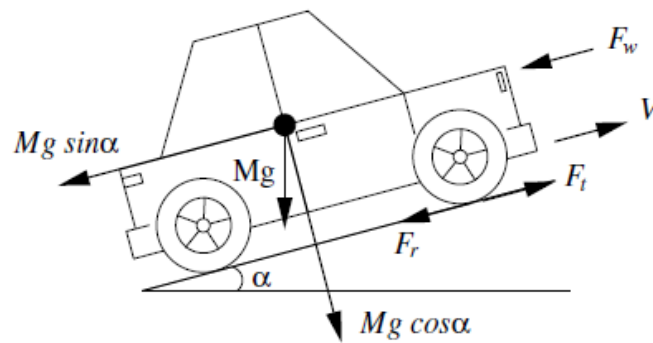


Figure 2.2 Force balance in simplified model [10, p. 2]

An even more detailed model has been developed in the Czech Technical University of Prague, in 2017, with the aim of studying the consumption of different vehicle models and the influence of various powertrain components [11, pp. 51-71]. In this research, after stating the required assessment, such as fully dependency of vehicle speed and slope on given driving cycles, constant operation weather and finite State of Charge (SOC), the implementation of the operational logic in the Matlab and Simulink environment has been described. The model balances out the energy consumed due to aerodynamic drag, slope, rolling resistance  $F_r$  to obtain the tractive one, which is then increased proportionately to the inefficiencies of the electric machine, the inverter,

the converter and the battery to obtain the energy drawn at battery level. Several cycles, such as Urban and Extra Urban driving cycles, NEDC, Artemis Cycle and Highway fuel economy driving cycle are then simulated to evaluate their consumptions and compared.

A relevant implementation of the electric vehicle characteristics has been found in the research supported by the TranLIVE University Transportation Center in 2015, in which regenerative braking application to simulation model was studied and achieved [12]. The energy recovered by braking is supposed to be proportional to the deceleration, following an exponential curve. The thermal energy that would otherwise be wasted by conventional brakes is stored into the batteries, increasing the SOC and giving a consistent advantage, in particular during city driving.

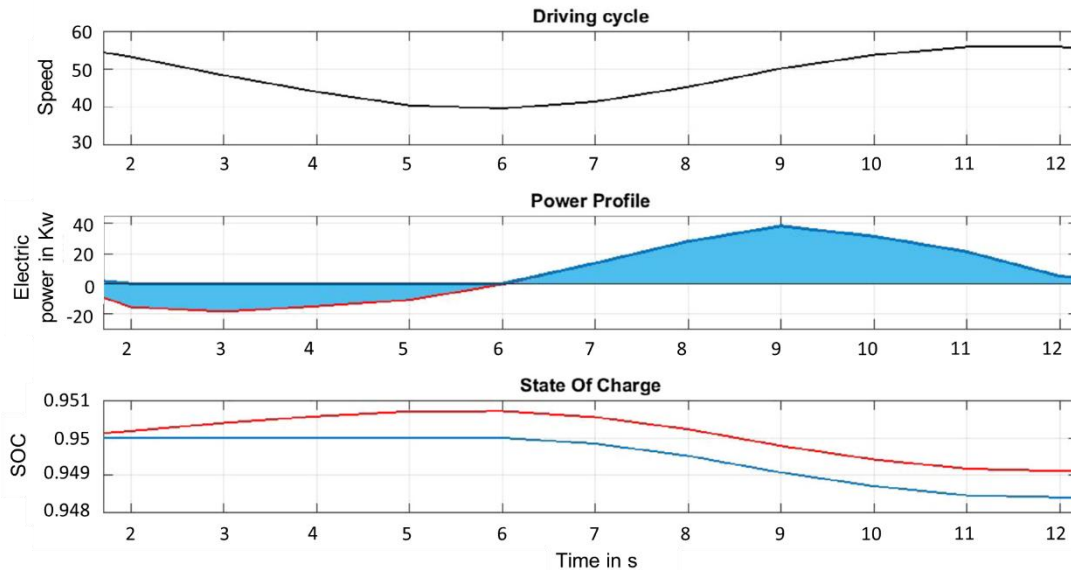


Figure 2.3: Section of cycle to represent regenerative energy stored into batteries [12, p. 263]

The adopted model exploits the inputs of instantaneous speed and EV characteristics, provided in the initialization by the user or by the cycle time-speed curve, to compute the overall and instant consumption, together with the SOC, by means of a quasi-steady backward approach.

In fact, vehicle models can be distinguished in forward facing models and backwards ones [13, p. 731]. The latter starts with the traction power requested at the wheel and evaluates the desired variables travelling backwards through the motor, power electronics and battery. The former, instead, uses the inputs given by the driver, such as throttle position or steering wheel angle, and evaluate the driving torques and other control outputs by means of several feedback controllers. This strategy is mainly used to develop controls and hardware, while the other is often adopted since it permits a shorter simulation time. Generally, however, the total time is strictly related to the level of details required by the model.

All the previous simulation models have been presented because they give a better overview since they share either the operation logic (balance of forces), or the environment (Matlab and Simulink), the tools, the driving cycles or some details (regenerative braking) with the model adopted for this thesis, the Topology Optimization Tool for Electric Mobility (TOTEM)

### 2.1.1 TOTEM

The Topology Optimization Tool for Electric Mobility (TOTEM) has been created by the Chair of Vehicle Technology (FTM) of the Technical University of Munich, Germany [14, pp. 17-19]. This tool allows to run a custom vehicle configuration on a desired maneuver or, by means of an automatic optimization procedure, to find the best compromise between driving dynamics, cost and consumption, once different parameters such as population size or number of generations have been set [15].

The working procedure is divided into three main steps: The first one is the initialization, in which the vehicle model is configured according to the different preferences set by the user. In the GUI, it is given the possibility to the operator to choose between different car segments and tire, to define the number and typology of driven axles, together with motor and gearbox specifications. Matlab calculation environment is adopted for this part. Different axle configurations are available: central motor with open differential, central motor with torque splitter, central motor with electric Torque Vectoring (eTV) and dual near wheel motors. In the gearbox settings, it is possible to define the number of gears for every axle and the relative gear ratios. Concerning instead the motors, both asynchronous induction and synchronous permanent magnet machines are selectable.

According to the preferences chosen, the glider is built and input parameters, such as vehicle dimensions, mass and geometry, tires characteristics, aerodynamic characteristics and chassis data are set. Those are based on the vehicle segment selected (A, B, C, E), since there are some default values for each. Motor torque and efficiency curves are created according to the nominal torque and speed, maximum speed and typology of electric engine set. An algorithm virtually designs the motor, starting from the inputs, and a series of electrical and thermal computations allow to predict the maximum torque providable and the efficiency in every operation point.

The total cost of the powertrain is also evaluated, considering the relative one of the motor, the transmission, gearbox and the power electronics. Concerning the input parameters for the simulation, the weights and dimensions of every part are evaluated, and the overall cost is estimated through an algorithm which sums the production costs, obtained with a reference production line creation, and the cost of raw material, together with the purchase cost of some minor parts. Number of pieces per year, production country and variable costs of the materials are also taken into account and influence the final figures [16, pp. 30-83].

The last part of the initialization consists in selecting the maneuvers to simulate, which may be divided in longitudinal dynamic (Acceleration, maximum speed, custom cycles and WLTP cycle) and lateral dynamic (steady state circular test, sinusoidal steering input test and steep steering input test).

The second phase is the simulation itself, which is run in a Simulink environment, and can be divided into three parts: The first one, called "Driver", uses the inputs of the maneuvers, as trajectory or speed, to evaluate the vehicle ones: steering angle or vehicle torque at the wheel. It also contains the feedback controllers which ensures that the model follows closely the instructions given. The following section, the "Vehicle", contains the evaluation of vehicle limits according to the tires and motors, together with the torque distribution and gears strategy for both efficiency and performance objectives, as better explained in the chapter 4.1. The backward facing consumption evaluation, vehicle model efficiency and the operation of torque splitter or torque vectoring are also included in here, together with the vehicle model itself (see Chapter

3.2). In the latter, the torque figures at each wheel are used to evaluate the operating conditions of the tires, through the Pacejka formulas, the vehicle trajectory, accelerations, steering angle and all the vehicle body and suspension motions. The last section, the “Environment”, collects all the data used to describe the working environment, such as the friction coefficient of the road, initial conditions of the road and the vehicle (Figure 2.4).

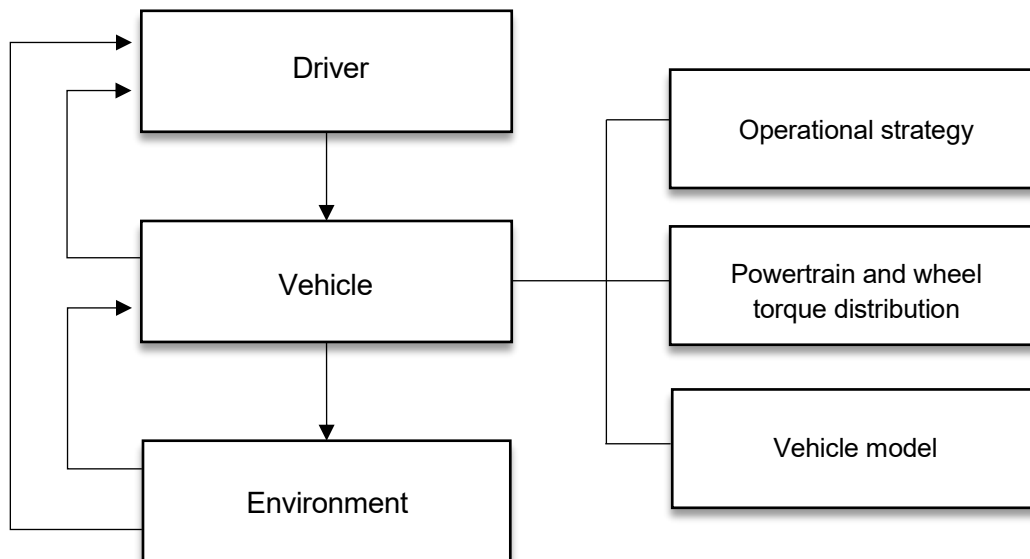


Figure 2.4 Model scheme

The concluding step is the evaluation of the results, in which, accordingly to the chosen maneuver, the outputs of the simulation are analyzed, and the outcome is presented to the user. For instance, if the custom cycle is selected, the battery status and distance covered would be used to evaluate the real consumption, while for acceleration maneuvers the different times of acceleration or elasticity test would be obtained.

### 2.1.2 WLTP Cycle

The Worldwide Harmonized Lightweight Vehicle Test Procedure (WLTP) is a laboratory driving cycle test introduced in 2017 to substitute the outdated New European Driving Cycle (NEDC), designed in the 1980s and based on theoretical driving data [17]. In fact, back when the NEDC was designed, carbon dioxide emissions were not tested and were not a source of economic advantage among the car makers [18, pp. 2-3].

This new test has been created by experts from EU, Japan and North America, to fight the continuously increasing difference between the official laboratory tests and real-world driving fuel consumption and CO<sub>2</sub> emissions, which increased from 7% in 2001 up to 30% in 2013 [19, pp. 8-9].

The resulting cycle is used to measure precisely the fuel consumption and CO<sub>2</sub> emissions of several passenger cars. The main differences, with respect to the previous one, are: a longer and more dynamic driving cycle, a higher vehicle test mass and lower engine temperature at test start. With a 30 min driving time, 23.25 km length, 46.5 km/h average and 131 km/h maximum speed, the new cycle promises to closely simulate the reality [20].

The WLTP is composed of three different classes (1 to 3), according to the power to curb weight ratio. The Class 3 groups most of recent cars (power above 34 W/Kg), while heavy-duty vans and busses usually belongs to the second class. Different speed and acceleration profiles are used for the different classes [21, pp. 35-38].

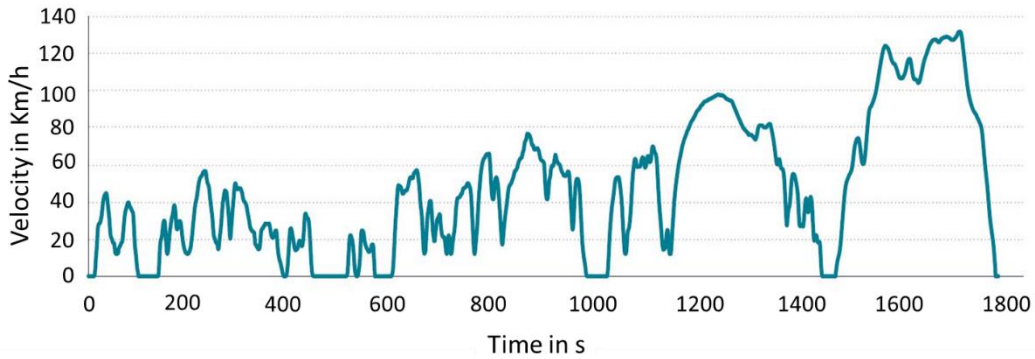


Figure 2.5 WLTP Class 3 Cycle [20]

## 2.2 Double and single track models

In order to describe the handling of a vehicle, in particular a double-axle one, two different models are selected according to the different circumstances and degree of precision required from the results [22, pp. 257-270].

The most accurate and adopted is the double track model. It considers the sideslip angle for every wheel and different condition of the steering angle. The tire model can also be non-linear, giving more precision and realism to the results.

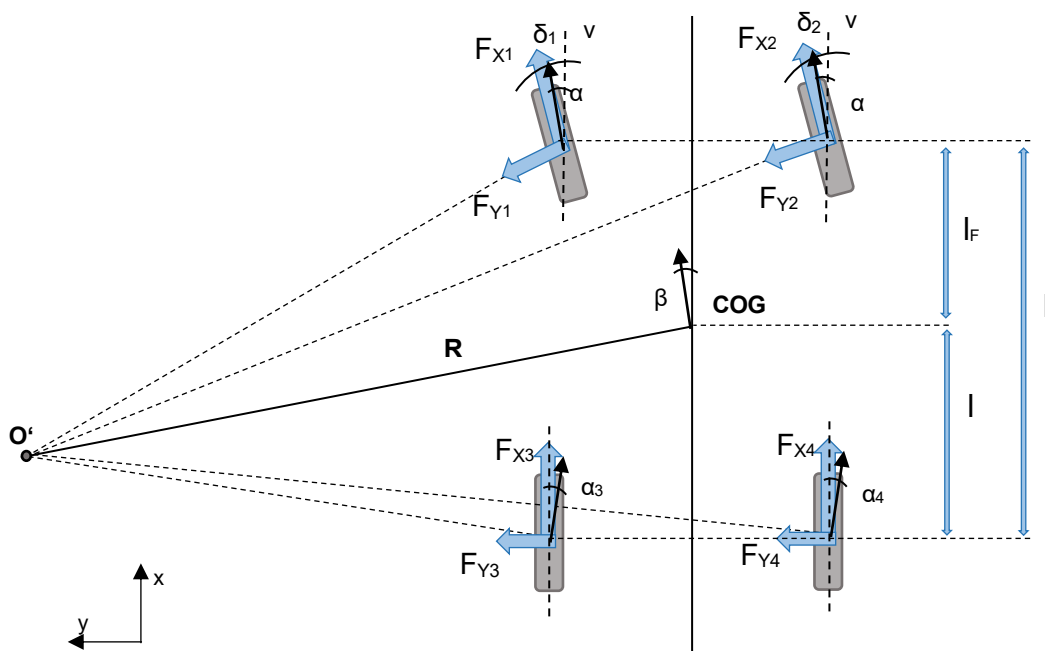


Figure 2.6 Double track model

Moreover, both the pitch and roll motions can be simulated, since the variation in the position of the center of gravity can be accounted for in any condition. Especially during tight radius cornering, the front wheels show a different steering angle ( $\delta_i$ ), with different tire behavior, and appropriate devices, such as the Ackerman steering, must be adopted [23, pp. 241-244].

The other possibility to describe the behavior is to adopt the so called “monotrack” or “bicycle model”. The present represents a simplified approach and its use is suggested only for high speed cornering or corners with a curvature radius ( $R$ ) much wider than the wheelbase ( $l$ ), hence when the side slip angle is significantly smaller. This last detail ensures the reliability of the results, despite the quite substantial simplification implemented. In addition, the second assumption necessary is to operate without any roll motion since, if this last condition is verified, a different behavior can be found in left and right tracks due to the center of gravity (COG) shift, making the approximation not valid. The tire behavior should also be linear to cope with the simplification done.

The equation which represents the equilibrium of forces in y direction can be described as:

$$\frac{mV^2}{R} \cos(\beta) = \sum_{\forall i} F_{x_i} \sin(\delta_i) + \sum_{\forall i} F_{y_i} \cos(\delta_i)$$

The equation for the equilibrium of rotation around G is expressed as:

$$\sum_{\forall i} F_{x_i} \sin(\delta_i) x_i + \sum_{\forall i} F_{y_i} \cos(\delta_i) x_i = 0$$

Since, as assumed, the  $\delta$  and  $\beta$  angles are negligibly small, the equilibrium equations can be summarized as

$$\begin{cases} \sum_{\forall i} F_{y_i} = \frac{mV^2}{R} \\ \sum_{\forall i} F_{y_i} x_i = 0 \end{cases}$$

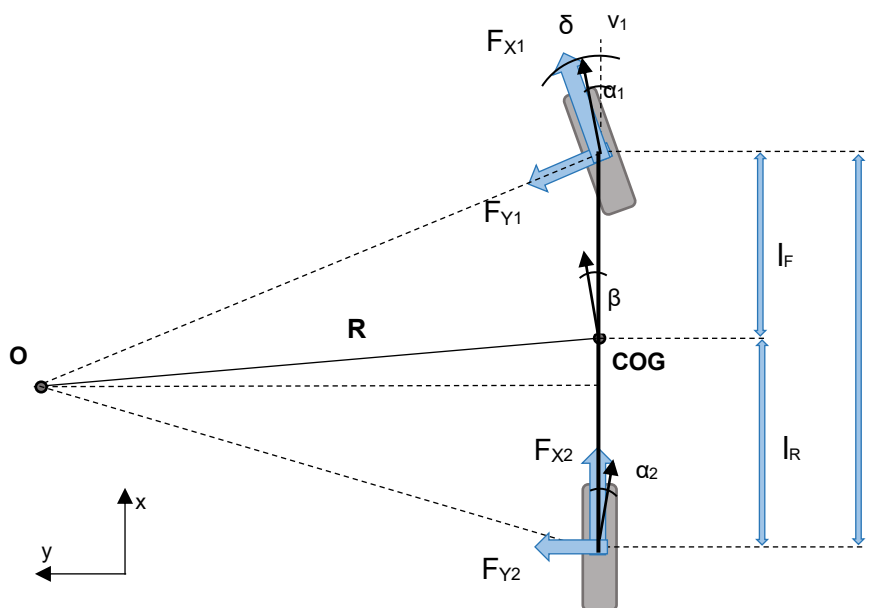


Figure 2.7 Monotrack or bicycle model

## 2.3 Comparison of front, rear, all-wheel drive layouts

Several researches have been conducted, with different objectives, on the influence of a power-train configurations on electric vehicles. The possibility to converge the torque on the wheels of the front or rear drivetrain can lead to relevant advantages in term of dynamics, handling and efficiency.

A team of the University of Surrey focused on the development of an optimal controller for Torque vectoring, considering the different layouts that an electric car can present [24]. The different configurations analyzed were single central motor Front-Wheel Drive (FWD), dual motor FWD, dual motor RWD, a mix of central and dual motor for All-Wheel Drive (AWD), and dual motor per axle in the AWD architecture.

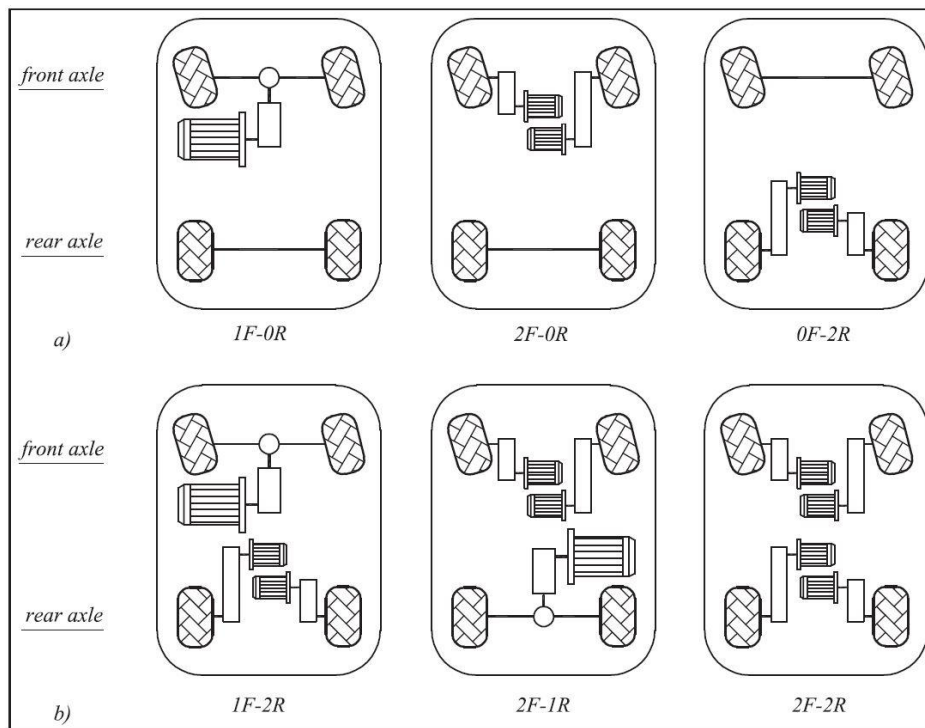


Figure 2.8 Examples of vehicle layouts with one to four electric powertrains [24, p. 2]

A yaw-moment controller, composed by a feed-forward part, in charge of creating the desired moment according to input requests, and a feedback part, responsible for keeping the system stable and avoid noise and disturbance interferences has been designed for the purpose. The selected model is an eight degree-of-freedom vehicle model, which consists in longitudinal, lateral, roll and yaw motions, and rotation of the four wheels. A flat road and small sideslip angles were assumed. For single driven axle a limited slip differential has been also included, and its loss considered in the evaluation of the input power of the drivetrain, based on look-up efficiency maps. For the simulation and validation, the Matlab/Simulink working environment has been adopted. In order to validate the model, a front wheel drive sport utility vehicle was tested in the proving ground of Lommel (Belgium), and step-steer and skid-pad tests were performed.

By means of transferring part of the overall required torque to a certain wheel, the team was able to design a controller which would affect the vehicle yaw moment and the understeer or oversteer characteristics of the model. To correct the undesired behavior, a look up table in function of steering angle, speed and pedal demand was created, and though an optimization algorithm, the ideal torque distribution for each wheel identified.

Different configurations were then compared, using as evaluation criteria the limit of linear vehicle behavior, maximum lateral acceleration and controllability. Interesting results have been obtained for what concerns longitudinal dynamics, where, despite the similar performance in braking conditions, in traction conditions the advantage of the AWD architecture has been highlighted and the benefit of torque vectoring is visible in the result in all the dual motor configurations (Figure 2.9). An increase of approximately 30% in performance between single motor single driven axle and dual motor, in which torque vectoring is enabled, is evident.

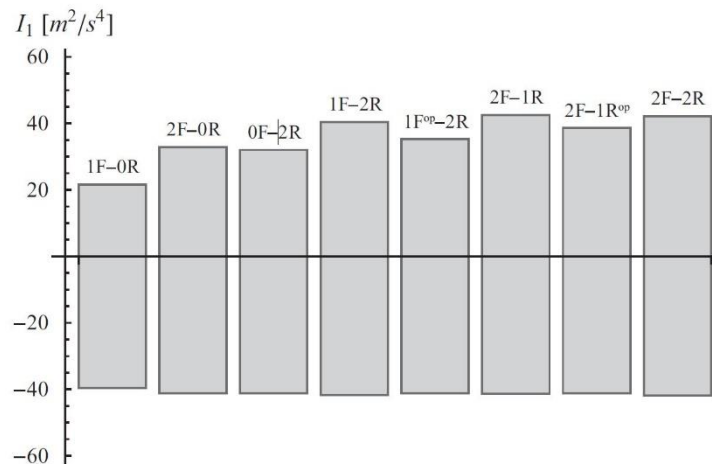


Figure 2.9 Results for longitudinal behavior of the research from the University of Surrey [24, p. 11]

The same team, subsequently, also investigated the effect of torque allocation to reduce the losses in AWD electric vehicles [25]. The aim was to design a controller which would allocate a different torque to the four motors reducing power consumption and minimizing tire slip.

An offline procedure was applied to identify among all the different combinations the most efficient, based on the data provided by the engine manufacturer, still maintain the desired acceleration and yaw moment. The driver controller, as described above, was able to achieve the desired level of yaw rate and simulate all the different vehicle behaviors. Different power consumptions have been obtained varying the working condition, in term of requested torque from the four motors and the allocation. The lower overall consumption has been so identified. Moreover, to avoid oversteering behavior, front axle bias has been preferred when possible.

The investigated maneuvers were straight-driving at 50 km/h and 100 km/h, ramp steer with constant steering rate of 10 deg/s at 100 km/s and sequence of step steers with variable amplitude at 100 km/h.

The results showed a minimal variation of power losses of 3.1% in favor of the optimized allocation in straight-ahead maneuvers, with an increase up to 5.8% and 4.5% for ramp steer and sequence of step steer maneuver respectively.

A further experiment has conducted in 2015 to demonstrate how a fine tuning of the understeering characteristics could further reduce energy consumption [26]. The test was carried out with a fully electric Range Rover Evoque prototype in the facilities of Flanders MAKE (Belgium). A series of 60 m radius skid-pad tests were performed and optimal regeneration-traction balance between left and right side of the drivetrain was studied. Optimal yaw moment and allocation strategy has been analytically identified. The conclusion highlights the presence of multiple solutions for optimal allocation, together with the possibility to evaluate a sub-optimal solution considering tire slip and a possible energy saving of at least 8%, with respect to the default allocation.

Still conducted by the same team, the optimal torque distribution depending on vehicle speed for equal drivetrains and monotonically increasing power loss characteristics has been investigated, with the aim of designing an easily implementable torque distribution strategy and validating it experimentally [27].

A controller has been designed to switch at the optimal point between the analytically evaluated two main optimal condition: the single axle strategy for low torques and even distribution for large ones.

The tested vehicle was an EV Range Rover Evoque, from the iCOMPOSE European project, with four identical onboard electric motors. The test maneuvers were the New European Driving Cycle (NEDC), Artemis Road driving cycle and Extra Urban Driving Cycle with 8% uphill road slope. A bench equipped with rollers has been used to evaluate the power loss measurements at every torque allocation, and the maneuvers were then simulated on a validated Matlab/Simulink model.



Figure 2.10 The iCOMPOSE EV at Lommel test center (Belgium) [28, p. 2]

The results confirmed that up to a certain threshold, a single motor was the most efficient configuration for low torque levels, while for higher ones as even distribution between front and rear axle was ideal. This strategy reduced the energy consumption between 0.1% and 5%, according to the cycle simulated. Even step steer maneuvers indicated a decrease of the consumption.

Based on the same prototype, an experimental assessment has also been realized to study the effect of different front to rear torque allocation on the vehicle behavior [28]. The test consisted in a series of ramp steer maneuver at 30, 60, 80 km/h in FWD, RWD, AWD layout with a 50:50 front-to-rear distribution. A Proportional Integral (PI) feedback controlled oversaw controlling the vehicle speed. The results were a more understeering attitude of the RWD with respect to the FWD layout, due to a destabilizing yaw moment caused by the steering wheel angle, especially highlighted in the 30 km/h test.

A similar study has been carried on at the Cranfield University (UK) to study the effect of torque vectoring on the ISO double-lane change maneuver [29]. The adopted model has been a seven degrees-of-freedom: longitudinal and lateral displacements, together with yaw rotation on z-axis and the individual rotation of the four wheels. Lift and drag were considered by means of constant coefficients. Pacejka magic formulas has been used to describe the tire behavior.

Differently to the previous experiments, the present has been based not on an EV platform, but on a conventional ICE one, with a 70:30 central differential, able to change to a 30:70 distribution (bang-bang control). The three simulated cases adopted three open differentials, the 70:30

central differential and torque-vectoring differential. The results have displayed an improvement of approximately 40% in terms of slip angle for the bang-bang controller differential case. The addition of an active central differential or a left-to-right torque vectoring device increased even more the difference with the base scenario.

A study which also focused its interest on the effect of vehicle behavior has been conducted by a team of the University of Nottingham (UK). The results of active torque distribution (Torque Vectoring) on the efficiency and dynamic attitudes has been investigated [30, pp. 1-9]. A seven degrees-of-freedom Matlab model has been used for the investigation, neglecting suspensions and body motions. Nonlinear model has been adopted for tires.

The study proved that front to rear and left to right distribution can have positive effects on leftward turns maneuvers of 100 m and 30 m radius at 10 Km/h, despite some occasional oversteering behavior. More relevant to the future studies is the concern on consumption reduction, which settles at 0.52% in case of an AWD with front-heavy mass distribution and 0.21% for a FWD rear heavy vehicle. The most relevant reductions occur at high speed (Figure 2.11).

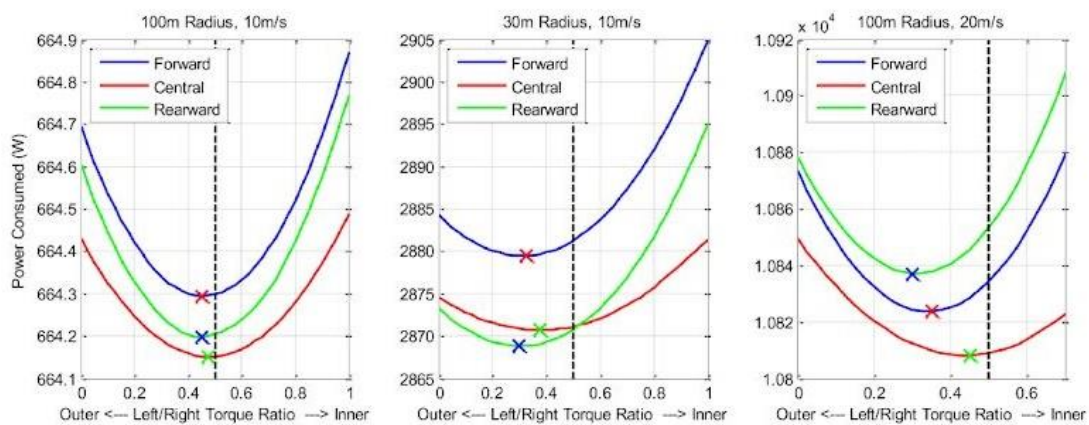


Figure 2.11 Power consumption varying torque split for different weighted vehicles and different maneuvers [31, p 7]

On similar aims was based the publication by J. Tobolář, R. de Castro, U. Bleck, C. Satzger, J. Brembeck and Y. Hirano [31, pp. 1-8]. The platform used was the ROboMObil (ROMO) developed by German Aerospace Center. Electric motors model was created to evaluate the losses, together with the inverter one. RWD central motor and dual near-wheel motors, AWD with torque vectoring or near wheel motors and all-wheel steering (AWS) were chosen as investigated configurations. All those layouts were simulated in Modelica for steady-state cornering, in-turn and straight acceleration, sinusoidal steering and double lane change. A higher efficiency for in-wheel motor was registered both for combined handling maneuvers (CM1) and combined highly-dynamic ones (CM2), compared to both RWD configurations, while AWD did not bring any significant advantage in terms of energy savings.

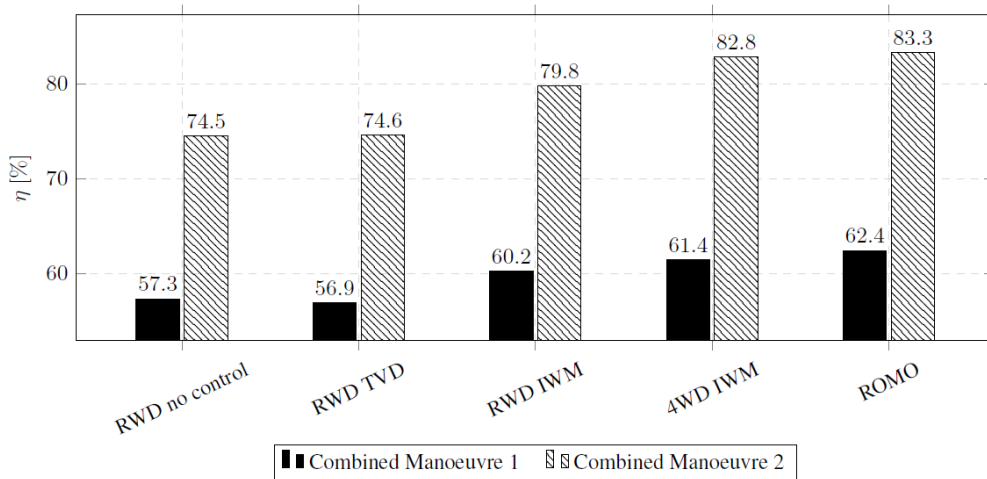


Figure 2.12 Average energy efficiency [31, p. 7]

Further detailed researches focus more on the efficiency aspect, rather than performances. A clear example is the investigation concerning in wheel permanent magnet synchronous motors (PMSM) losses [32]. The aim was to search for a method to determine torque distribution which would lead to the lowest consumption.

A mathematical model to evaluate the losses in PMSM and in inverter systems has been designed and validated, by means of bench testing a motor and analyzing the power outputs. Four ranges of speeds (100 1/min, 200 1/min, 300 1/min and 400 1/min) were chosen as different values to validate. Once the optimal torque distribution strategy has been defined, according to motor and inverter losses, the model was simulated for straight acceleration and braking for 100 N m, 150 N m, 200 N m.

Motor loss, and in general system efficiency, has been discovered to be a convex function for identical motors, and maximum efficiency can be found at 50:50 front-to-rear torque distribution. For different motor parameters, the ideal torque distribution has been also mathematically investigated, but no general conclusions can be made since the optimal torque bias is dependent on motor characteristics.

To validate the optimization for torque distribution, a four-wheel-drive EV with four identical PMSMs was tested on a dynamometer, and through the Battery Management System (BSM) and the data from the teste bench, the strategy has been validated. The tests consisted in a run at 5 km/h, 6km/h and 7km/h for 80 N m and 120 N m overall and in a run at 10km/h, 20km/h and 30 km/h for 200 N m, both in acceleration and in braking conditions.

All the results denote the 50:50 torque distribution as the most efficient, with worsening energetic consumption as closer it gets to full torque on one axle [Figure 2.13-14]

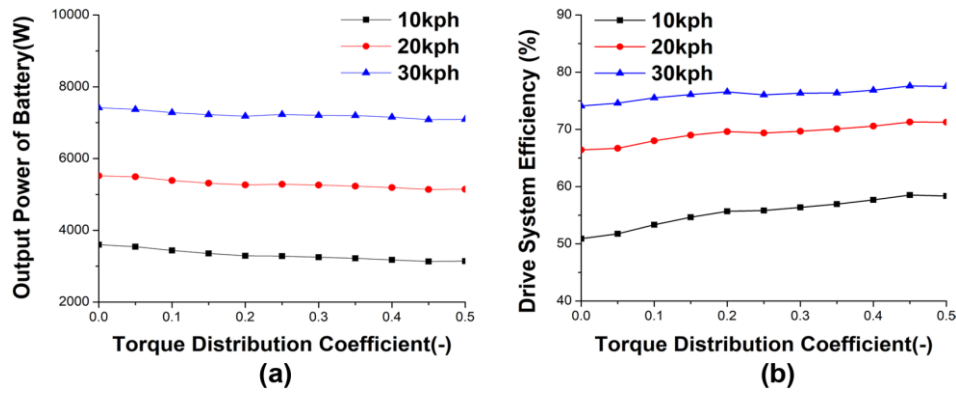


Figure 2.13: Results from the Dynamometer test at 200 N m for different torque distributions under acceleration conditions (a) Battery Output Power (b) Drive System Efficiency [32, S 15]

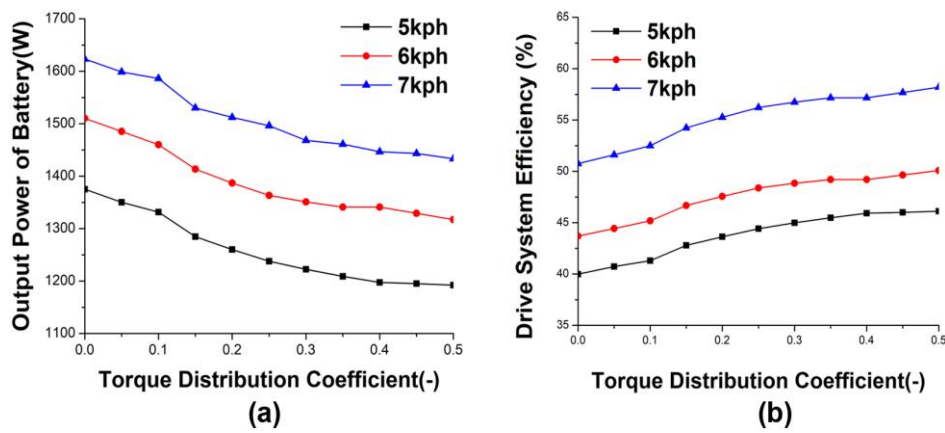


Figure 2.14: Results from the Dynamometer test at 120 N m for different torque distributions (a) Battery Output Power (b) Drive System Efficiency [32, S 14]

Several analyses have also been carried on for in-wheel electric motors, with similar objective as the previous ones. A group of researchers from the Tsinghua university of Beijing (China) investigated, in 2012, a method for an optimizing the efficiency of electric vehicles with in-wheel motors [33, pp. 764-770].

They developed a mathematical evaluation of the losses of both the motors and the inverters, and validated the results testing a motor on a dynamometer test bench. With those results it has been discovered that the best configuration is an even distribution of torque among the motors. The final tests consisted in runs at 20 km/h, 30 km/h and 40 km/h in both 4WD and 2WD configuration for acceleration and braking. The results show a better efficiency for AWD vehicles, although their previous literature researches indicated the 2WD configuration as the optimal one at low speed (Table 2.1). The justification can be found in the neglect of the efficiency of the disabled axle, which is instead relevant to the results.

Table 2.1: Test results in driving conditions [33, p. 770]

Vehicle speed in km/h	Total driving Torque in N m	Battery power in AWD in W	Battery power in 2WD in W
20	20.5	779.7	834.6
30	26	1366.8	1427.7
40	31	2062.2	2150.3

Another publication regarding efficiency of electric vehicle with in-wheel motors was presented by Xinwei Jiang, Long Chen, Xing Xu, Yingfeng Cai, Yong Li and Wujie Wang [34, 2-8]. The model adopted is a EV prototype with four 3 kW motors. The efficiencies of the latter and of the battery have been studied through several tests on a dynamometric bench, by simulating the Economic Commission for Europe urban driving cycle. After developing the logic for the energy optimization by torque allocation, a Matlab/Simulink model has been tested in the same cycle, both in 2WD and 4WD configuration. When torque is below a certain threshold, rear allocation only is preferred, while above it an all-wheel drive distribution is favored. However, energy consumption has dropped by 0.12 kJ/m compared to all-wheel drive in general and 0.31 to rear wheel drive.

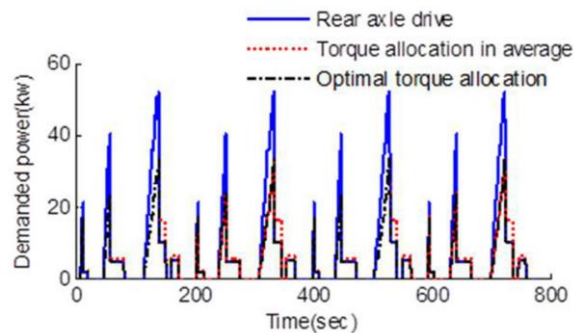


Figure 2.15: Demanded power for three different allocation strategy [34, S 8]

A research including both electric and hybrid vehicles has alternatively been conducted by Sang-Jae Lee, Yong-Gi Kim, Tal-Chol Kim and Ki-Nam Kim [35, pp. 1-6]. The team investigated the possible reduction of consumption of a hybrid vehicle with both electric and thermal engines at the front and a fully electric rear powertrain by activating and varying the load of the rear motor. Simulating the FTP and Highway cycles, it was discovered that rear unit intervention increased the efficiency of 0.1%-0.3% (according to the cycles) in fully electric mode, and 0.2%-0.6% for the hybrid mode. Additionally, by enabling regenerative braking, a further increase of efficiency was available.

A relevant paper for the subsequent work considers the studies about a smart torque vectoring algorithm for full electric vehicles [36, pp. 1-8]. The operation strategy is divided into an iteration for torque split ratio for minimum losses, when the battery has sufficient power, and the same iteration but only with the energy that the low-level battery can provide, in case of reduced power. As in the future investigation of this thesis, the models are simulated on Matlab/Simulink, with the WLTP cycle. The smart strategy can reduce the consumption by 2.9% in case of torque split ratio of 1 (FWD) and 1.6% in case of 0.5 (AWD with a 50:50 distribution).

A completely different approach for the differences between vehicle layouts has been brought by J. Lee and D. J. Nelson in their examination of the influence of rotating inertia for electric vehicles [37, pp. 1-7]. With the development and validation of a back-tracking model, three possible configurations (FWD, RWD and AWD) have been analyzed through five driving cycles to understand the impact of inertia over energy recovered in braking and propulsion. The net energy comparison, obtained subtracting the energy regenerate from the require for propulsion, shows an energetic requirement 8.7% and 4.9% lower for AWD and FWD layout, compared to a vehicle without regenerative braking. In fact, part of the energy of the powertrain is stored in rotating parts and can be fully retrieved by regenerative braking.

The following research focuses its attention on braking conditions, in particular on energy regeneration in braking conditions [38, pp. 686-697]. A torque allocation algorithm has been designed to minimize power losses. A longitudinal only vehicle model has been adopted and a loss model has been studied to predict PMSMs and battery efficiency. Based on the former results, a controller has been designed to allocate the negative torque distribution to the most efficient configuration. Particular consideration has been given to the losses through slip. The simulation, conducted in the Matlab/Simulink environment, for double lane changing maneuver, deceleration from 80 km/h and NEDC highlights how the ideal torque allocation varies with speed and how the even torque distribution is overall the preferred (Figure 2.16).

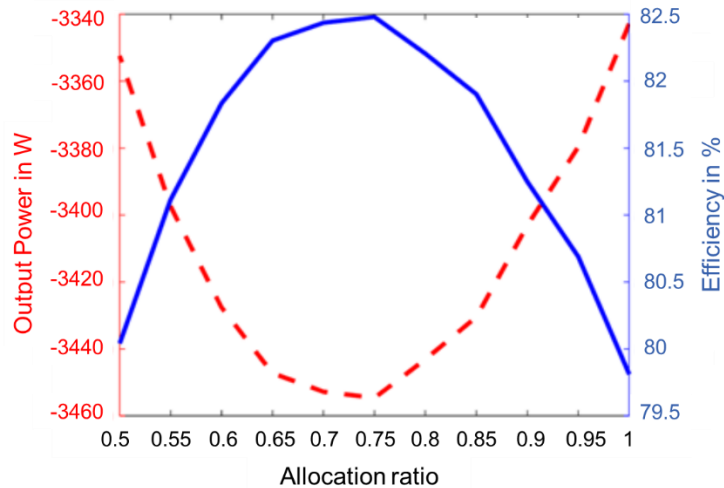


Figure 2.16: Experimental results of different allocation ratio [38, S 696]

The second-last document which is mentioned presents the comparison under a point of view of pure performance. The traction during accelerations is analyzed, especially for off-road vehicles [39]. The model has a 14 degrees of freedom, to be as precise as possible, and both rigid and flexible tires can be simulated. The test has been conducted at various speed on both dry sand and loamy terrain. The results highlighted that the most efficient allocation to transmit power to the ground is an all-wheel drive layout, with torque distribution offset on the rear axle. Moreover, the effect of load distribution has been found not to give any significant advantage on the tractive efficiency but only on traction. The Figure 2.17 shows the results on loamy conditions at 50 Km/h. As visible, the lowest power to achieve the previously set results has been found for a value between 50 % and 60 % repartition of torque at rear axle.

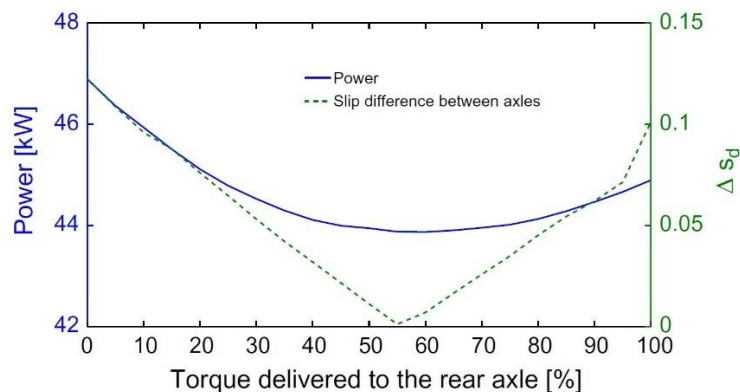


Figure 2.17: Power transmitted at ground at a speed of 50 Km/h on loamy terrain [39, p. 11]

The last and probably most relevant publication analyzed has been based on a former version of the TOTEM tool, the same used in this thesis, and with similar objectives. The effect of power allocation in AWD configuration has been studied for consumption, cost and performances. In this case, a reduced custom driving cycle, lasting 90 seconds, with a top speed of 58 Km/h and an average of 34 Km/h has been adopted to run the consumption comparison. The vehicle model has been optimized on the cycle to find the best input parameters and based on those the nominal torque has been shifted front to rear to compare all the possible configurations. Several power levels have been also considered, to widen the analysis. The performance investigation has been obtained by an average of several longitudinal and later maneuvers. As results in Figure 2.18 highlights, the most efficient distribution lies between 0.15 and 0.5, while the performances are best enhanced by a rear predominant AWD configuration. The costs show a gradually increase in the AWD configurations as the even distribution is approached and a more severe rise as the model shifts from 4WD to 2WD.

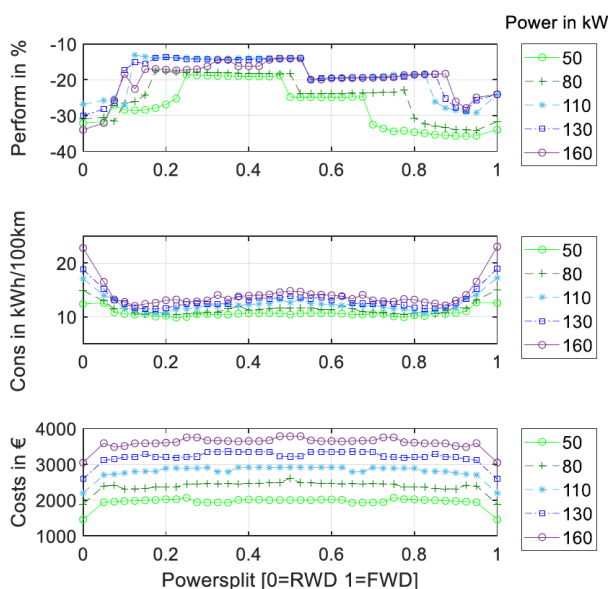


Figure 2.18: Performance, consumption and cost results of the comparison [40, p. 3]

### 2.3.1 Conclusion on the state of the art for the comparison

The analysis of various publications and researches on the subject led to point out some general trends.

The results highlighted a higher efficiency of front-wheel driven configuration in longitudinal acceleration with low torque and speed with respect to the all-wheel-drive one, which excelled in all the other conditions, especially due to the possibility to optimally control the torque vectoring.

A reasonable amount of research has also been conducted with the aim of performance analysis, mainly evaluating the improvement brought by torque vectoring in both 2WD and AWD configuration. Some publications were also supported by physical investigations, while others realized simulation of longitudinal and cornering tests. In any case all the documents supported the superiority of the all-wheel-drive configuration both performance-wise and efficiency-wise, also due to the availability of tailor made torque vectoring, highlighting the limits of 2WD layout, both due to dangerous behavior for RWD vehicles enhanced by the adoption of torque vectoring, and to the limited case of better efficiency for FWD at low speed only.

The publications which instead focused just on the efficiency comparison, analyzed the problem also varying some of the details of the drivetrain. The adoption of a gearbox highly influences the torque bias according to the selected gear since the parameters of optimal working point of the motors change. The presence of different motors on the front and rear axle may shift the ideal working point but motors choice can improve longitudinal acceleration. Focus on optimal Torque vectoring also revealed possibility to better improve efficiency and energy recovery in the presence of AWD configuration.

Nevertheless, no comparison has been carried out considering the cost as a variable, apart from the publication by the TUM institute, which is limited by a cycle too short (lasts 30 seconds) and with lower power demand and speed (has an average speed short of 12.5 Km/h) with respect to the homologation reference (WLTP). Car manufacturers deeply investigates the increase of the cost before considering a new investment, and the proportionality between this and the advantages are a constant concern. In addition, most of the literature investigated did not compare the same simulations with different objectives, but either efficiency or performance were examined, one at a time. This limit justifies the further investigation of this thesis, since the result may allow several interpretations of the best alternatives based on the aims to achieve, hence being more relevant for its flexibility.



# 3 Reduction of the driving cycle simulation time

## 3.1 Time analysis

The initial point of this thesis has been the reduction of the time required for the simulations. This, for the dynamic behavior maneuvers, lasted approximately less than a minute each, while the WLTP cycle (see Chapter 2.1.1) finished over 10 minutes later. Due to this inconvenient, the feasibility of any analysis which requires simulation of multiple configurations was compromised from a quite long waiting of the results. Since the objective of the TOTEM instrument is to give the possibility to investigate all the available combinations of choices in vehicle structure, this drawback could not be accepted in the given conditions of the research.

To understand the sections of simulation in which most of the time is spent, a casual configuration has been chosen.

Table 3.1: Parameters input for the reference simulation

Parameters	Value / Choice
Segment	C
Front axle	Near-wheel motors
<ul style="list-style-type: none"> <li>• Motor typology</li> </ul>	Permanent magnet synchronous machine
<ul style="list-style-type: none"> <li>• Motor nominal torque</li> </ul>	100 N m
<ul style="list-style-type: none"> <li>• Motor nominal speed</li> </ul>	5000 1/min
<ul style="list-style-type: none"> <li>• Motor maximum speed</li> </ul>	10000 1/min
<ul style="list-style-type: none"> <li>• Number of gears</li> </ul>	1
<ul style="list-style-type: none"> <li>• Gear ratio(s)</li> </ul>	9
Rear axle	Central motor with open differential
<ul style="list-style-type: none"> <li>• Motor typology</li> </ul>	Asynchronous machine
<ul style="list-style-type: none"> <li>• Motor nominal torque</li> </ul>	100 N m
<ul style="list-style-type: none"> <li>• Motor nominal speed</li> </ul>	5000 1/min
<ul style="list-style-type: none"> <li>• Motor maximum speed</li> </ul>	10000 1/min
<ul style="list-style-type: none"> <li>• Number of gears</li> </ul>	2
<ul style="list-style-type: none"> <li>• Gear ratio(s)</li> </ul>	11 / 8

The table above (Table 3.1) illustrates the parameter choice, which has been selected to be as work intensive as possible. The maneuver which has been selected is the WLTP cycle.

The required time analysis can be divided into initialization, simulation and result processing time. The former and the latter are neglected since they are significantly smaller than the main simulation time. This, in fact, is over ten times longer than the others, which require together less than

a minute. In any case the times of this sections were analyzed with the time counter tools in Matlab. The result is a running time of 773.99 seconds, to be divided into initialization (51.63 s), simulation (720.73 s) and post-processing time (1.63 s).

The tool used to analyze the time spent in simulation, which runs in Simulink, a graphical programming environment for modeling integrated with the rest of Matlab environment, is the Profile instrument. This performance instrument collects the data and generates a report with the time spent relatively to each function which has been run, helping to identify the parts of the model on which to focus for optimization [41].

The results consist in a list of all the functions, with the addresses in the simulation, the relative times, calls and time per call. This table has been summed up according to the subgroups to which they belong (Figure 3.1).

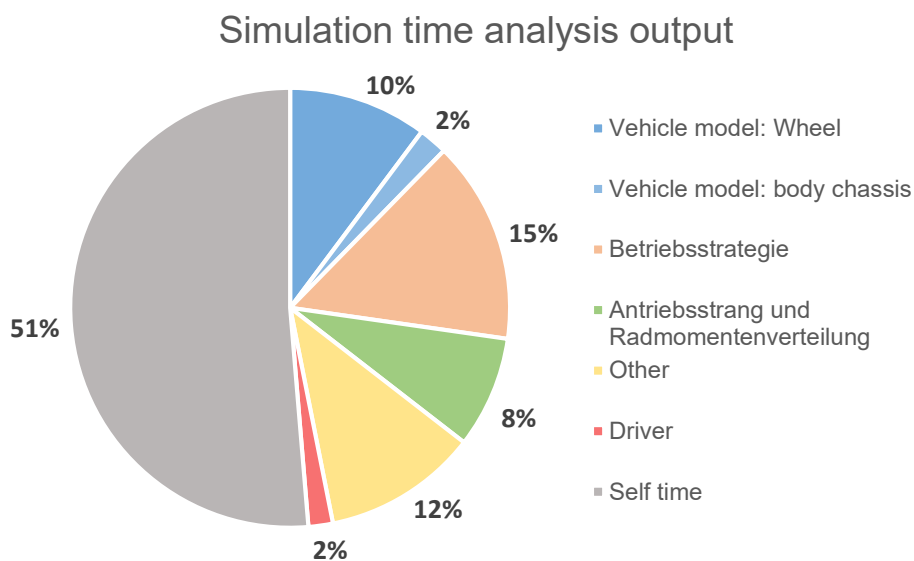


Figure 3.1: Time division of the simulation

From a first look it can be observed that significant concentration of the time has been spent in the wheel model. Eighty-four seconds are spent in the simulation of the tire model, based on the Pacejka magic formulas, with an average of 21 seconds per tire (2.5 %). On contrary, a relatively small amount is related to the remaining part of the vehicle model, the body motion evaluation (only 2%). A significant percentage is consumed in the operational strategy section. The dense presence of lookup tables and S-functions justifies the high computational effort and the time consumed. Similar reason explains the percentage of the powertrain and wheel torque distribution part. The remaining time is divided between self-time and other functions not groupable under significant associations. The self-time, which represents the biggest percentage, is the time spent in the simulation itself, not calling any child function. Since the aim of the Profile tool is to identify the bottlenecks to optimize the model, not all the functions are mentioned, but only the most relevant ones. This self-time is the results of all the functions not analyzed but grouped under a major heading.

An second regrouping of the functions, according the typology, has been conducted to understand whether there is the possibility to cancel or reduce some of those. The results are shown in Figure 3.2.

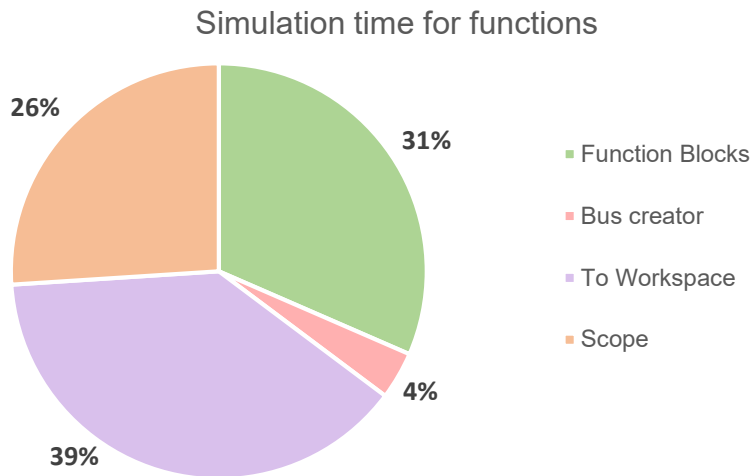


Figure 3.2: Time division according to functions

As predictable, most of the time is spent in functions and to workspace blocks. Anyway, a substantial percentage is linked to scope blocks. Those tools are used for debugging and to study the variables which change over time but are not necessary for correct operation of the model.

## 3.2 Method

As a first step of the model optimization, the unnecessary scopes have been eliminated to fasten the simulation.

Secondly, a study on the necessity of all the To Workspace has been carried on. Those blocks collect the data during while the model runs and save them all in the Matlab workspace during the termination phase. Most of those blocks are either used for the rest of the maneuvers, especially lateral dynamic ones, or are required for post processing analysis tools and not directly for the final output. To properly ensure the optimized functioning, the unrequired ones must be temporarily disabled just when the driving cycle is run, while they should be enabled for the remaining procedures. This can be achieved by setting the “commented” parameter to “off” when the WLTP is run. If the user desires to have the complete data to run afterwards one of the analysis tools, a selection box in the maneuver choice has been implemented to allow it.

The latest and most demanding optimization operation accomplished aims at reducing the time spent in the function blocks of the vehicle model. Half of the functions related to the tires could be eliminated if the vehicle model would be simplified to a Single-Track Model (See chapter 2.2).

This simplification is possible because all the driving cycle maneuvers, as the WLTP, are designed to run on dynamometric roller benches, on which no steering input can be applied. Hence, those cycles are completely simulated as a straight-line path with variation of speed in function of time [42, pp. 136-147]. The absence of steering input, which lead to negligible side slip angles are the main requirement, as explained in Chapter 2.2. Designing a new model which simulates only half the track of the vehicle but can give results for the full vehicle, thanks to perfect

symmetry of the geometries and forces, would reduce the simulation time by approximately 42 seconds, which is a reasonable amount to justify the planned work. In addition, in the bench tests there is the possibility to simulate an inclined road by applying extra braking torque to the rollers, to mimic the additional effort required by a steep track. This feature should still be included in the simplified model. Note that no modification has been applied on the operation logic: the tire model, suspensions and vehicle dynamics still use the same rationale and only some minor components have been removed when not used.

The Figure 3.3 illustrates the operation of the so obtained simplified vehicle model: The input of drivetrain and brake torque, arriving from the “Powertrain and wheel torque distribution” (See Chapter 2.1), together with tire parameters, road characteristics and initial position, coming from initialization, enters the tire calculation block, inside of which tire behavior is evaluated. The outputs (longitudinal and lateral forces, radius and wheel lift) enter the body calculation block, in which the vehicle characteristics and motions are determined. Global results consist in the model velocity and acceleration, suspension motion, pitch angle, aerodynamic and damper power. An algebraic loop is also present since, to use the Pacejka magic formulas, camber angle and force on z-axis are required.

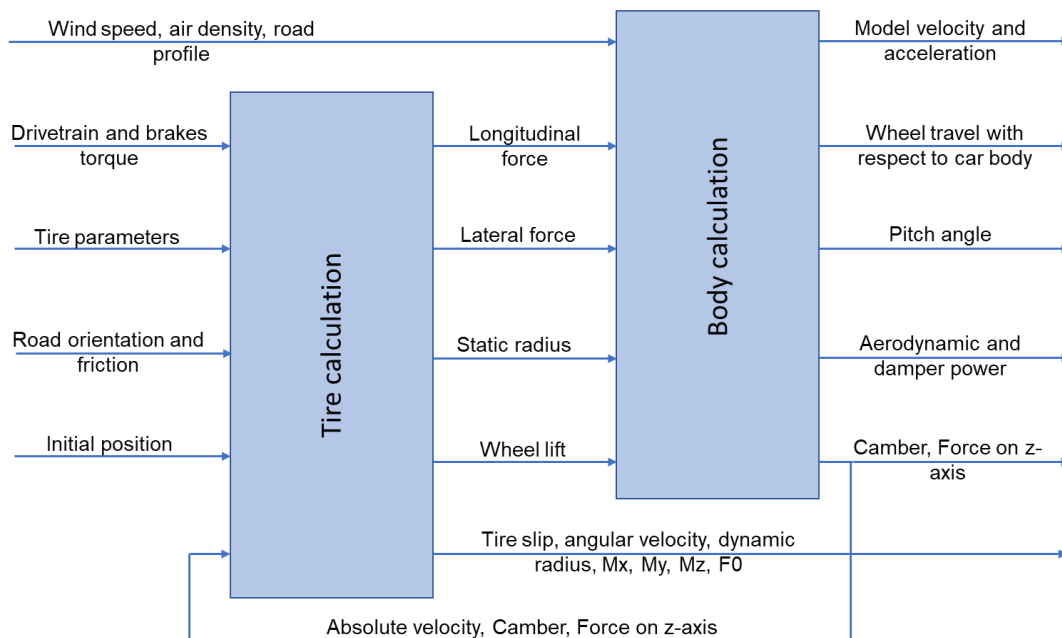


Figure 3.3: Vehicle model scheme

Analyzing the operation more specifically, to understand the modifications done to the model, the Tire calculation block structure is presented (Figure 3.4).

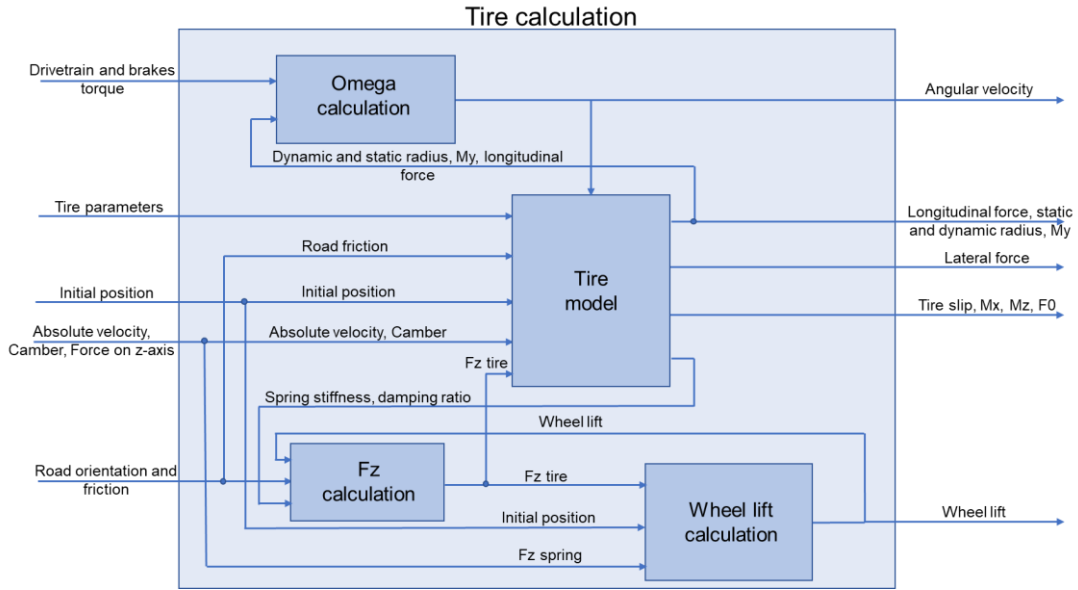


Figure 3.4: Tire Calculation structure

Inside “Omega calculation”, all the torques at the wheel are balanced and integrated over time to evaluate the wheel angular velocity, later needed in Tire model. The torque related to left and right sides are averaged to obtain a single value per axle. In the “Fz calculation” block, the displacements on the tire and their stiffness and dumping coefficients are used to obtain the forces in z-direction. The “tire model” block contains the Pacejka magic formulas computation. Here the tire functions are reduced to two, cutting down the simulation effort, hence the time. “Wheel lift” section evaluates the wheel travel according to suspension geometry and coefficients, with ground reference frame. In this case only one side of the suspension system is considered.

In “Body calculation” section instead, chassis motion such as pitch and suspension travel are evaluated, together with the Kinematic compliance (Figure 3.5). Roll motion and anti-roll bar functions have been eliminated since their effect is mostly negligible both on a dynamometer and in a driving cycle.

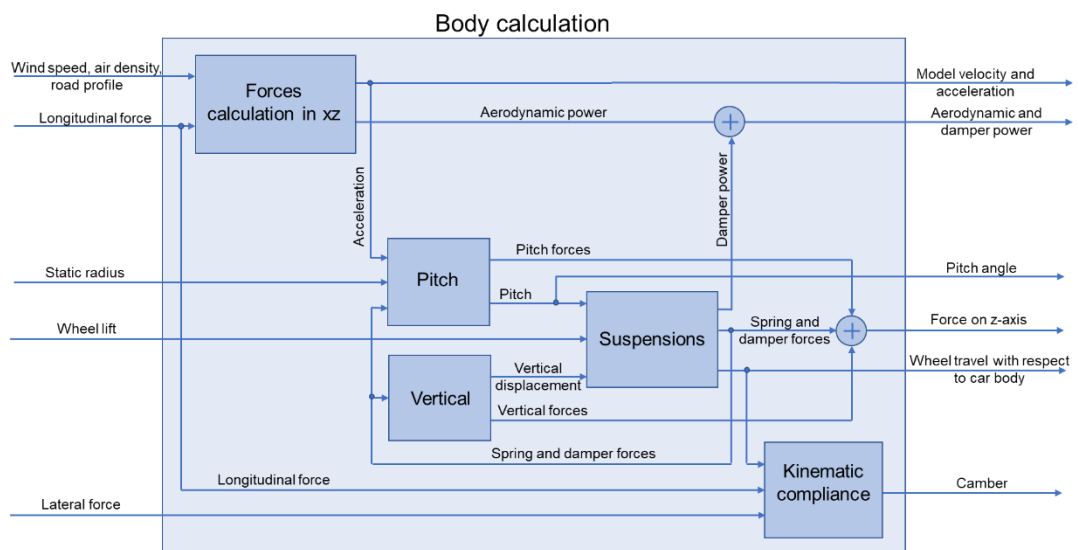


Figure 3.5: Body calculation structure

The pitch block, still present since it works on longitudinal dynamic only, balances the rotation of the vehicle around the pitch center, whose position has been evaluated in the initialization (Figure 3.6).

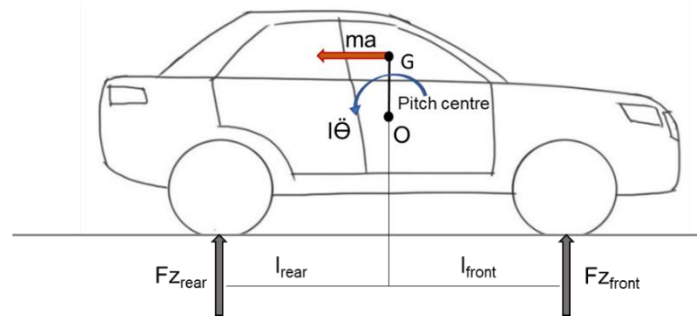


Figure 3.6: Rotation around pitch center

The forces and torques balance is described by the following formula:

$$2Fz_{front} \times l_{front} + 2Fz_{rear} \times l_{rear} - ma \times OG = I\ddot{\theta}$$

The pitch angle ( $\theta$ ) is found by integrating the solution

$$\ddot{\theta} = \frac{2Fz_{front} \times l_{front} + 2Fz_{rear} \times l_{rear} - ma \times OG}{I}$$

which, in case of single track model becomes:

$$\ddot{\theta} = \frac{Fz_{front} \times l_{front} + Fz_{rear} \times l_{rear} - \frac{1}{2}ma \times OG}{\frac{1}{2}I}$$

Mass ( $m$ ) and inertia ( $I$ ) are halved since force on z-axis now refers to only one axle.

The “Vertical” block contains the equation describing forces exchanged on z-axis between the chassis and the wheel. The wheel travel is obtained with the integration of wheel acceleration, gathered from the formerly mentioned equation. “Suspension” subsystem uses the output of the previous blocks to evaluate the dynamics of the geometry, travel and forces. In “Kinematic compliance”, the camber of the tires is calculated by means of polynomial evaluation. Lastly, the “Forces calculation in xz-axis” system contains the driving dynamic calculation (Figure 3.7) [22, pp. 185-188].

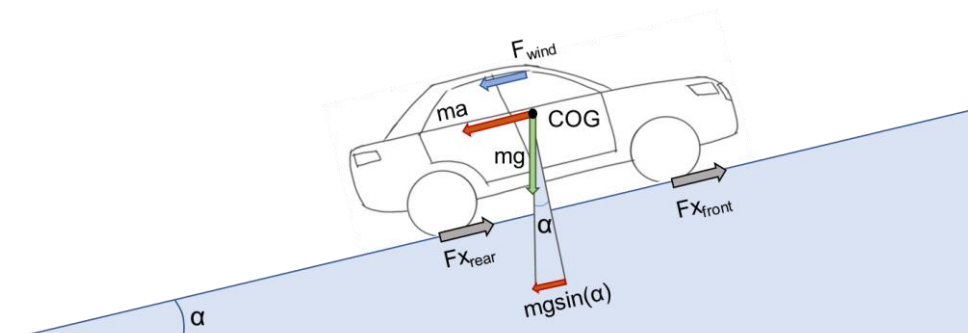


Figure 3.7: Driving dynamic calculation

The balance can be described by the following equation:

$$ma + 2Fx_{front} + 2Fx_{rear} - mg \sin \alpha - F_{wind} = 0$$

The acceleration in case of single track model becomes:

$$a = \frac{F_{x_{front}} + F_{x_{rear}} - \frac{1}{2}mg \sin \alpha - \frac{1}{2}F_{wind}}{\frac{1}{2}m}$$

Where both the mass (m) and the aerodynamic force ( $F_{wind}$ ) have been halved since the vertical forces have been reduced. The road inclination angle ( $\alpha$ ) is obtained through the road altitude variation over space.

The rest of the modifications which have not been quoted in the description are minor ones, required to adapt the operation of the monotrack model to the rest of the simulation. All of them are mentioned in the Table 3.2. Additional subsystems have been created to duplicate the outputs and mimic the ones of a double track model.

Table 3.2: Modification to vehicle model

Subsystem	Location	Modifications
Delta (steering angle)	Tire model	Removed since absent in new configuration
Beta (side slip angle)	Tire model	Removed since negligible in new configuration
Phi (roll angle)	Body calculation	Removed since negligible in new configuration
Z_wheel_body	Tire calculation	Removed since not needed in the new configuration
V <sub>x</sub> and V <sub>y</sub>	Tire calculation	Substituted with general Velocity
Aligning torque vars	Tire calculation	Removed since not needed in the new configuration
Friction save	Tire calculation	Removed since not needed in old configuration too
M <sub>antr</sub> and M <sub>bremse</sub>	Tire calculation	Averaged between left and right
V <sub>0_korr</sub>	Tire calculation	Modified to work with two wheels only
Calc_Fz	Tire calculation	Modified to work with two wheels only
Wheel_lift	Tire calculation	Modified to work with two wheels only
Road orientation	Body calculation	Removed roll angle influence
Body_chass_vert	Body calculation	Removed y-axis component and Mz
Aerodynamic	Forces calculation	Removed y and z components
Forces calculation	Body calculation	Removed y-axis components
Roll	Body calculation	Removed since not needed
Spring and Damper	Suspension	Modified to work with two wheels only
Anti-Roll Bar (ARB)	Body calculation	Removed since not needed
Pitch	Body calculation	Modified to work with two wheels only
Vertical	Body calculation	Modified to work with two wheels only
Kinematic compliance	Body calculation	Modified to work with two wheels only

### 3.3 Results

After all the modifications applied to the simulation, the tool was run to evaluate the results and the effects on the consumption of the WLTP cycle. The Table 3.3 shows that, of the three optimizations, the most effective of which is the scope removal. The time for the simulation has been reduced to 542.35 seconds. The time required for the operation of Scopes and To Workspace blocks has been reduced as expected from the initial analysis, while the monotrack model improved the simulation time of almost 10 seconds more than forecasted. This extra time saved consists in a small self-time reduction, since the simplified model reduced the Simulink structure not only for the Pacejka tire model, but also for the body calculation, since most of the blocks used more twice, once per track, have been halved.

Table 3.3: Time reduction achievements

Status	Time reduction	Percentage
Starting conditions	720.73 s	100 %
Scopes removed	- 82.27 s	- 12.11 %
To Workspace commented	- 41.91 s	- 5.81 %
Single-track model	- 54,2 s	- 7.52 %

The profile report creator tool has been used a second time to analyze the new time distribution among functions and systems and to assess if the aims of time reduction and the expected values have been achieved (Figure 3.8).

Simplified model time analysis

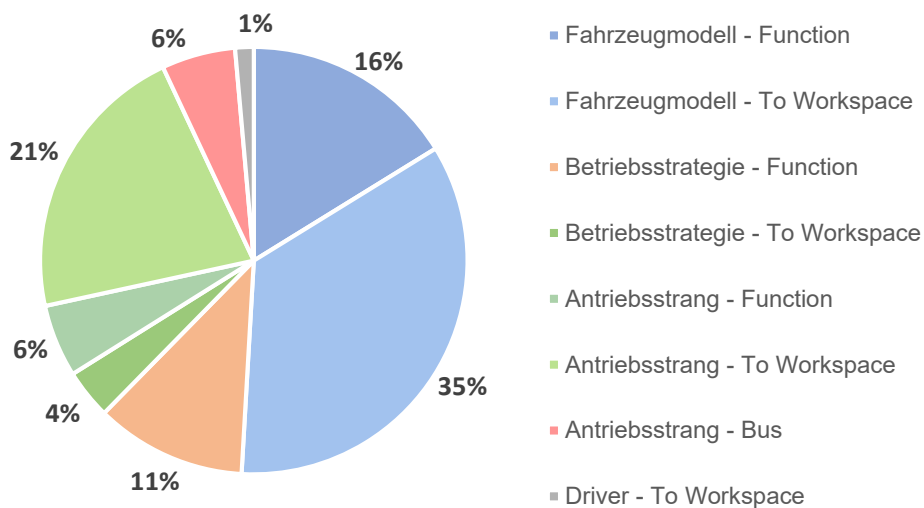


Figure 3.8: Time analysis after optimization

The analysis reports exactly the expected results. Scopes disappeared from the Profile report, To workspace have been reduced by a substantial percentage and vehicle model functions were reduced as well. The overall shortening of simulation time may induce in the reader the idea, created by comparing the pie chart prior to the time optimization, that time decrease due to the

vehicle functions contraction with the monotrack model is smaller than effectively, but it must be remembered that it is a cut down by 7.52 % of the original time. Only the proportion to the other functions remained approximately constant. The self-time seems to increase as well, but this is only an impression given by the reduction of all the other functions.

It is worth stating that the Profile report tool has not shown the level of precision required for a deep level optimization, since it has been created to investigate only the most relevant slow-downs of the model. The presence of the abundant percentage of selftime has set a limit to the study of time consuming systems and subsystem in the model. However, as confirmed by the Matlab support, this method is the most effecting without having to implement a new ad-hoc instrument, which would not be worth the time invested.

The result, which is slightly worse than the expectations, given by the imprecision of the above analyzed tool, is still significant if it is considered that the simulation now takes 25 % less time than before this operation. The future work which will be conducted on this model can now be achieved faster, allowing a more detailed research, since results are available significantly earlier.



# 4 Model improvements and optimizations

## 4.1 Efficient torque allocation strategy

Torque allocation is one of the great advantages of all-wheel drive vehicles since it permits to distribute the torque between front and rear axle according to the requirements. In case of performance requirements, for instance with an acceleration from low speed, torque is preventively distributed to the axle with more traction according to the wheel slip evaluation algorithm and corrected based on wheel speed variations. This allows to achieve much better performances than having a fixed split ratio, since the latter is not adapted according to the real conditions of the vehicle and of the road.

When efficiency requirements are analyzed instead, the strategy is different: the aim is to reduce as much as possible the electric consumption, by allocating the torque to a single axle, or a combination of both which present better efficiency in that given moment. As investigated in the state of the art (Chapter 2.3), the motor efficiency curves and power electronic efficiency are the key points for this decision.

In the TOTEM tool, allocation strategy has already been implemented, for both the requirements. The motor and torque limits are evaluated, based on vehicle conditions, such as speed, acceleration and steering angle, and the results are the inputs for the allocation strategy. Performance allocation works by evaluating the limit torque which could be transferred to each axle, without having a significant amount of slip. This algorithm has been implemented by Tobias Zuchtriegel in his semester thesis at TUM [43]. Efficiency allocation strategy has also been already implemented, but due to imprecision of the results it had to be profoundly modified. The prior design has been created by Tim Lübbers [44, pp. 20-29].

In the latter, the inputs necessary for the correct evaluation of the torque allocation are the limits of the tires and of the motors, the instantaneous radius and the angular speed of each wheel and the overall torque required to be applied to overcome aerodynamic and resistance forces and achieve the speed and acceleration demanded by the simulated maneuvers. The limit of the tires is evaluated through the maximum longitudinal and lateral potential forces, calculated by the Pacejka magic formulas in the tire model and, with the friction cycle formula [22, p. 118], the maximum potential force is obtained. The limits of the motors are, instead, the maximum torque that the motors are able to produce at a certain angular speed, given by the velocity of the vehicle itself and the transmission ratio. Those are evaluated with a look-up table, based on the motor characteristics [45, p. 42]. The wheel radius is calculated according to the tire vertical stiffness, a design parameter of the selected tire, and on the vertical force applied by the suspension. This value changes along the simulation, due to roll and pitch motion, road inclination and vertical components of the aerodynamic force, hence it is necessary to measure it in every instant and a constant value would be a too general approximation. The overall torque required by the model, evaluated in the Driver block (see chapter 2.1), is evaluated integrating the driving cycle speed to obtain the necessary acceleration, if it is not a user input itself. The force forecast to be

achieved is obtained balancing the traction forces, drag, resisting forces and inertia ones, and given the instant wheel radius the torque is trivially calculated. The minimum and maximum limits between tire and motor are set as the reference longitudinal limits.

The efficiency-based torque allocator is composed by seven main blocks, as visible in Figure 4.1 and Figure 4.6: The limit determination block, the vector creation, the engine torque calculation, the power evaluation, the torque allocation evaluation, the torque distribution, the gear selection and the torque variation limiter.

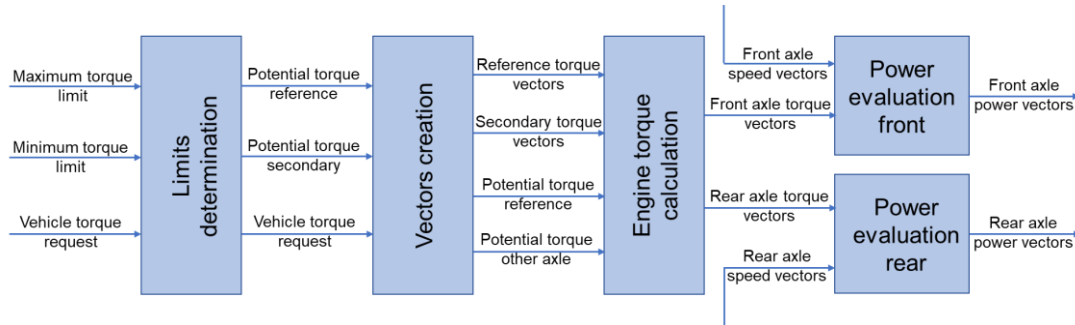


Figure 4.1: Power evaluation of the combinations

In the first block, the limit is chosen according to the phase of the cycle the model is simulating. For acceleration conditions the upper torque limit is chosen, since the model could not be able to provide the required torque to achieve the desired acceleration or the tires could slip, hence not being able to transmit the potential force to the ground. For braking conditions instead, the lower limit is selected, since the model could lock the wheels, not slowing down the vehicle sufficiently, or the maximum motor negative torque could be reached. In this case, the risk of not having enough negative torque to reduce the speed is not encountered because the brakes take care of the extra torque required. Moreover, driving cycles never present strong deceleration which undermine the braking system, while the possibility that the user's motor settings are not adequate to the cycle is more probable.

Once the limit for each axle is chosen, the front and rear are compared to select the reference axle for the future evaluations. The axle with the minor limit is selected, and the torque value for the reference axle is chosen as the minimum between the overall torque requirement and the torque limit itself. If this axle is potentially able to provide all the torque required by the maneuver in a given moment, the choice of making the other axle deliver part of it will only be a decision based on vehicle efficiency. If not, the other axle will be in charge of supporting the reference one by providing the remaining torque necessary to satisfy the request. Additionally, in the same block, the torque request is limited to the maximum capability of the front and rear motors combined, so that future evaluation is based on actual vehicle capabilities only.

In the second block, the possible combination of torque split between front and rear axle are evaluated. The torque values of the reference axle are divided in a hundred possible figures, from zero the entire value, with evenly spaced intervals. Every torque number is then subtracted from the total torque requirement to evaluate the torque allocated to the secondary axle. What is so obtained are a hundred possible combinations of torque front to rear which still satisfy the overall torque demand.

Figure 4.2 represents a section of the operation of the torque allocator for a configuration with front engine significantly more capable of the rear. It is clearly visible how the reference motor (the rear) comes to its limit in terms of torque and the front compensates it.

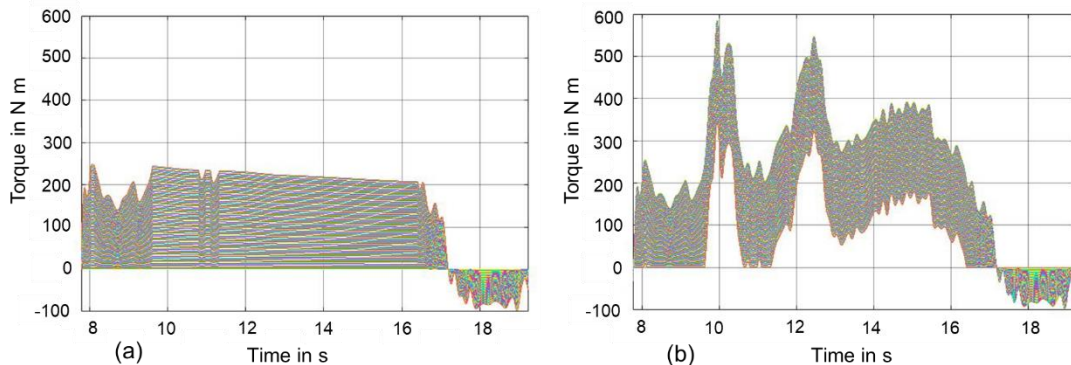


Figure 4.2: Torque combination. (a) reference axle torque, (b) secondary axle torque

The reason of choosing the axle with smallest capability as the reference is here explained. In case of a reference axle with capabilities above the other axle, the subtraction of the combinations from the general torque demand would create a situation in which the motor is not able to provide the torque requested. Figure 4.3 illustrates now the case in which, with the same configuration as the one described above, there is no selection of a reference motor. The torque allocation configurations are, for more than half, not feasible due to rear torque limit.

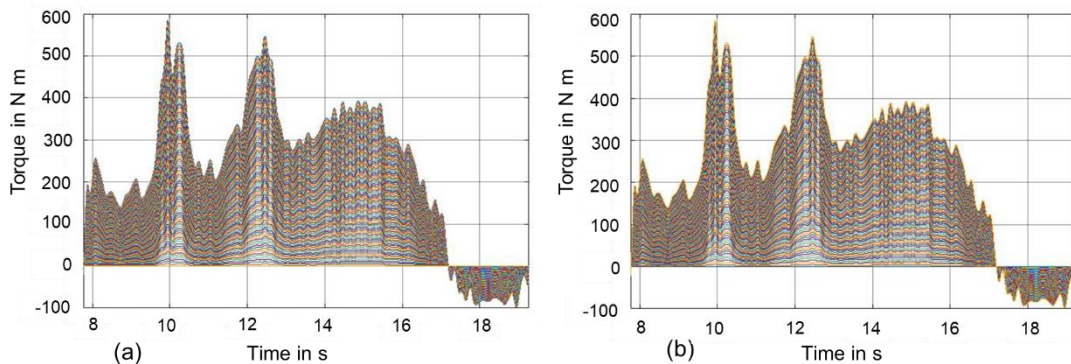


Figure 4.3: Torque allocator without reference axle. (a) Rear, (b) Front

In the following block, the engine torque calculation, the effect of gearbox efficiency is considered. To deliver the required torque to the wheels, the previously evaluated values must take into account the efficiency, so that the motor torque is the sum of the torque delivered to the wheels and the losses which will occur in the drivetrain, such as gearboxes and differentials. The efficiency value adopted is the constant figure later used in the powertrain and wheel torque distribution block for the final evaluation of transmitted power. In addition, the wheel torque is converted to motor torque, according to the transmission ratio of the selected gear.

Once the possible torque combinations have been evaluated for a given time instant, the expected electrical power consumption can be evaluated for both front and rear axle. The first step is to find whether the torque comes from a central motor or near motor configuration. In case of a near wheel motor configuration, the torque is halved and the power is evaluated for only for one wheel, since each side has its own dedicated motor and power electronic, as described in the semester thesis by Frederik Seeger [46, pp. 3-4]. After this assumption has been made, the electric power requirements of the motors are investigated.

The efficiency is obtained through a 2-D Look-up table, which relates the torque and angular speed of the motor to its efficiency. According to the torque sign, positive for traction and negative for braking, different tables are used. Those have been research object of Horlbeck [47] and Eroglu [16].

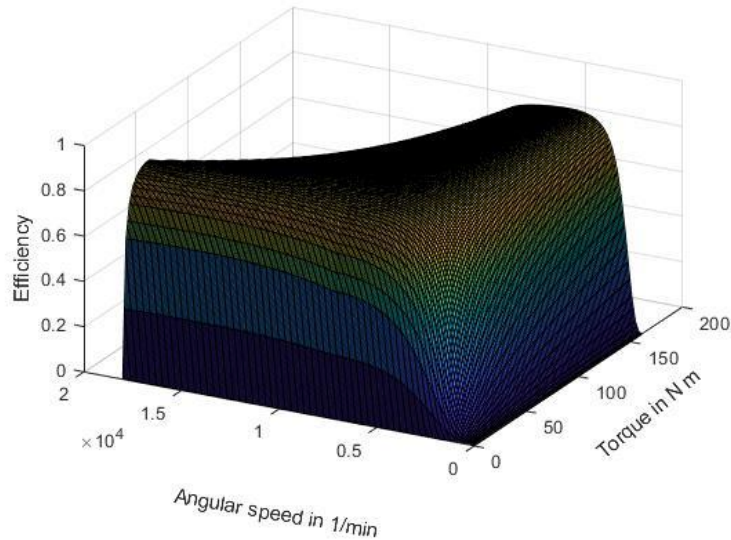


Figure 4.4: Efficiency curve for electric motors

The mechanical power is obtained multiplying the angular speed, equal for all the torque configurations, with the latter. Using the following formula, the electric power entering or exiting the motor is evaluated:

$$P_{out} = \eta_{motor} P_{in}$$

In case of positive torque, the electric power entering the motor is going to be higher than the mechanical output, since efficiency range is always between 0 and 1. For negative torque entering the motor, the electric output is going to be smaller than the mechanical input for the same reasons listed above.

For the evaluation of the power electronic efficiency no difference is stated between the use of the electric machine as a motor or as a generator. Its value is obtained through a 3-D lookup table, whose inputs are the voltage, the current and the power factor. The voltage is considered as constant since the variation with respect to the overall value is mostly negligible. The current is evaluated starting from the electric power to be delivered to the motor and the power factor, which is acquired through a 2-D lookup table, based on motor torque and its angular speed.

With the same method described for the motor, the electric power entering or exiting the device is evaluated. In case of electric energy provided by the battery, the value is lowered due to the efficiency of the power electronics. For energy produced by the electric machine, operating as a generator, the net amount delivered to charge the battery is lowered by the losses of the electronics. The final output is doubled in case of near wheel motors. As explained above, the power analysis has been conducted for one side only in the evaluation of this motor configuration. The Figure 4.5 summarizes the previous steps necessary for the evaluation of the electric power entering or exiting the battery.

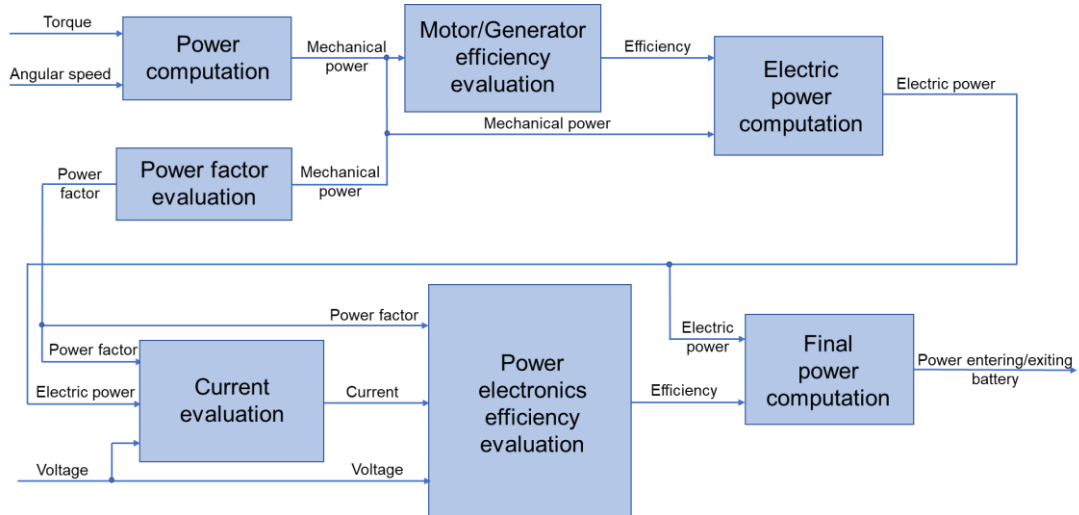


Figure 4.5: Electric power evaluation diagram

The process last described is used for the evaluation of both the front and rear axle power combinations, but this procedure is not sufficient alone to determine the suggested torque allocation which would provide the best efficiency among all the previously determined. In order to achieve so, a subdivision must be done, between 2WD vehicles and 4WD ones (Figure 4.6).

In case of 2WD vehicles a decision has still to be accomplished. The model, in fact, is capable of simulating front-, rear- and all-wheel drive models which are equipped with one or two speeds gearboxes. This procedure is responsible of defining the most efficient gear to run in for a given instant of a selected driving cycle. Obviously, this operation only occurs with multiple gears configurations. To achieve it, the power outputs of both the gear ratios are compared and the gear which provides minimum power is chosen for traction conditions, while the maximum is selected for regenerative braking conditions. The output of this block are the gear selection and the optimum power.

If, instead, an all-wheel drive vehicle is simulated, the situation is more complex. A dedicated system has been designed to control the torque allocation changes (Torque allocation evaluation 4WD in Figure 4.6).

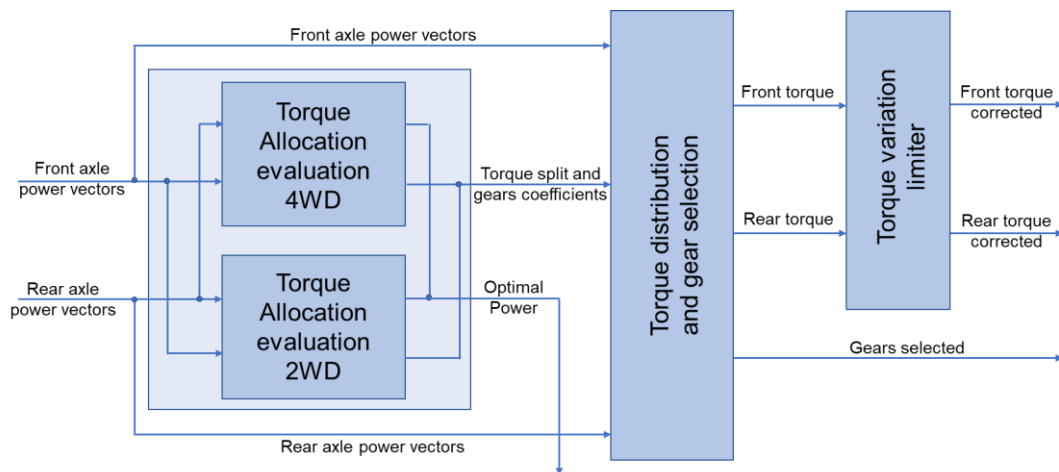


Figure 4.6: Torque allocation and distribution

Due to the similar consumption of front and rear axle, in case of model configuration with identical front and rear powertrain, the shifts between those two axles would be too frequent, to the point that the model wouldn't be stable anymore and the consumption would only increase, due to the power spent during the change of torque distribution. For this reason, the controller limits the changes according to some defined criteria:

- In any case, as for the 2WD controller, the minimum power is chosen for traction conditions and the maximum is selected when in regenerative braking conditions.
- If the new suggested allocation does not give an advantage in terms of power saved or recovered of at least 2.2% with respect to the previous allocation, the controller does not allow the change between the twos.
- If the suggested allocation changes with respect to the used one in less of 0.5 seconds, the controller does not allow the change until half a second has passed from the last torque allocation change.
- If the torque changes from positive to negative or vice versa, which would indicate a change of behavior from acceleration to deceleration or the opposite, the two limits set above are bypassed and the best torque allocation from the new condition is chosen.

These conditions are fundamental to guarantee the correct operation of the model. The value of minimum gain of 2.2% and 0.5 seconds have been found with a detailed analysis of the consumption in the WLTP cycle with identical front and rear configuration. The Figure 4.7 shows clearly the results of the ideal torque allocation with (in red) and without (in blue) the controller which limits the torque distribution changes.

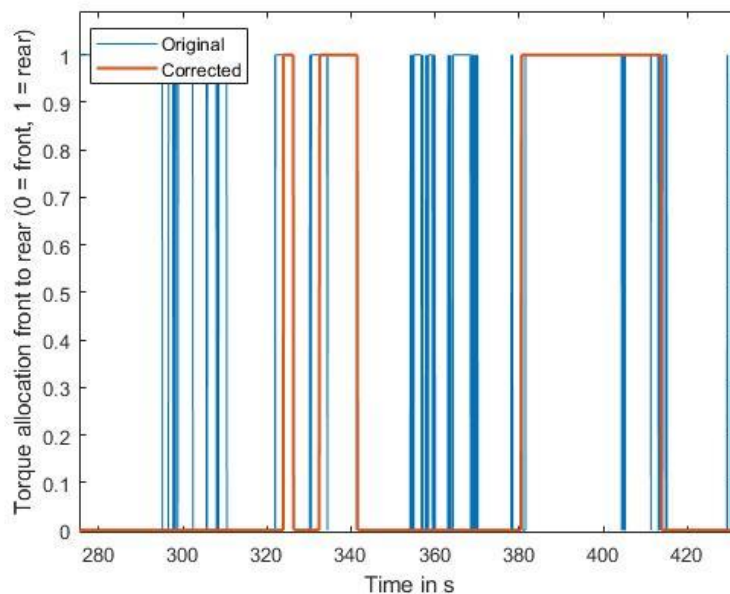


Figure 4.7: Effect of controller on torque distribution

Because of the time the model takes to pass from an allocation to the other, this change is not energy free. The torque figures have to pass through the allocations in between the new and the old one, where efficiency is lower, and extra energy is spent with respect to keeping the assigned torque distribution. Nevertheless, the minimum gain of saved energy is not enough to contrast this problem alone, since a too high value would cancel the advantages of having an efficient torque allocation algorithm, and a too low value would lead to instability in the tire model, as

experienced during the execution of the thesis. For this reason, a further limit, the maximum frequency of changes, has been introduced and its value has been fine tuned.

The defined torque allocation coefficient is then used in the “Torque distribution and gear selection” block to select the final torque to be transferred to both the axles. Between the several torque combinations earlier evaluated, the coefficient selects the correct one to transmit to the following block. Moreover, the correct gear ratio is set according to the selected gear to obtain the correct torque at the wheel.

The last block which handles the torque is the torque variation limiter. This system had to be implemented due to the high instability of the model when the torque allocation is changing. The rationale behind it is to limit the torque change to a given rate, still maintaining the overall torque value unaltered. This has been obtained by applying a rate limiter to each wheel torque, and evenly distributing the difference between the so obtained overall torque and the expected one to the four wheels. In case of the WLTP maneuver, the rate has been based on a realistic value obtained by the analysis of a restrained number of documents [48, p. 6, 49, p. 140]. The variability of this parameter with typologies of motors and their design and control does not justify the identification of a precise number, but to obtain realistic results from the model the correct order of magnitude is sufficient. For this reason, a reference response time of 20 ms has been selected. The response time is the time which passes between the input for the new torque and the achievement of the latter. From this value, the rate can be easily obtained knowing the gear ratio.

The operation of the torque limiter is clearly visible in Figure 4.8. A segment of a driving cycle has been selected to represent the shift between front to rear-wheel drive. The blue curves represent the original torque input, with immediate change, while the red curves represent the damped change in torque distribution.

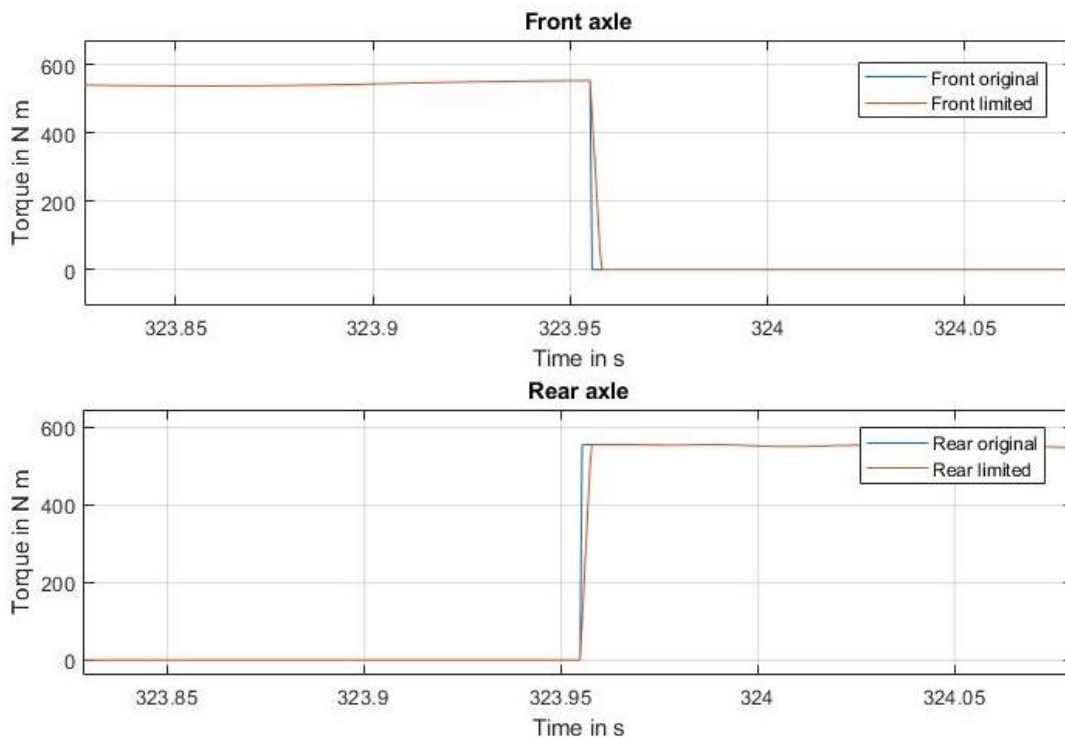


Figure 4.8: Torque limiter operation

### 4.1.1 Differences with the previous design and reason of changes

As it has been explained before, the efficient torque allocation system has been already implemented before, but due to incorrectness in operation it had to be restructured profoundly. The changes which have been implemented are listed below:

- The algorithm did not have any variable reference axle, but the front was always considered as reference. The downside of this logic is that for front motors less capable of the rears, the model is correctly creating the possible torque combinations, but when the configuration is inverted, as presented above in Figure 4.2, half of the combinations are not feasible due to the limit of the motors in deliverable torque, and so are eliminated. This unevenness between the two symmetric configurations leads to an unjustified difference in consumption. In addition, when an all-wheel drive configuration is simulated with a low power motor at the front and a significantly higher power on the rear axle, the elimination of more than half of the combinations leads to a significant loss of precision in evaluating the most efficient allocation. Both the problems have been solved with the creation of a reference axle.
- In the engine torque calculation block, the gearbox and differential variable efficiency prediction has been eliminated since the forecasted torque losses were not realistic and a constant efficiency value has given better results.
- The power evaluation logic has been completely renewed. The former rationale was based on the evaluation of the losses, which was not as accurate both for the implementation and for the logic. The evaluation of the required or provided power for all the combinations gives the possibility to directly compare the forecast with the real energetic demand and directly links the evaluation to the consumption, avoiding possible unexpected external factors influencing the consumption.

Together with the addition of the torque limiter and the allocation controllers, the obtained system works properly. The Figure 4.9 illustrates a representative section of a driving cycle where it is clearly visible the small difference in predicted and real power delivered by the battery, mainly caused by the drivetrain losses which are not forecasted.

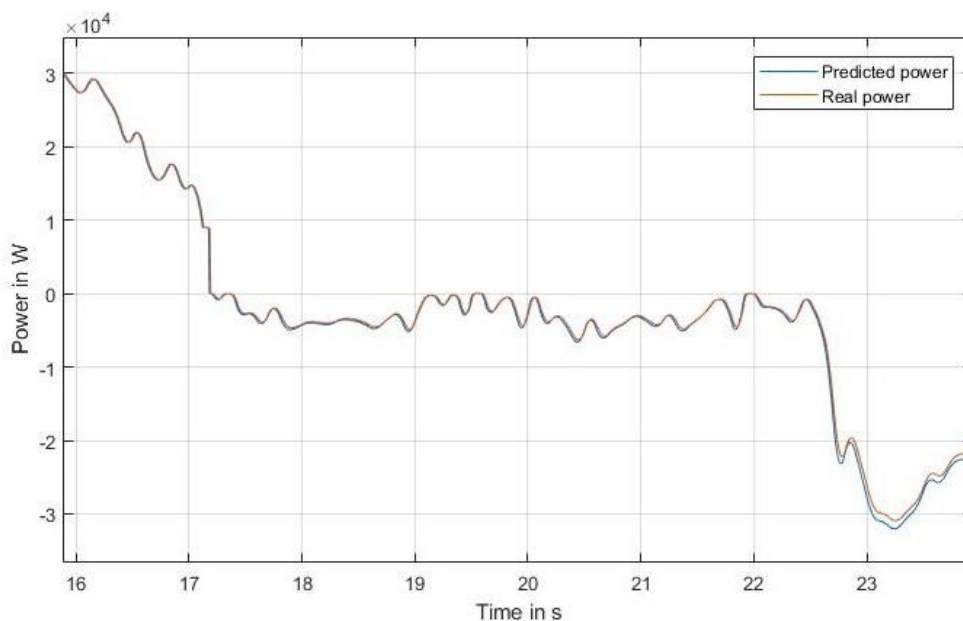


Figure 4.9: Results of power prediction

## 4.2 Powertrain and drivetrain efficiency calculation

The TOTEM tool, as described in the overview (Chapter 2.1.1), has the great advantage of being able to simulate a variety of configurations, for motor layout, motor typology, gearboxes and differentials. An important feature given by this instrument is the possibility to analyze the efficiencies of all the components in a given instant. This feature has been implemented by Frederick Seeger during his semester thesis [46, pp. 53-68]. The efficiency of the power electronics, as described in the previous chapter, is evaluated through a 3-D lookup table, while for the motor one a 2-D lookup table has been used. For the gearbox, instead, a constant value based on the selected gear is considered, while for the differential the efficiency is calculated based on lookup tables which consider the torque transmitted, for the open differential, or simply with the ratio between the input and output power, for torque splitter and eTV.

However, a further system has been implemented to evaluate the efficiency of the powertrain and drivetrain at the front axle, rear axle and overall vehicle. The entire values not only give an idea of how much energy is lost in converting the electric energy delivered by the battery into mechanical energy able to propel the vehicle, but it also shows how this changes through the cycle.

To evaluate the correct efficiency, the order of the components must be considered. The efficiency of a series of components is given by:

$$\eta_{series} = \eta_1 + \eta_2$$

Where  $\eta_1$  and  $\eta_2$  are the efficiencies of the components in series [50, p. 7]. For parallel components instead, the total efficiency is:

$$\eta_{parallel} = \frac{\eta_1 P_1 + \eta_2 P_2}{P_1 + P_2}$$

Where  $\eta_1$  and  $\eta_2$  are the efficiencies of the components in parallel and  $P_1$  and  $P_2$  are the powers transmitted through those [50, p. 8].

The Figure 4.10 highlights how the combination of components can be in series and in parallel inside the vehicle.

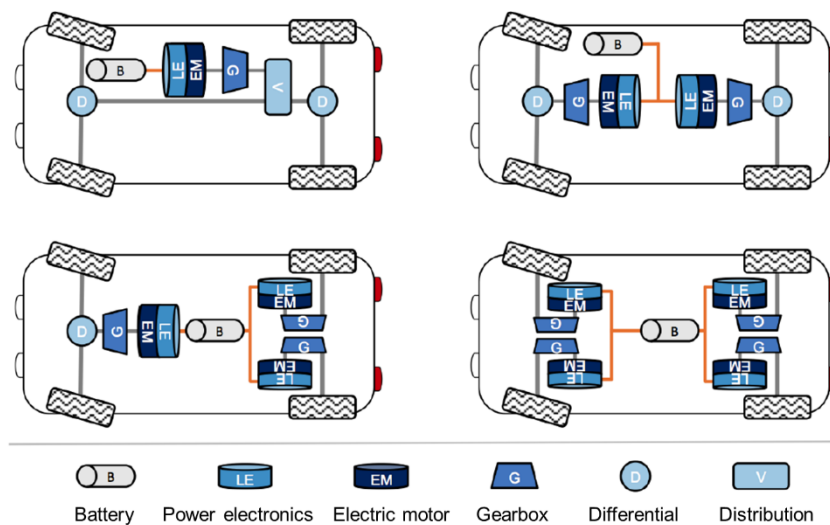


Figure 4.10: Possible powertrain and drivetrain layout configurations [46, p. 4]

The Figure 4.11 illustrates the diagram used for the evaluation of front, rear and overall vehicle efficiency. As clearly visible, the near wheel motor configuration does not necessitate of a differential, but the efficiency is individually evaluated for left and right side of the axle, and then both the systems are considered in parallel to calculate axle efficiency. For central motor instead, all the components are connected in series. In case of all-wheel drive configuration, front and rear are considered in parallel to obtain the overall vehicle efficiency.

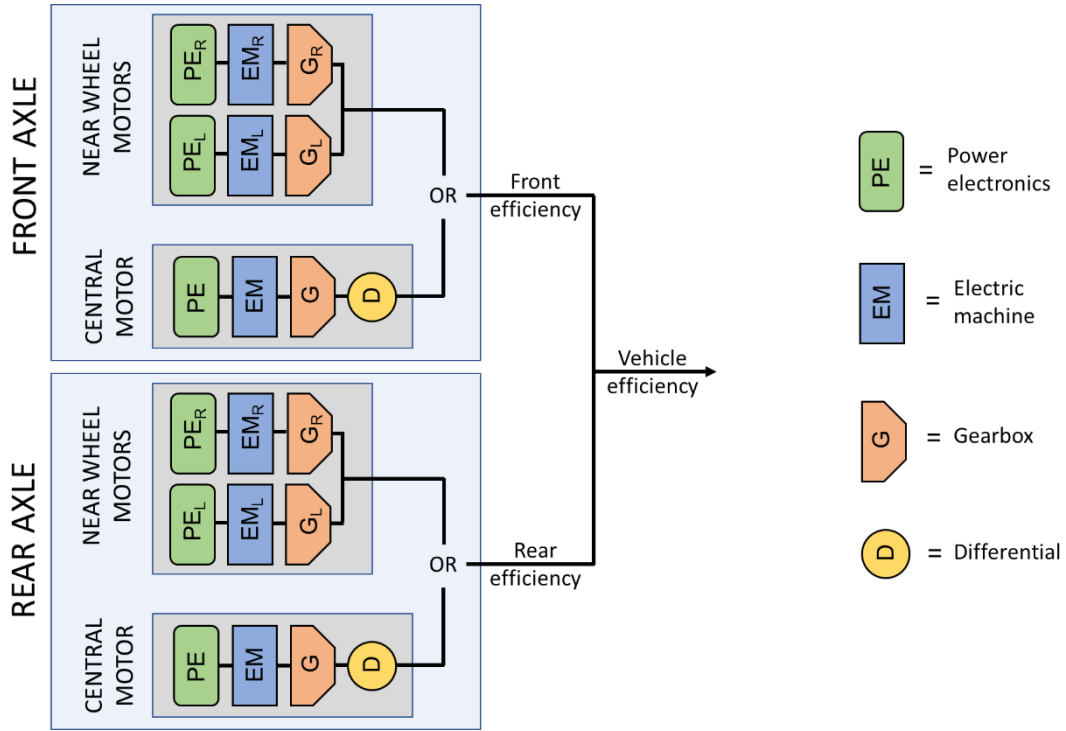


Figure 4.11: Layout of components for the efficiency calculation

# 5 Validation

## 5.1 Strategy and cycle parameters definition

### 5.1.1 Validation cycle creation

The model is now complete and correctly functioning, but this must be proven through a proper confirmation procedure. Despite most of the components have already been verified by the former students and research associates in their theses and publications, the validation of the those does not necessary imply the validation of the entire model [51, p. 4].

As E.A. MacNair, K.J. Musselman, P. Heidelberger reported, "Model validation is performed by comparing model behavior with system behavior when both model and system are driven under identical input conditions" [52, p. 67]. The methods for validating the simulations are several, among which two have been used: The first is the graphical comparison, which is an heuristic approach which contemplates the observation of the values of the same variable over time from both the model and the studied system, and analyses the differences in trends, similarities and other variations [53, p. 140]. The seconds consists in a sensitivity analysis, which contemplates a change in the input parameters of the simulation, with a scientific method, to study the influence on the results. If unexpected behaviors emerge, it might be a sign of incorrectness of the model [52, p. 69].

To validate the model with the first approach, a certain driving cycle must be simulated both from a real electric vehicle, possibly with all-wheel drive layout to ensure reliability of the successive comparison, and from the model created on Matlab/Simulink in the TOTEM tool. Due to the impossibility of creating a driving cycle and simulating it on a dynamometer bench, because of the unavailability of the resources in the short term, it has been decided to use the data recorded by Andreas Holtz, a former master student at the Technische Universität München (TUM), during his research for the master thesis [54].

Holtz simulated a series of maneuvers with a Tesla Model S 85D, one of the few fully electric all-wheel drive vehicle available on the market, and data were recorded with the data management system integrated in the Tesla and a GPS tracker. Additional records of the journey to and from the proving ground, mostly composed by country roads and highway, have been saved and documented as well. Those, despite being divided in segments of about eight minutes on average, are a reliable and precious source for a custom cycle to validate the model.

Among the portions, the most representative one has been chosen (Figure 5.1). Its duration is higher than the average (approximately 470 seconds) and the speed range is the widest and most significant (from almost still to 90 km/h). An attempt to create a combined cycle, merging the segments recorded, has been done but, due to the time intervals presents between the data sets, a longer reliable cycle was impossible to obtain, and the authenticity of the existing ones has been preferred to the major duration and range of a combined cycle. That said, the model still necessitated to be prepared to be simulated. From data recorded a tool was designed to evaluate the inputs necessary to run the validation.

The first operation has been to filter the data collected and to create a speed profile curve, the main input, with the same timestep as the one used by the model, which is  $5 \cdot 10^{-4}$  seconds. The timestep is the time which passes before a new input is delivered to the model. The data has been instead recorded with a frequency of 100 Hz, which translates into a timestep of a 0.01 second. Moreover, the original records presented a significant amount of noise, especially in speed and acceleration records. To solve this inconvenient, all data were averaged in time sections of 0.1 s. Subsequently, with the spline function, a curve with the desired timestep has been obtained. This function interpolates in a given time interval, in this case the complete cycle duration, a given set of points, the averaged speed values, so that the newly created function is continuous up to a certain derivative order [55]. The same treatment has been necessary for the altitude input (Figure 5.2).

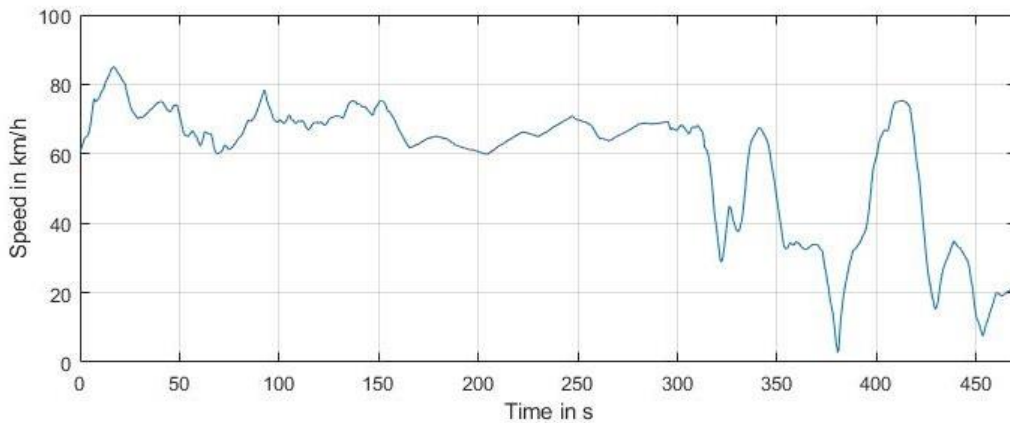


Figure 5.1: Validation cycle speed profile

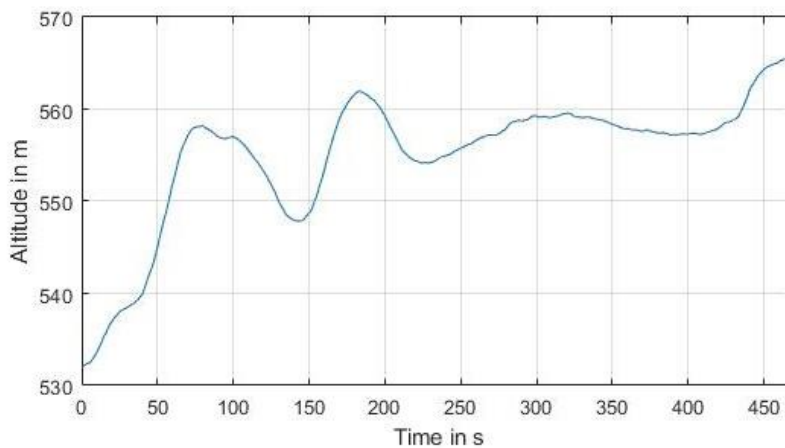


Figure 5.2: Altitude profile

Figure 5.3 shows the magnification of a part of the cycle where the difference between the original cycles and the ones created for validation is clearly visible. The more evenly distributed speed curve is necessary for a smooth operation of the model during the simulation for validation.

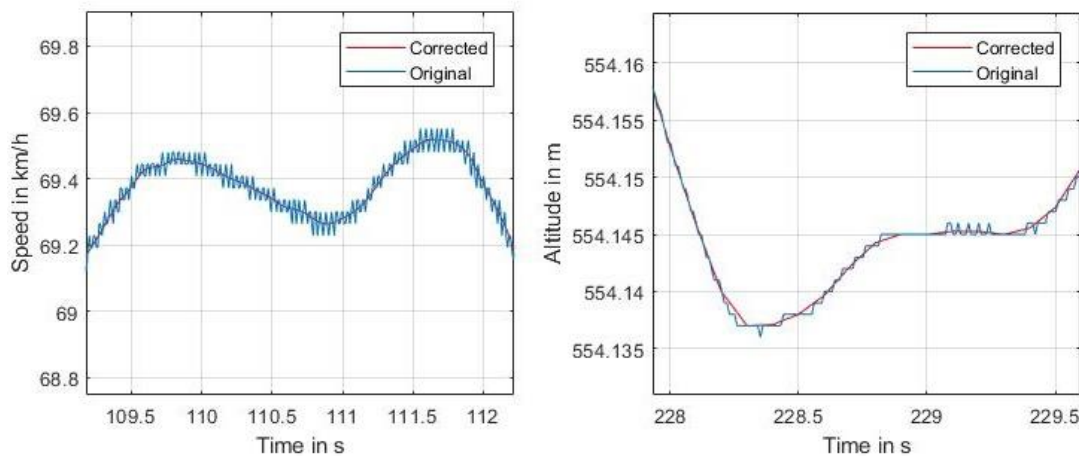


Figure 5.3 Speed and altitude profile magnification

The second input required from the model is used to evaluate the road inclination and it is the altitude above sea level of the four wheels of the vehicle. To obtain this value, since the vehicle altitude was present in the recorded data, the average height of two intervals, preceding and consecutive the analyzed point, has been evaluated (Figure 5.4). The width of those intervals is the same as the one used to evaluate the vehicle altitude, but the intervals are shifted of half the length. Once the average altitudes ( $h_{avg1}$  and  $h_{avg2}$  in Figure 5.4) have been evaluated, the difference between the two ( $\Delta h$ ) was calculated and, knowing the distance covered between the two instants ( $d$ ), the road inclination angle ( $\alpha$ ) obtained with the following formula:

$$\alpha = \tan^{-1} \frac{\Delta h}{d}$$

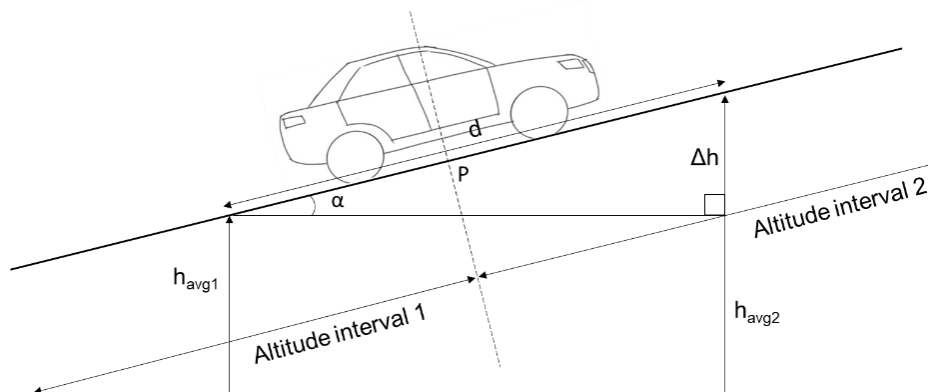


Figure 5.4: Road inclination angle evaluation

With the value so gathered, one more passage has been necessary to find the height of the wheels (Figure 5.5). Knowing front and rear wheelbases ( $l_{front}$  and  $l_{rear}$ ), with respect of the center of gravity (COG), the evaluation of the relative altitude variation ( $\Delta h_{front}$  and  $\Delta h_{rear}$ ) has been obtained through the sine evaluation:

$$\Delta h_i = \sin l_i$$

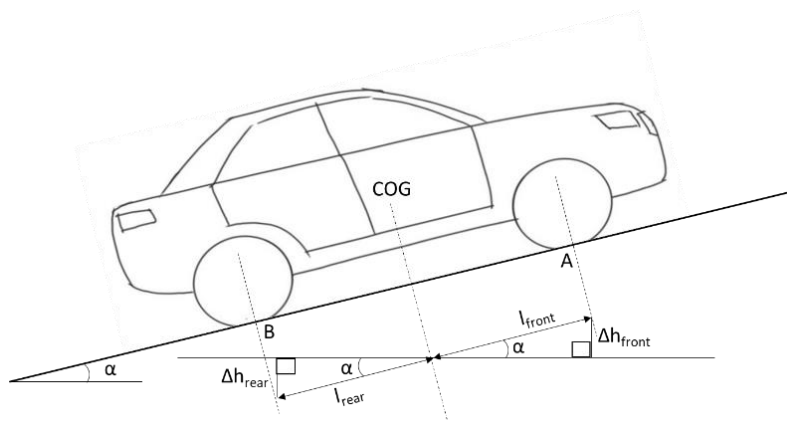


Figure 5.5: Wheel altitude calculation

The wheelbase variation with suspension travel has been neglected, since the order of magnitude is significantly smaller and would imperceptibly affect it. The wheel altitude has been then evaluated adding the so found values of altitude variation to the vehicle altitude expressed with the height profile curve (Figure 5.6). As expected the front wheels have higher altitude when the latter increases while the rears are positioned lower. This behavior is inverted when the inclination changes. Moreover, the steeper the road, the higher is the difference in altitude.

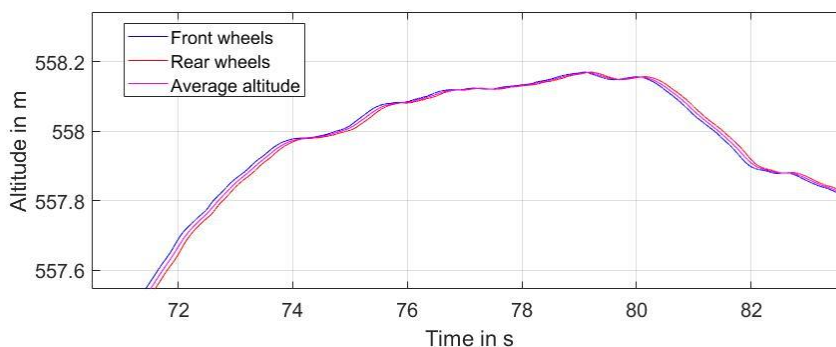


Figure 5.6: Altitude variation for front and rear axes

### 5.1.2 Motor parameters definition

Once the cycle has been created, the remaining inputs for the validation to be found were the exact motor parameters to input to correctly reproduce the Tesla Model S in the model. The Model S 85D has all-wheel drive with central motors and open differential: in fact, D stands for Dual motors [56]. They are asynchronous induction motors, but its specifications are not available to the general public, apart from the maximum angular speed of 18000 1/min. The gearbox consists in a single gear speed reduction system with an overall ratio of 9.34.

In order to obtain the nominal torque and speed of the motor, a tool has been created to simulate several power configurations and compare those with the data available from tests performed on the real vehicle. As documented in Andreas Holtz’s master thesis [54, p. 16], various acceleration tests have been conducted with two passengers and with full homologated weight. The data gathered from those experiments included the wheel torque and angular speed, which being at full load, can be assumed to mostly resemble the original shape and values of the maximum torque curve. Throttle position and acceleration was also analyzed to verify the former statement. The extracted information is provided by the vehicle CAN (Controlled Area Network)

and, while angular speed is measured by sensors, torque is obtained considering the working conditions, so a level of uncertainty is to be expected in the output.

Nevertheless, curves obtained by acceleration tests were not sufficient, since the test has been interrupted before the high-speed sections were reached. So, a section of the free highway driving in which full load conditions occurred has also been used. The change of the conditions, test after test, due to heating of the drivetrain and electrical components, is the explanation of the shift of the results, clearly visible in Figure 5.7

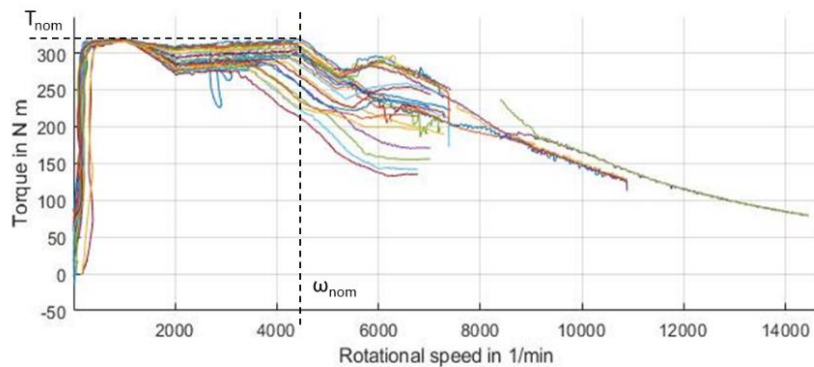


Figure 5.7: Torque data from Tesla Model S

As mentioned in Holtz's documentation [54, p. 43], from the results it was possible to identify the values of the nominal torque ( $T_{nom}$ ) and speed ( $\omega_{nom}$ ). The nominal torque is the theoretically constant value that is obtained at full load from zero to the nominal speed, which is the value starting from which the curve assumes a hyperbolic descending behavior. However, the figures so obtained (320 N m and 4300 1/min) did not provide the input data for the simulation. Asynchronous induction motors can be overloaded for a short period of time to achieve better performances, still maintaining the same nominal speed. This procedure consists in delivering a higher voltage than the nominal, causing higher current to flow and higher torque to be produced [57, p. 19]. For this reason, setting as input the obtained results would have created a model much more capable than the reference vehicle, falsifying the outputs.

To obtain realistic consumption and performance capabilities, the curve that better matches the Tesla one has been investigated. As described above, the reference nominal speed found could be safely assumed as a starting point for this study. This allowed the simulation of several nominal torques with an interval of 1 N m from 100 N m to 300 N m (Figure 5.8).

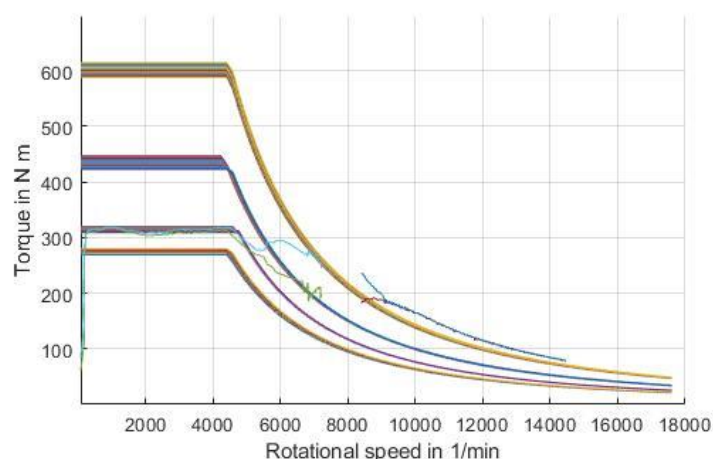


Figure 5.8: Torque curves result based on nominal speed

As clearly visible in Figure 5.8, there is no curve which closely matches the real one of the Model S. The reason can be found in the operational logic of the initialization tool, which creates the torque and efficiency maps for the desired parameters (See Chapter 2.1). The tool is based on virtual design of the motor, whose dimensioning is done through an algorithm which operates in steps and not linearly, and the obtained motor model is then electrically and thermally tested to obtain the torque curves which reflect these characteristics. Nevertheless, the overload ratio varies according to the design, and is not exactly proportional to the nominal value.

To find a curve which best matched the Model S curve, the so created tool has been modified to simulate a range of combinations between 100 and 200 N m with 1 N m step and from 4000 1/min to 8000 1/min with 200 1/min step. The obtained curve closely matches the constant torque and the high-speed sections of the original. The values which has been obtained as inputs are 108 N m of nominal torque and 7000 1/min of nominal angular speed (Figure 5.9).

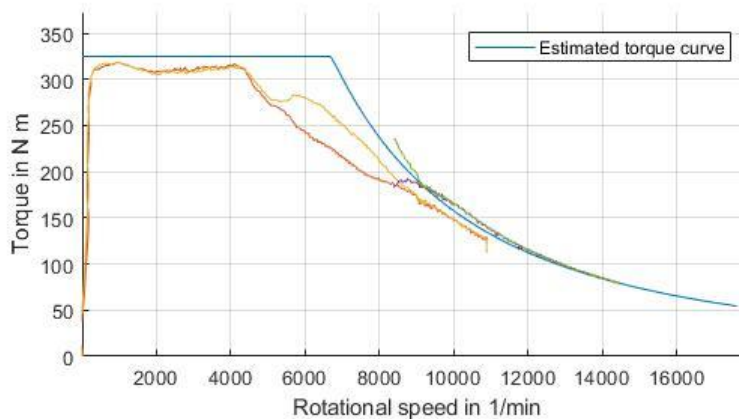


Figure 5.9: Estimated Tesla Model S torque curve

### 5.1.3 Validation criteria and validation tool development

Once the cycle has been created and all the input for the validation were present, the remaining step was to define a validation criterion. The variables to be compared have been defined and a tool for the analysis developed.

- The first parameter which has been compared between real and simulated results is the vehicle speed. This is necessary to verify that the model undergoes the same exact conditions of the real vehicle, so that also the rest of the outputs can be examined in contrast.
- The second had to be the acceleration of the vehicle. Also this one certifies that the model behavior is the expected one, moreover the inertia force ( $ma$ ) is necessary for the analysis of external forces and their influence, as explained in successive points.
- The third fundamental quantity is the axle torque. In both the model and vehicle cases it is measured in the drivetrain, as it exits the motor, before being amplified or reduced by the gearbox. Front and rear must be analyzed separately, since different torque distribution strategies are applied in the model, with respect to the Model S. This aspect is relevant for the consumption results since the torque allocation influences the efficiency of the whole drivetrain and power electronic system.

- Even the overall vehicle torque has been analyzed. This data indicates the mechanical force which is applied to the vehicle to achieve the desired speed and acceleration. It is required to assess the correctness of aerodynamic, resistant and friction forces.
- Engine angular speed is used not only to ensure the correct overall transmission ratio, considering gearbox, differential and wheels, but also, together with the torque, to evaluate the mechanical power provided by the motor.
- Additionally, the energy leaving and entering the battery, during acceleration or regenerative braking, is compared to evaluate the energetic demand and understand the efficiency of the power electronics. It is provided in form of battery voltage and entering current, but the power can be trivially calculated. The difference between the mechanical power provided by the motors and the electric energy at battery level gives an interpretation of the efficiency of the motors and the electronics combined.
- The distance is needed also, for the evaluation of the consumption and the difference between the real and simulated cycles. In fact, the data recorded in the Tesla Model S refers to free driving, which includes not only longitudinal driving, but also a certain number of turns and changes of direction which may have influenced the reliability of the records. The lower the difference between the twos, the higher is the probability that the information gathered on the real vehicles are safe to be used for validation.
- The power of driving losses, a derived variable from the previous ones is also relevant. It includes the aerodynamic drag, resistant forces, losses due to the efficiency of the power transfer through the tire, differential and gearbox. It is mathematically presented by the following formula, and the related forces are presented in Figure 5.10:

$$F_w + mg \sin \alpha + F_{loss,tire} + F_{loss,transmission} = (M_f + M_r)R_{wheel}\tau_{transmission} - ma$$

where  $P_w$  is the aerodynamic power,  $mg \sin \alpha$  represents the extra force needed due to road inclination,  $F_{losses}$  are the forces due to losses in gearbox and tire,  $M_i$  is the motor mechanical torque,  $R_{wheel}$  is the radius of the tire and  $\tau_{gearbox}$  is the overall transmission ratio of the gearbox and differential together.

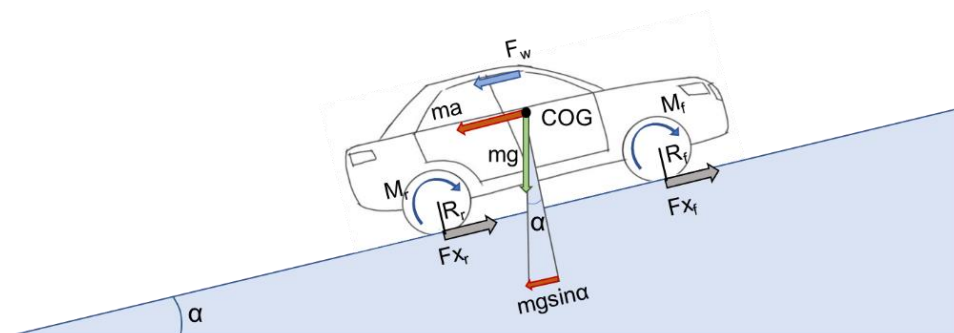


Figure 5.10: Driving losses and forces

The only value which has not been already presented but has been obtained by its average value through the simulation is the wheel radius, set to 0.301 m. This value is continuously changing, and the instant value could be retrieved from the simulation, however, for comparison purposes, a fixed value has been chosen since it was not possible to evaluate the precise amount in retrospect from the already obtained data of the Model S.

Once the parameters to analyze were chosen, the tool was built. To filter the signals from the noise present in the recorded data, the same method as described in chapter 5.1.1 has been

adopted. The signals were averaged in intervals of 0.2 second, a value chosen to eliminate the persistent oscillations in the acceleration variable, losing as little information as possible, giving the most readable and significant results.

To have a further input for the comparison, the average difference between all the previously mentioned parameters were computed taking the data from real and simulated cycle every 0.2 seconds.

### 5.1.4 Summary parameters and information on the vehicle

As previously said, the vehicle chosen for validation is a Model S, a 5-door hatchback car produced by Tesla since 2012. The model is available both in RWD and AWD configuration. Table 5.1 summarizes the input parameter for the validation and the correspondent in the Model S 85D.

Table 5.1: Summary validation parameters

Parameters	Tesla Model S 85D [54, pp. 51-52]	TOTEM simulation
<b>Electric Motor</b>		
• Number of motor	2	2
• Position	Central, Front / Rear	Central, Front / Rear
• Typology	ASM	ASM
• Configuration	AWD	AWD
• Maximum torque	658 N m	650 N m
• Maximum angular speed	18000 1/min	18000 1/min
<b>Gearbox</b>		
• Number of gears	1	1
• Gear ratio	9.34	9.34
<b>Differential</b>		
• Position	Front / Rear	Front / Rear
• Typology	Open differential	Open differential
<b>Tires</b>		
• Manufacturer	-	Bridgestone
• Model	-	Potenza RE050ARSC
• Dimensions	245/45 R19 102Y	215/45 R18 85Y

## 5.2 Validation result and analysis

The results of the validation show that the driver controller is capable of closely follow the speed input curve, with an average difference in speed of 0.0056%, which is small enough to be considered negligible (Figure 5.11). As expected, maximum difference can be found at a time of 381 seconds, where the speed is the slowest and the ratio between the difference and the overall speed is 3.62%. However, this difference is only 0.041 Km/h, thus not so relevant to influence the simulation and the validation.

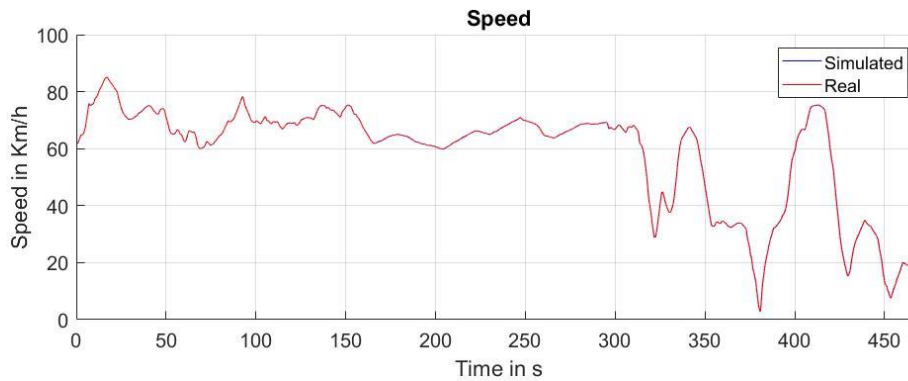


Figure 5.11: Speed result

The acceleration also shows an expected behavior (Figure 5.12). As predictable, its peaks are in the steepest parts of the speed plot when the acceleration and deceleration are higher.

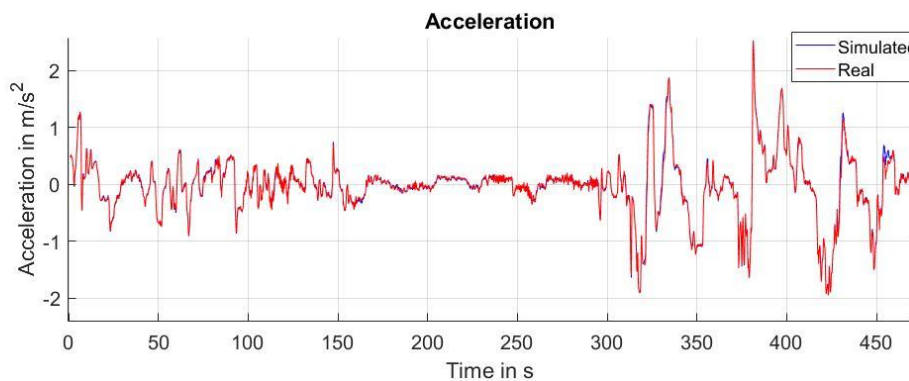


Figure 5.12: Acceleration results

This variable shows a more evident variation from the measured data. The average difference is 1.735%, which is not so relevant to represent a concern or have a major influence on the following analysis. A couple of time intervals have been analyzed for further investigation of the causes of divergency. In particular, between 455 and 460 seconds, a major difference is visible. The analysis of the simulated and real speed highlight that there is no variation and being the acceleration the derivative in time of speed, there cause can be attributed to an error in the recorded data, probably caused in postprocessing by the excessive noise present in the acceleration signal.

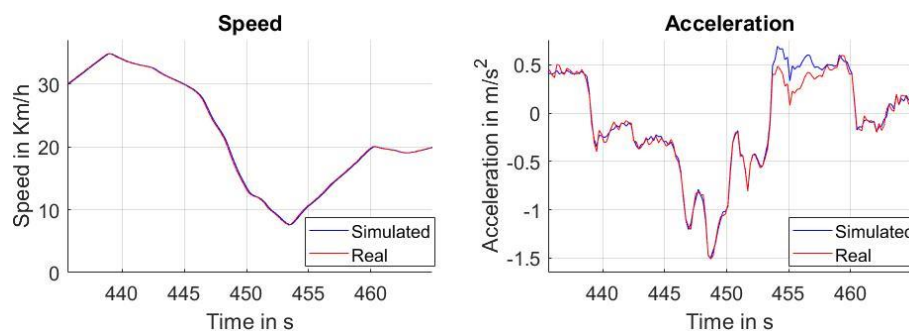


Figure 5.13: Speed and acceleration analysis of the relevant interval

Moreover, the difference of  $0.2 \text{ m/s}^2$  for an interval of 5 seconds only constitutes approximately 1.2% of the totality of the cycle, so its effect can be neglected. In any case this interval will be also monitored in the following analysis.

Analyzing the torque delivered by each axle (Figure 5.14), a different torque allocation strategy is clear. The Tesla Model S delivers mainly the torque to the rear wheels, and only requires both the axles for strong acceleration, for instance at 380 seconds or for long and severe deceleration, at 320 and 420 seconds in the cycle.

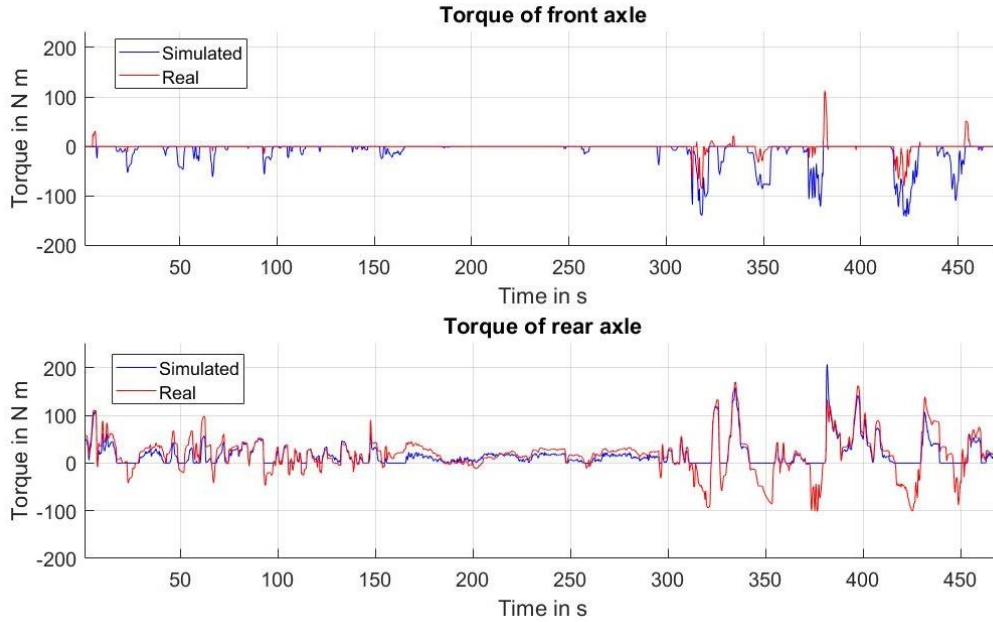


Figure 5.14: Torque delivered to front and rear axle

The model, instead, operates always with a single axle, preferring the front or the rear based on the driving conditions. The model, as in the reality, is more front heavy, hence the front wheels are more loaded than the rears (Figure 5.15). This remains true until the model undergoes acceleration: in this eventuality, the center of mass above the road level induces a pitch rotation which loads the rear axle more than the front, as visible at 320 seconds in the cycle. Due to this behavior the wheel radius is always smaller for front tires, since they are normally more compressed, aside from when the forces change due to the behavior described above.

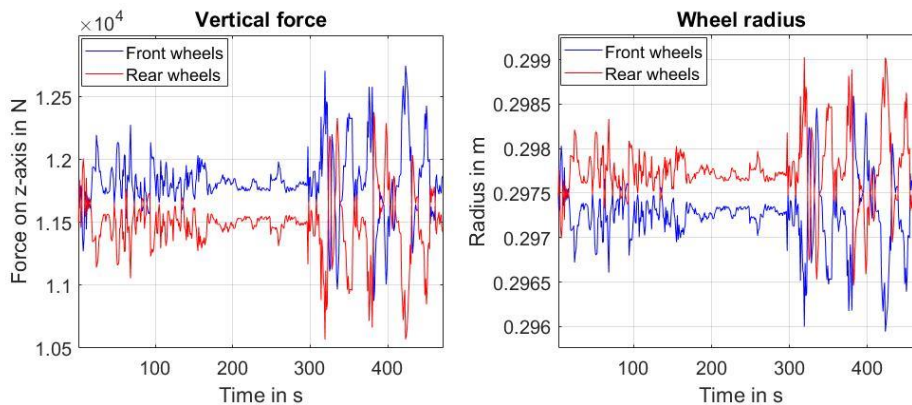


Figure 5.15: Vertical force and wheel radius of the simulation

Because of the change in torque radius, given a certain vehicle speed, the rear axle will rotate faster than the front under acceleration, since  $\omega = \frac{Velocity}{radius}$ . For this reason, the torque allocation controller will prefer the rear axle for acceleration and front for deceleration. As visible in Figure 5.16, the increase the angular speed brings an advantage in efficiency for the operating region of the validation cycle, highlighted by the red points on the efficiency map.

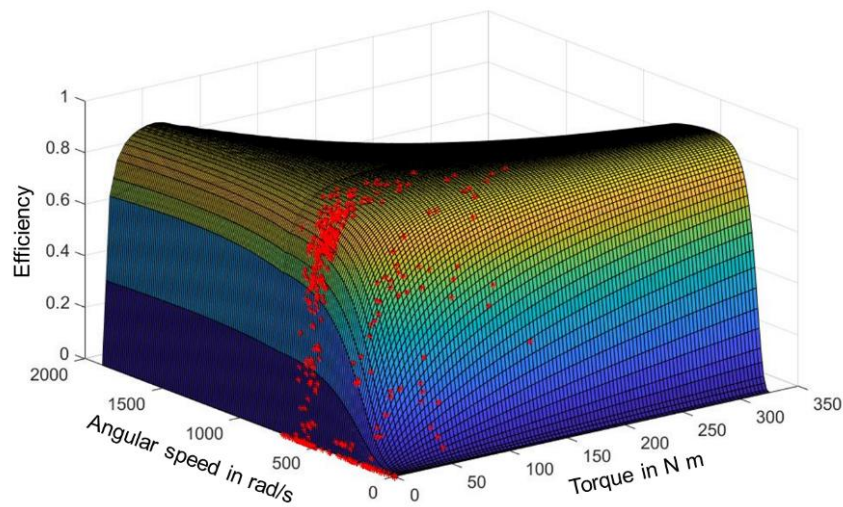


Figure 5.16: Motor efficiency map

The decision of the torque allocator to select one axle only and avoid an all-wheel drive allocation is justified by the efficiency map and the validation cycle. As visible in the picture above, the torque required barely gets to the high efficiency area of the motor, hence dividing it with a similar engine would only result in a lower overall efficiency. In case of less powerful and capable motors or harder acceleration or speed, the motor would get to the upper limits, where the efficiency drops, hence an all-wheel drive allocation would then be suggested to reduce the consumption. To prove it, the same model has been simulated on the WLTP cycle, which has similar torque demand compared to the validation driving cycle. The torque allocation value has been manually changed, bypassing the efficiency algorithm, to prove the correct forecast of the consumption in using only one axle at a time (Figure 5.17).

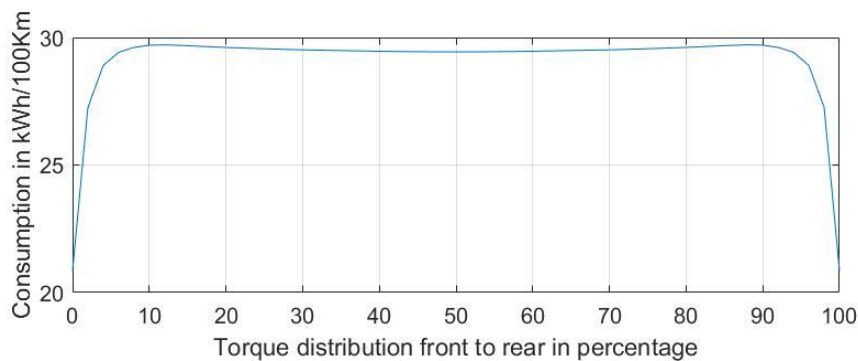


Figure 5.17: Consumption based on torque distribution

After stating the correct operation of the torque allocation, the overall torque can be analyzed (Figure 5.18). As stated in the previous chapter (5.1.3), this comparison is significant to analyze the losses and the forces acting on the vehicle.

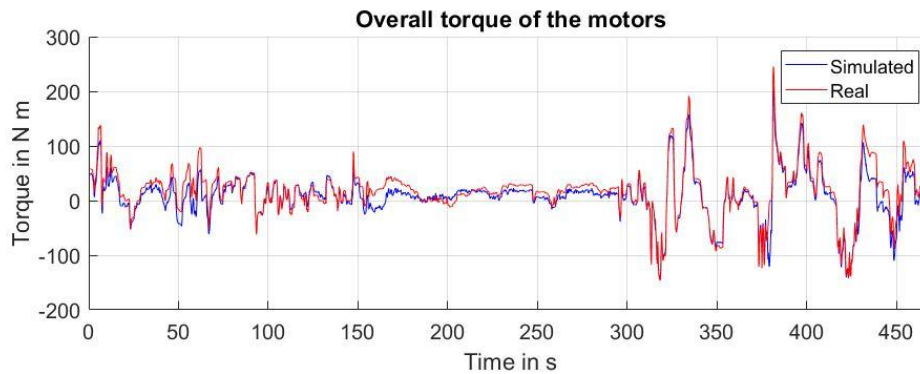


Figure 5.18: Overall torque

It is clearly visible that the simulated torque is mostly lower than the actual one. Several causes could explain this behavior: a first hypothesis is that the simulated vehicle is lighter than the real one. This could justify the minor torque in acceleration but not the one in deceleration since the lower inertia should require a lower negative torque as well. Moreover, for both the vehicles the mass is set to 2374 Kg, which is the weight of the vehicle with the driver and a passenger. The absence of fuel further reduces the variables which could influence the measurements.

A second possibility which would justify this behavior is a miscalculation of the aerodynamic drag. This would explain the lower torques but the divergence of torques should be depending with the vehicle speed. However, the model has similar torque figures not only for low speed conditions, such as at 320 seconds and 380 seconds, but also at higher speed. Moreover, for similar speeds, the torque values get both similar and different at certain times: at 165 and 180 seconds the speed is around 50 Km/h but the torques are off by 30 N m in one case and 0.5 in the second, hence also this hypothesis must be excluded.

A third consideration can be the dependency on the road inclination. In some parts of the cycle an influence of the road inclination is conceivable, especially between 150 and 180 seconds, where the difference is bigger (see Figure 5.2). Even though the road inclination is evaluated with a method that considers some approximations, a road inclination which varies between 3 and -2 degrees, as shown in Figure 5.19, can be assumed as correct for an altitude range of 30 meters in 7.62 Km. Thereafter, the road inclination can have an influence, but it is not sufficient to justify the divergence in certain sections.

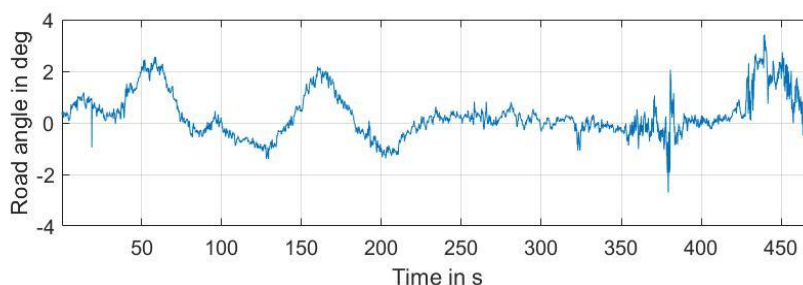


Figure 5.19: Road inclination of the simulated cycle

To further investigate the problem, the driving losses have been considered. As described in Chapter 5.1.3, it is evaluated balancing the inertia, traction and braking forces. The Figure 5.20 shows that the losses in the analyzed interval are lower between 150 and 180 seconds than for the rest of the graph. Moreover, due to the noise present in the acceleration signal, the major influencing factor in driving losses, the difference is not as clear as expected. An average of 3 kW of difference in losses is present in the considered section.

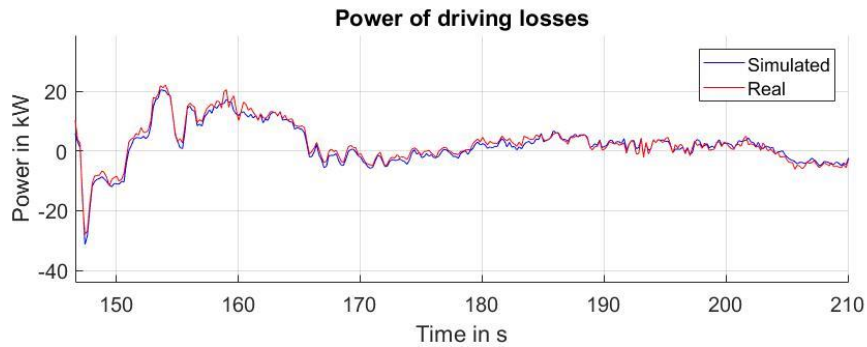


Figure 5.20: Power of driving losses in a section of cycle

These losses can be attributed to several factors: the inefficiency of the tires in transmitting the force to the ground is not considered in the model. Moreover, the gearbox efficiency, which is considered constant and equal to 0.98 in the model, has a different behavior in the reality. It is dependent on the torque and on the speed. Another influence is given by the steered tires. As a matter of facts, when tires are at an angle, the component of the lateral force along x-axis, small but not negligible, is oriented in the opposite direction of the vehicle speed, hence it slows the vehicle [58, pp. 18-19]. The Figure 5.21 illustrates the steering angle, and for some intervals when the wheels are steered, a difference in torque can be noticed.

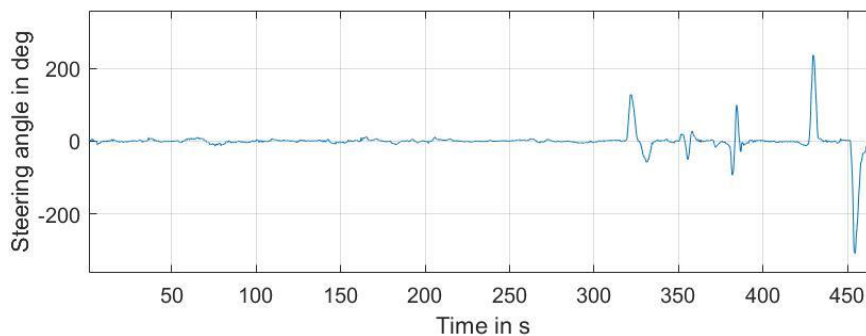


Figure 5.21: Steering angle of the Tesla Model S

In addition to this, while the model is capable of reducing the speed only through the regenerative braking, it is not known if in the sections of the cycle when the throttle position is null, a brake pressure has been exerted.

The difference in torque in the interval from 450 to 480 seconds is not bigger than the average difference in the cycle, hence the acceleration variation of Figure 5.13 can be attributed to an error in measurement of the acceleration in the Model S, otherwise a substantial difference in torque should have been visible.

Once the mechanical point of view of the validation has been discussed, it is possible to analyze the operation of the electric components, namely the electric machine and the power electronics. The validation of those components is fundamental, since in the following comparison the same vehicle will be used but several topologies will be implemented to analyze the influence.

To examine its effect, it is necessary to compare the difference between the electric power which is delivered from or to the battery and the mechanical power generated or delivered to the motor both in the Tesla vehicle and in the model, during the cycle (Figure 5.22).

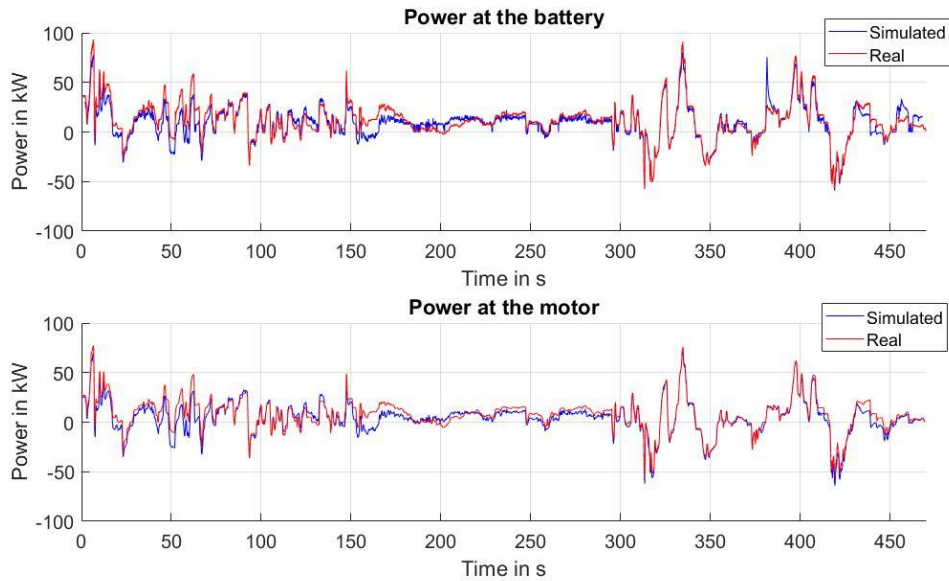


Figure 5.22: Power at the battery and at the motor

As visible, the same difference present between the two torques is now also present between the two powers. This assesses that the rotational speed of the two engines is the same, since a major deviation would be otherwise present, and this is also guaranteed by the former validation of the speed of the vehicle. Concerning the electric power instead, the behavior is the expected one. For negative torques the electric machine works as a generator, delivering power to the battery, hence the current through the battery is negative because it is recharged. For positive torque instead, current is delivered from the battery to fuel the motors and produce positive mechanical power.

The major changes between the two graphs are the present at 380 seconds and 460 seconds. If the Figure 5.11 is also considered, it can be noticed that the difference in electric power is significantly higher for low speed. In fact, whenever the vehicle is at a speed lower than 10 Km/h, the electric consumption immediately increases, even if the mechanical power delivered does not justify this behavior. The cause of this can be found analyzing the efficiency map of the motor. Its efficiency drops drastically for low speed, for all torque figures, causing the significant current absorption for the low mechanical output. In Figure 5.23 it can be observed how the efficiency starts dramatically decreasing from 2000 1/min on. Even without analyzing the Model S motor efficiency map, it is possible to state from the results that the efficiency drops drastically at a lower speed, since a peak in consumption is present as well but significantly more reduced than in the simulated model.

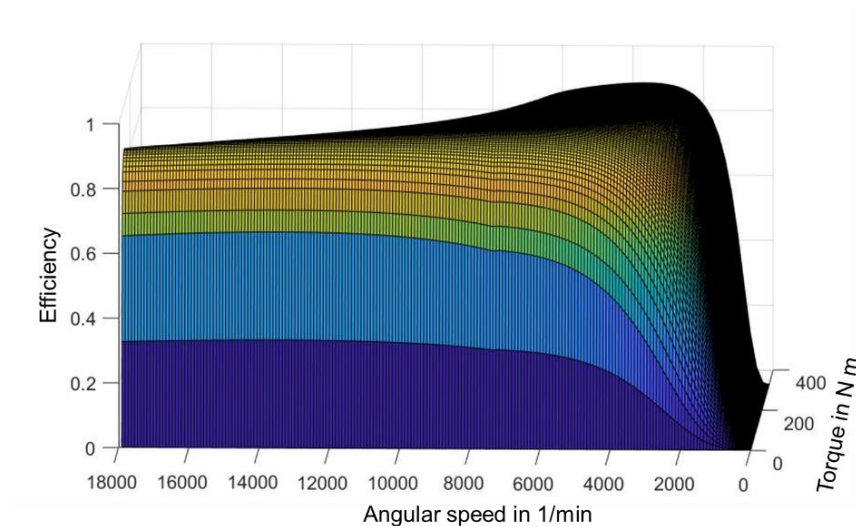


Figure 5.23: Efficiency map of the model

The Model S instead, despite showing an increase of consumption for low speeds too, has an overall efficiency higher, not far from efficiency in other working conditions.

For this reason, a lower bound has been set for speed below 10 Km/h, so that the efficiency in this condition never drops below 0.2. The electric power plots are the results obtained with this limit. This highlights that the energetic demand before was even higher and could not be justified. Nevertheless, due to the short duration of this variation, the overall energy demand is not affected in a reasonable manner to justify further actions to limit it. Increasing the efficiency limit would lead to a substantial change in the shape of the efficiency curve, which would then cause an unjustified unevenness in the efficiency map itself.

A final comparison between the two powers is possible analyzing the arithmetic difference between the motor mechanical power and the battery electric power for the real and simulated model (Figure 5.24). This value represents the power which is loss in the form of heat converting the electric energy from the battery into mechanical energy in the motors. A distinction between the losses in the motor and the ones in the power electronic was possible in the model but not in the Tesla. The Battery Management System (BMS) did not provide the voltage and current entering the motor, hence any further analysis of it in the model would not find a correspondence in the real vehicle.

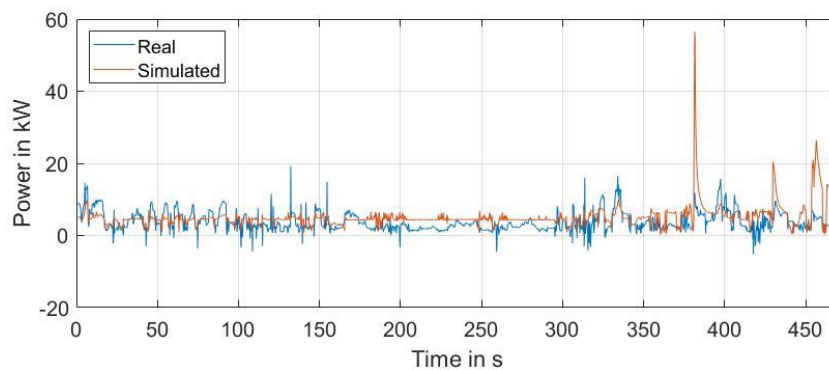


Figure 5.24: Power losses in electric components

As stated before, the main difference is present at low speed. Another observation is that the Model S has a wider range caused by the different operating conditions, while the simulated

model has smaller variations in losses. However, the wider range of the signal recorded on the Tesla is only affected by the change of torque, since with low speed, as for instance at 320, 380 and 460 seconds, when the speed significantly changes from the average value, no major differences are visible. This can indicate that the efficiency values, which in the model are quite similar once a defined level of torque has been achieved (as noticeable by the upper flat portion of the efficiency map in Figure 5.23), are more influenced by the torque figures in the actual condition of operation of the Model S motors. A further detail to be specified is the presence of noise in the real measured data: the losses, as shown by the model, can never reach negative values in reality. This is an indication that the torque figures measured by the integrated system in the vehicle might not be as accurate as it can be normally considered.

A last data to compare is the consequence of the electric demand. For a similar distance covered, 7.6 Km in the reality and 7.57 Km in the simulation, the result of consumption is 19.75 kWh/100Km and 15.9 kWh/100Km respectively, with a difference of 19.52%. This value has been obtained integrating over time the electric power demand in both the cases. It is the result of the minor torque required to complete the same cycle and the difference in losses caused by the electric motor and the power electronics.

### 5.3 Sensitivity analysis

A method of further investigating the correct operation of the model is to conduct a brief sensitivity analysis on the same validation cycle but with different configurations, as stated at the beginning of the chapter. The aim of the sensitivity analysis is to study the effects of different inputs on the outputs and to find the limits of the adopted instrument. The influence on the latter has then to be justified to state the accuracy of the tested tool, in this case the TOTEM model.

The configuration which will be analyzed are:

- Front-wheel drive configuration with central motor;
- Rear-wheel drive configuration with central motor;
- All-wheel drive configuration with central motors;
- All-wheel drive configuration with near wheel motors;
- Front-wheel drive configuration with dual near wheel motors;
- Rear wheel drive configuration with dual near wheel motors;

Of those configurations the first three will be tested with 3 different nominal torques of 54 N m, 108 N m and 216 N m. The aim is to understand how the consumption is affected by doubling or halving the nominal power of the powertrain. The rest of the inputs will remain the same as described in the previous chapters for the validation.

The Table 5.2 shows the results of the analysis, expressed in consumption as kWh/100Km.

Table 5.2: Sensitivity analysis consumptions

Nominal torque of each axle	FWD	AWD	RWD
	Consumption in kWh/100Km	Consumption in kWh/100Km	Consumption in kWh/100Km
54 N m	12.76	13.13	12.74
108 N m	15.37	15.9	15.34
216 N m	21.36	22.49	21.35
108 N m with Near Wheel motors	17.79	19.66	17.75

It is firstly noticeable that the all-wheel drive topology has always the highest consumption between the configurations of the same nominal torque. In fact, they all share the same drivetrain and powertrain relative to each axle, but the all-wheel drive, which has twice the driving axles, weights 140 Kg more that the 2WD equivalent in the 54 N m torque configuration, 253 Kg in the 108 N m one and 409 Kg in the 216 N m. The torque allocation, which delivers the torque in the most efficient combination, prefers one axle only, to have the highest efficiency possible. The difference between the 2WD and AWD is hence given by the extra weight of the vehicle, which requires extra force, hence supplementary torque to achieve the same acceleration. More energy is provided to the motor, which leads to an increase in consumption, small but noticeable.

The second observation which has to be done is related to the increase of energetic demand relative to the increase of nominal torque. In fact, increasing the latter, also the weight increases. This, alone, has always a negative effect on the electric consumption. In addition, also the motors become more capable and the increase of weight is not proportional to the increase of performance. Hence, for a slightly bigger torque demand, a more powerful and heavy motor is provided. This causes the vehicle to operate with a lower efficiency, since the for qualitatively similar efficiency maps, the same efficiency of a more powerful motor is obtained at a higher torque with respect to a less powerful one. This causes the increase in consumption which is clearly visible in the table.

It can be additionally noted that front and rear-wheel drive vehicles have similar consumption, but with a small difference. As explained in the chapter 5.2, it is related to the weight distribution, and pitch motion of the vehicle under acceleration and deceleration. Moreover, the overall uphill cycle loads the rear tires even more, giving an imperceptible but existent different in consumption.

The last topic to be analyzed are the near wheel motor configurations. As said before the difference between AWD and 2WD is justified by the increase in weight. In this case, however, it is particularly significant since the motors are two, with two power electronics and two gearboxes. Compared to the variation in weight of the central motor configurations, the near motors show an increase of 420 Kg versus 253 Kg. Moreover, the division of the torque between left and right motor causes them to operate in a lower efficiency zone, leading to higher consumption with respect to the central motor layout for the same nominal power.

The analysis of these configurations is not only relevant for the validation of the model, but also to ensure the proper operation in the future task.

## 5.4 Conclusions of the validation

The results of the validation achieved with the graphical comparison highlighted some relevant differences between the real vehicle and the simulated model. Despite the small errors which can be safely be assumed to have been caused by noise or faulty values in the recorded data and which did not have a major influence on the results, the cycle has been precisely reproduced by the model. A clear difference is present when the torque figures are analyzed. This can be caused by several factors, among which the simplifications made to the drivetrain which considers the efficiency of the gearbox constant, the ideal transmission of torque through the tires, which instead has some relevant losses due to the compliance of the rubber and its internal friction [23, pp. 30-69], the friction of the bearings and all the other mechanical parts which are in charge of delivering the torque from the motor to the wheels. In addition, since in the Model S the torque figures have been probably obtained with a look-up table, as no torque sensors are present on the axle, the reliability of those values cannot be guaranteed for high precision investigations. The cycle itself has been created with already obtained data, hence a detailed driving cycle, aimed at testing several conditions to better investigate the behavior of the model could not have been adopted.

Considering the electric devices, such as the motor and the power electronics, the losses are quite realistic. However, even if a correct trend is shared between the two cases, the simulated values have a smaller variability in dependence on the operating conditions. Nevertheless, the average loss is correct, and the qualitative behavior is the expected one. This divergence can be caused by the quantitative difference between the real and simulated efficiency maps. The tool has been designed to simulate a large variety of configuration, and it cannot be expected to have excessive precision in reproducing each real motor and power electronic. Due to this reason, together with the former, the consumption results are off by a 20% approximately.

However, the exact correctness of the result has not been the objective of this validation, but the correct operation of the model and the response of the sensitivity analysis proved that, for the successive comparison, the model is sufficiently valid [51, p. 2]. If a total and precise validation of the model would have been the objective, the real vehicle should have been tested on a dynamometric bench, to ensure minimal influences of external parameters, the efficiency and torque maps should have been obtained from bench testing the motors and the power electronics, and a globally significant cycle, as the WLTP, should have been used. For this research, instead, the limits found on the model can be neglected, since the unreliability of the mechanical efficiency does not provide a concern because the comparison uses the same cycle and quite similar torque and speed figures have to be expected, hence the error is equally reproduced in all the cases. Also, the divergencies of the electrical power are not particularly significant, since, as proven by the sensitivity analysis, the influence of the variation of parameters affects the model in the forecasted way, and the quantitative reliability is important but only second to the qualitative one, for pure comparison purposes. Nevertheless, a deeper investigation has to be done to study how the differences influence the results and what is the cause of those divergencies can be corrected or taken into account for further researches.

Efficient torque allocation strategy, which instead has been a major concern, has proven to operate correctly, as explained by the correct allocation selection, which lead to the lowest consumption available for the intended cycle. This is fundamental to ensure the correct working and results of the next research.

# 6 Comparison of front-, rear- and all-wheel-drive topologies

## 6.1 Comparison maneuvers and parameters

In the developing world of electric vehicles, several alternatives have been presented to the growing market. Different philosophies have led the car manufacturer to adopt different configurations for the powertrain and drivetrain. Among the car makers, Ford, Opel and VW have presented their own interpretation of new electric mobility, respectively with the Focus electric [59], Ampera-e [60], the e-Up and the e-Golf [61]. These all share a front-wheel drive layout. In most of the cases, driving the front wheels is a choice dictated by the economy of scale. These vehicles share the platform with previously existing internal combustion engines vehicles. In those, the front driven configuration is chosen since they have been conceived with the aim of reducing the development and manufacturing costs, in order to offer to the final client an adequate vehicle at a lower price. For this reason, modifying the platform would lead to an increase of costs which would further raise the already high price of electric cars.

An alternative configuration is the rear-wheel drive layout. This is present in most of the compact electric vehicles produced in the last years, from the Smart electric [62], the Renault Twizy [63] to the BMW i3 [64]. Due to the sitting position of the driver and passengers, it possible to position the motors, the electronic and sometimes also the battery under or behind the seats, shortening the front overhang (Figure 6.1).



Figure 6.1: Renault Twizy. Motor and battery position [63]

Positioning the powertrain in the front would cause a major overall length, since the leg distance must be considered, and the space integration of the rear axle with the passenger back would not be so efficient as for the front steering wheels with the legs.

A different motivation to adopt the RWD layout is presented by the Tesla Roadster [65]. This electric vehicle has been produced with the sole objective to approach the electric cars to the sporty drivers' market, which is more attracted by the dynamics and performance of the vehicle rather than the ability to drastically reduce the consumption and to avoid additional pollution [66].

In this case the rear driven layout shows better acceleration capabilities, both in straight line and under cornering, due to the loading of rear axle under acceleration by pitch motion (Chapter 2.3). Moreover, the absence of a driving motor on the steering wheels permits to have a higher grip on the front axle, since the lateral maximum force is dependent on the longitudinal force, as described by the tire ellipse [23, p. 138], and to not to influence the force feedback communication between the driver and the wheels.

The last possibility, which is becoming more and more common, is to offer an all-wheel drive configuration for mid-size cars. Tesla has been offering the Model S, Model X and now the Model 3 in AWD [67], Mercedes Benz the SLS Electric drive [68] and Porsche is going to present soon the Mission E [69], its latest full electric sport vehicle. The AWD capability is clearly known for its ability to guarantee a better traction on low friction conditions such as when dirt, water and snow are present. However, it has been preferred lately due to its better capabilities performance-wise. Being able to transmit torque on all wheels permits the vehicle to accelerate faster and reduce the time losses due to slip of the tires, since each tire must sustain a lower force compared to the equivalent power level in 2WD configuration. Moreover, due to Torque Vectoring, also the dynamic behavior can be improved with ad how torque delivery to each wheel.

Given this brief analysis of the market and market requests, together with the research conducted in chapter 2.3 it is possible to analyze and evaluate the criteria for comparing the different configurations:

- The consumption has certainly to be one of the subjects, due to both battery limited capacity and environment impact. In fact, the actual know how does not allow to have electric vehicles with similar effectiveness and driving range as ICE cars. This, together with the higher costs, has been one of the limiting factor to the spread of this new technology [70]. Any improvement in efficiency would only increase the duration of the batteries. In addition, since the modern world is not able yet to sustain itself on renewable sources only, most of the electric energy is still obtained with fossil fuels [71]. This means that every kilowatt of electric energy used causes the emission of a significant amount of pollutants and CO<sub>2</sub>, which only worsen the already problematic environment situation.
- The costs must be analyzed as well, since any small variation has a big effect in the mass production, and car manufacturers are continuously trying to satisfy the customers with the best product at the lowest cost. Any reduction in the latter, with same objective achievement is a point of interest from this industry. Moreover, due to the high cost of lithium batteries and the relatively low spread of the electric drivetrain, the final product is already significantly pricier than the equivalent petrol-powered version. Managing to make the EVs more accessible to the global public would only reduce the popularity of conventional vehicles, lowering the emissions related to the mobility [70].
- Performances are also relevant. As previously said, the market is interested in this feature, hence it is task of the car maker to satisfy the demand. In a future world where the fossil fuels will be substituted almost entirely with electricity, the desire of performance that the car industry have created during the last decades by offering always better and more powerful engines, still has to be appeased [72].

### 6.1.1 Consumption analysis

To obtain a valid comparison, the model has to run the same cycle for all the configurations. During the driving cycle, the power requirement at the battery is recorded and the losses of the battery itself are also considered to evaluate precisely the energetic consumption. Once the simulation has ended, the power demand is integrated over the simulation time, to obtain the energy utilization. This value, divided by the distance covered results in the consumption of the electric vehicle, expressed in the unit of measure of kWh/100Km.

Concerning the driving cycle adopted, the Worldwide Harmonized Lightweight Vehicle Test Procedure (WLTP) has been selected for several reasons. This cycle, as explained more in depth in the chapter 2.1.2, has become since 2017 the reference for homologation of new vehicles. Thanks to this new regulation, it is possible to evaluate a benchmark with present and future models which will be tested on the same driving cycle.

To define the WLTP as input, a maneuver has been created to provide the model the exact speed profile to follow, with a timestep of 0.0005 seconds. Nevertheless, the driving cycle which has been provided with different timestep of one speed input per second. To adapt it to the model requests the spline function has been adopted to recreate a reliable speed curve with the requested definition. The Figure 6.2 illustrates the results.

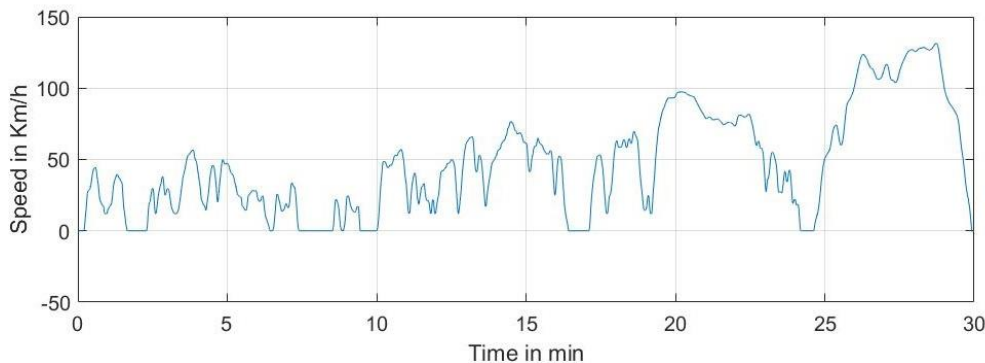


Figure 6.2: WLTP cycle speed profile

The WLTP is composed of several low speed accelerations and decelerations, to simulate urban and extra urban driving, with stop times and a high-speed section, up to 130 Km/h, to reproduce the highway driving behavior.

In addition to the consumption itself, the efficiency of the vehicle is also considered. It is important to understand the operating conditions of the model and to figure out if the consumption figures are related to the variation of the mass of or the motors and electronics. The value later analyzed is the average throughout the whole cycle.

### 6.1.2 Cost analysis

The costs that are going to be evaluated are only concerning the electric powertrain, the drivetrain and the battery.

The price of the battery is evaluated based on the capacity of the vehicle in the model. For comparison purposes a capacity of 90 kWh is set as reference, and its weight and price are evaluated based on this. This value can be considered a reliable average for mid-size electric vehicles, since the Tesla offers 75 kWh battery packs and the Audi e-tron a 95 kWh one [73].

Regarding the drivetrain, the process it is significantly more complex. The cost calculation is divided in motor, gearbox and power electronics. Concerning the latter, its price is evaluated based on the production number per year and the nominal power of the motor they have to control, according to some preset intervals. For the motors, the total cost is dependent on the price of the raw material, such as aluminum, copper and magnets, the cost of purchased components like bearing and connectors and the production cost, made of workforce, energy needed and depreciation of the tools and machinery. The transmission costs evaluation is subdivided in gearbox and differential. The gearbox costs are proportional to the number of gears and the torque it must withstand. For the transmission also, the costs can be collected in raw materials, purchased components, like O-rings and screws, and production costs.

An additional influence on the price is given by the so called secondary parameters, which are tunable according to user specifications, such as the production location, the trend of the rare earths magnet price (ascending, stable or descending), and the number of vehicles produced per year. Those, for our comparison, have been set to have a production location in Germany, with an hourly cost of 25.5 €, a constant cost of magnets of 81 €/Kg and a yearly production of 100.000 vehicles.

### 6.1.3 Performance analysis

For the comparison of the performances, the two most relevant maneuvers have been selected:

- The acceleration from 0 to 100 Km/h has been used as benchmark for testing vehicle capabilities in the entire world. In the countries where the metric system is not extensively used, such as the United Kingdom and the USA, an equivalent test from 0 to 60 mph (0-97 Km/h) is adopted. This test evaluates the time the car needs to accelerate from standing still up to the desired speed. The lower the time, the more capable is the car.
- The acceleration from 80 to 120 Km/h is called the elasticity test. This is normally used in conventional vehicles to evaluate the characteristic of the vehicle and motor at full load in the top gear [74, p. 210]. In electric vehicles, however, the torque reaches its maximum already at very low speeds and starts decreasing after the nominal speed has been reached. This test, hence, can represent the effect of the decrease of torque during the acceleration.

Those tests are conducted as a single maneuver in the simulation. From still condition the vehicle is instantly required to accelerate to a very high speed, above the test ranges, and the times for both the 0-100 Km/h and 80-120 Km/h are recorded. The maneuver has been optimized by Guillaume Lestoille, in his master thesis [75].

The model, however, considers the slip of the wheels, so the maximum torque available from the motor cannot always be delivered. A controller, developed by Tobias Zuchriegel during his master thesis [43], evaluates instant by instant the tire conditions and the maximum longitudinal force that can be transferred. Based on this, the torque input is evaluated. In this way minimum slip is always preventively guaranteed and minor losses in time are present.

### 6.1.4 Vehicle parameters

For the comparison, the Tesla Model S has been chosen since its segment is critical for the spread of electric vehicles and since the EV model has already been validated.

Given the market research and the study of the state of the art, the configurations to be compared are the front-, rear- and all-wheel drive topologies. However, to have a more complete investigation, several front-to-rear power distribution ratios have been included. The overall nominal power is kept constant, but it is distributed between front and rear axles with intervals of 5%, to obtain power allocations of 0:100 (RWD), 5:95, 10:90, etc.

Three nominal power levels of approximately 160 kW, 110 kW and 60 kW have been selected. The first refers to the nominal power of the Tesla model S, so that a comparison is possible with an existing configuration. The latter is a reasonable lower power limit for the selected vehicle segment, since the model with the selected gear ratio has discrete performances, such as a 0-100 around 10 seconds and a top speed of 195 km/h. Lowering this limit would result in a configuration not plausible compared to the market offer, hence any research would not find a correspondence in the real world. A third power level has been selected in between, to illustrate the variation of the results lowering or increasing the nominal power.

To ensure reliability of the results, only the nominal torque for each axle will be altered, since the vehicle has been proved to operate correctly for the given figures, but the overall one will remain consistent. The vehicle nominal power is kept constant since the nominal speed is unvaried. The gearbox, differential, and most of the powertrain parameters will remain unaltered. The Table 6.1 summarizes the inputs of the simulations for the comparison

Table 6.1: Input parameters summary

Model Specifications	Unit	Value
Drivetrain configuration	-	FWD / AWD / RWD
Motor		
• Position	-	Central motor – front / rear
• Typology	-	Asynchronous induction motor
• Maximum speed	1/min	18000
• Nominal speed	1/min	7000
• Nominal Torque	N m	216 – 150 – 90
Transmission		
• Number of gears	-	1
• Gear ratio	-	9.34
• Differential	-	Open differential
Tires	-	215/45 R18 85Y

## 6.2 Comparison results and analysis

### 6.2.1 Results with Horlbeck's motor parameters

The results provided several relevant information. The power distribution is represented with a ratio front to rear, where 0 is fully RWD and 1 is FWD. The consumption plot (Figure 6.3) showed a general shared trend for all the power levels.

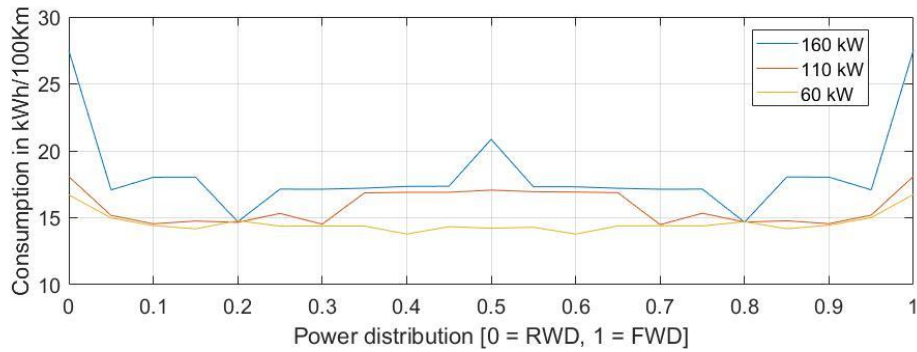


Figure 6.3: Consumption results

The energetic demand reaches its maximum for the two-wheel drive configurations, without presenting any clear difference between the front and rear configuration, as expected from the validation results (Chapter 5.2). The consumption then decreases as the power is divided between the driven axles, with an ascendant behavior approaching the even front-to-rear split ratio, more or less evident according to the selected power. The minima are reached between 20:80 and 40:60 front to rear, lowering the divergence as the power diminishes. It can be also noticed that the graph is relatively symmetric, without any relevant difference between left and right. Concerning the average efficiency, the trends have a strong correlation with the previous graph.

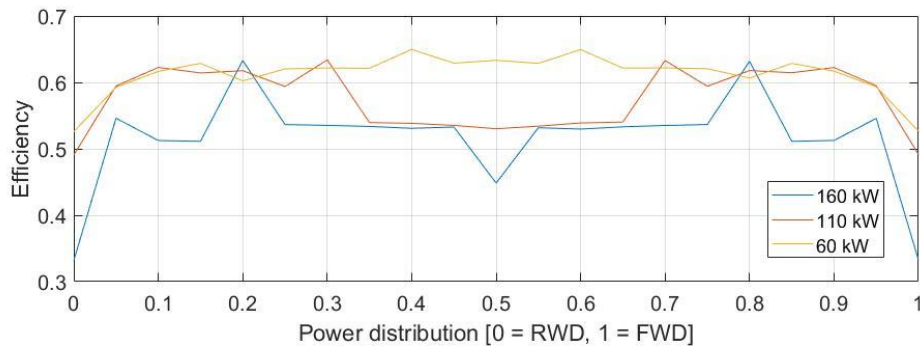


Figure 6.4: Vehicle efficiency results

As clear in the Figure 6.4, the vehicle overall efficiency is inversely proportional to the power demand. To be noticed are the values itself. For the 160 kW configuration, the figures for 2WD layouts are significantly small, reaching values as low as 0.33, not far from the maximum numbers of ICEs vehicles [76, p. 10]. Lowering the nominal power, the efficiency rises significantly,

with a maximum of 0.525 for 60 kW powertrain. The maximum values are reached in this power level, with 0.65.

The costs of the powertrain and battery reveal important information, as is visible in the two plots of the Figure 6.5.

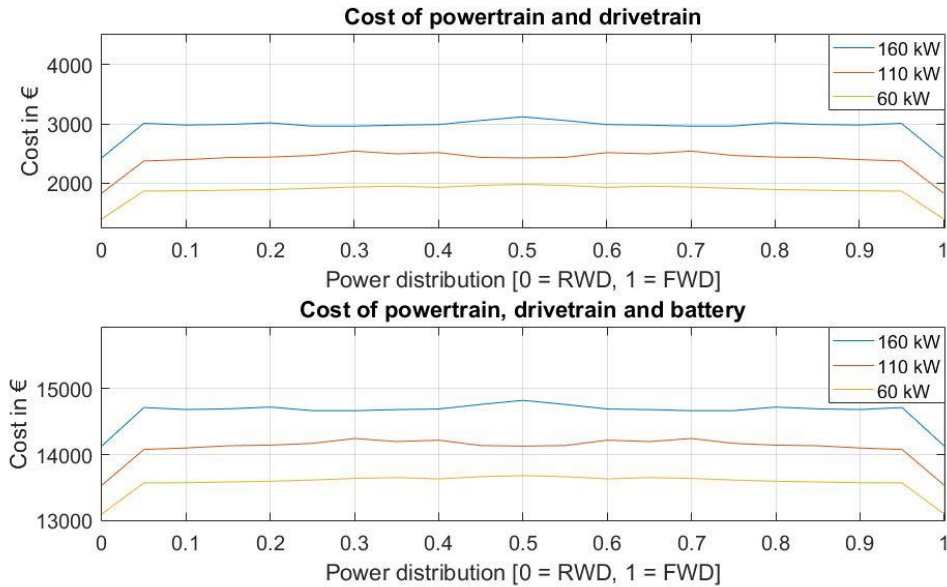


Figure 6.5: Cost of the powertrain and the battery

As predictable, the cost of the front- and rear-wheel drive layouts is lower with respect to the AWD. Moreover, due to the symmetry of the design inputs, also the price is perfectly symmetric. Nevertheless, the difference between 2WD and AWD is not as remarkable, especially when the price of the battery is also included (around 5-7 %). A general ascending trend can be denoted as the power distribution reaches the even split ratio. Concerning the maneuvers aiming at measuring the performance, the results are not immediately clear, as noticeable in Figure 6.6

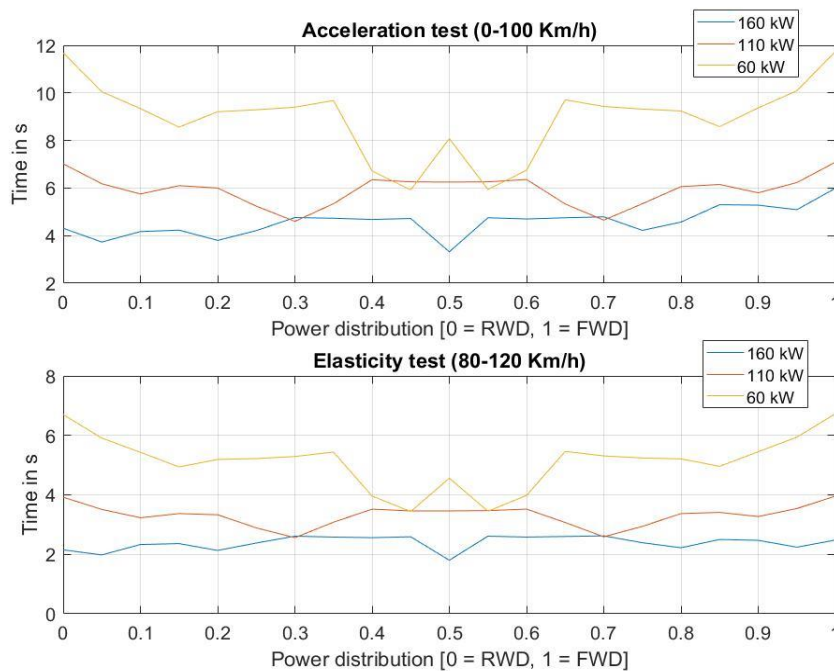


Figure 6.6: Acceleration and elasticity tests

Despite showing a predictable general descending trend in all the power levels as the distribution gets towards the AWD configuration, the time figures are strongly oscillating, with a trend recognizable in both the tests and different for each curve. The causes of this behavior, also present in the previous results, has been found in the initialization of the model, precisely in how the torque and efficiency maps are evaluated. The model, in fact, uses the user inputs to virtually design the electric machine, so that the nominal settings are achieved. However, when it comes to the maximum torque capabilities evaluation, it also considers the possibility of overloading. This method consists in providing the motor more electric power than what it is designed for, to create a higher output without having to increase dimensions and cost. Especially with induction motors, the resulting torque can be as high as two to four times the nominal value. The downside to this is that it can be used for relatively short time periods, since it causes a rapid internal increase of the temperature, which may lead to deformation or even melting of the components and, in case of permanent magnet synchronous motors (PSM), the demagnetization of the rare earths magnets. To avoid this inconvenience, the model evaluates the electrical and thermal behavior which would lead to a safe operation to compute the maximum torque curve. For this reason, the latter are not evenly distributed, as the nominal inputs are, but have a very high dependency on the design algorithm. The Figure 6.7 shows this distribution for the 160 kW configuration.

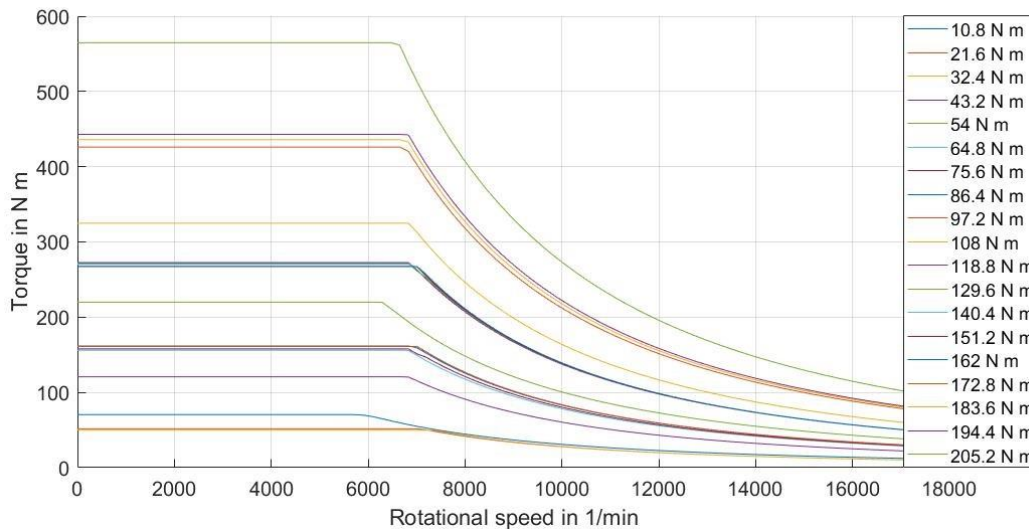


Figure 6.7: Comparison torque curves for 160 kW configuration

As clearly visible, not only the curves are not evenly distributed, but they are not ordered as well for certain torques, as for 162 N m curve (in blue), which is not the fifth curve in order of torque, as it should be from the nominal inputs. Since the efficiency maps are later calculated to fit the torque curves, also those are shifted.

For this reason, the acceleration and elasticity times are completely dependent on the power level. The mass, which is highly influenced by the weight of the motor and the gearbox, is also varying significantly due to this. The Figure 6.8 highlights the overall maximum torque of the vehicle, which should be approximately constant, and instead is changing significantly according to the configurations.

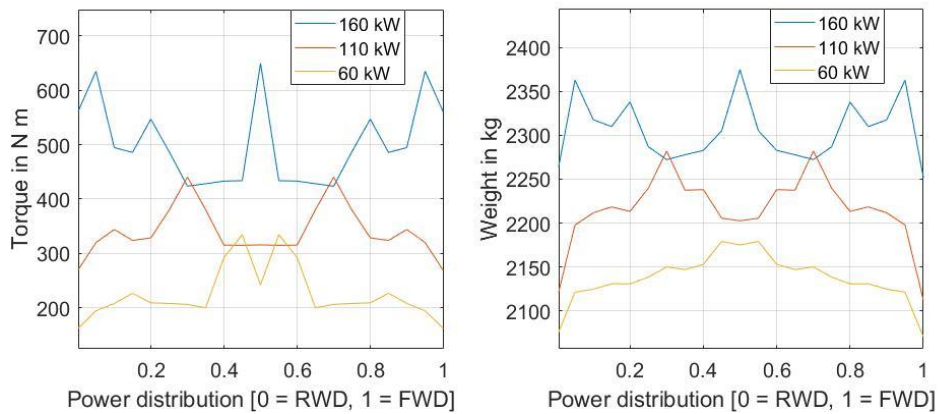


Figure 6.8: Maximum torque and weight of the configurations

If now the consumption plot is analyzed (Figure 6.3), is clearly visible that, despite the general trend which is reasonable and expected, the oscillation and unevenness of the results are given from this inconvenience. The maximum torque trend can be found also in this plot, similar for each power level. Looking at the acceleration and elasticity tests (Figure 6.6), this behavior can be recognized as well, just inverted, since the times are inversely proportional to the power of the tested vehicle.

Only for the highest power level a difference is present between left and right side. This is caused by the slip of the vehicle, or better the limitation of the transmitted torque to avoid so. To prove it, a parallel simplified simulation has been run with tires considered as a fully rigid element with infinite friction coefficient. The result, based on the same vehicle capabilities of the acceleration test, were subtracted by the ones obtained with the realistic tires and the difference plotted in Figure 6.9.

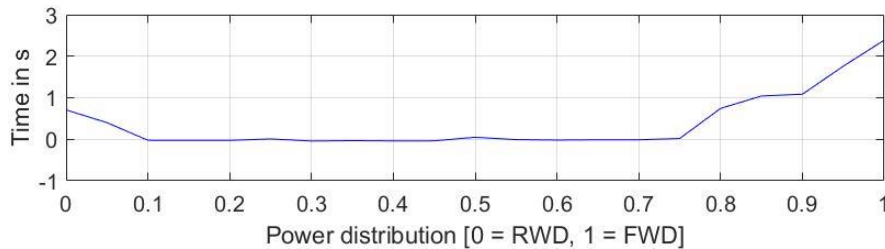


Figure 6.9: Acceleration difference with real and ideal tire

The variation is approximately null for most of the all-wheel drive configurations, while it increases as the power distribution reaches the 2WD layouts. As expected, when most of the torque is allocated to the front axle (power distribution close to 1), the difference increases more with respect to the results with torque more allocated at the rear.

Nevertheless, the outcomes are not qualitatively optimized, so a further simulation with a different motor specification algorithm has been done.

## 6.2.2 Results with Tschochner's motor parameters and analysis

In this second section of the results presentation, the model for the motor characteristics generation has been changed from the one design by Horlbeck [47], to the Tschochner's model [77], to obtain results which were qualitatively better. The latter, more simplified with respect to the previous, has some intrinsic behaviors and limits which influenced the results in a specific manner.

In this new model, the motor torque curve on which the efficiency map is generated is not a versatile and configurable as the previous was. The maximum rotational speed has still been set to 18000 1/min, but the nominal speed is now a function of the latter, exactly set at 0.4785 times the maximum rotational speed, which in this case equals to 8612.4 1/min. This value is not far from the 7000 1/min figure which has been defined as reference given the validation carried out, compared to the maximum limit, so the effect should be minimal. Moreover, the overload ratio is now fixed to twice the nominal torque, so that there is proportionality among the motors tested, and a better qualitative result can be expected. Due to this latter characteristic, the nominal power had to be recalculated so that they match the previous assumptions, so the three levels of power tested are 270 kW, 180 kW and 90 kW.

However, the efficiency maps generated are qualitatively sufficiently similar to the preceding, but quantitatively they are not. The new motors appear to have a global better efficiency, but for comparison reasons, this limit is still acceptable.

The Figure 6.10 shows the results of the comparison with the new model. As immediately visible, the plots are qualitatively better, with a more linear and expectable behavior. However, the trend is the same as the former model results, which proves the reliability of the former as well, despite the unevenness.

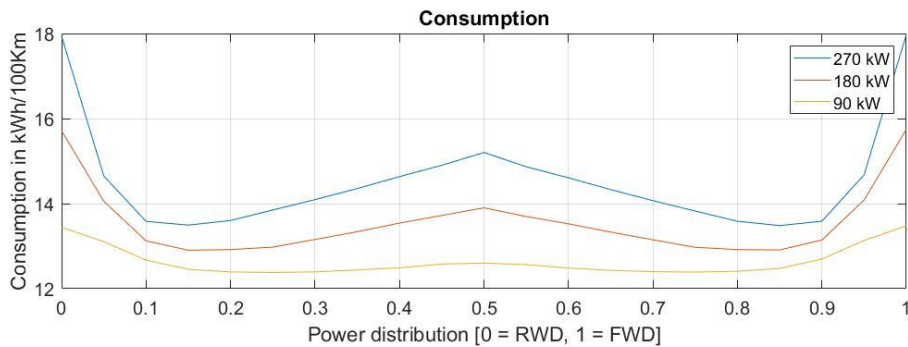


Figure 6.10: Consumption results with Tschochner model

Predictively, the consumption of FWD and RWD layouts are the highest within the same power level. This is caused by the motor dimensions and capabilities. Since the vehicle has to provide the same nominal power as all the other configurations, but with one powertrain only, the motor is significantly bigger and more powerful. This causes the electric machine to operate in lower efficiency zone for the same mechanical outputs, since its high efficiency region is reached for significantly higher torque demand with respect to smaller motors. As a result, the consumption is fairly higher compared to the rest of the same power level configurations. In addition, no difference is present between front and rear-wheel-drive, since both the motors are capable of regenerating all the mechanical power during the cycle, hence no advantage is given to the front axle configuration, which is theoretically able to retrieve more power due to the dynamic load shift under heavy braking which loads the front tires and increase the wheel locking limit with respect to the rear axle. Clearly, for the same reason previously explained, as the power level lowers, the motors are more efficient, and the consumptions decrease as well, but at a lower rate with respect to the power.

For all the curves, it is also visible that the power demanded diminishes drastically as the all-wheel drive layout is chosen. The efficient torque allocation, in fact, loads the front motor (in case of 5:95 distribution ratio) so that it reaches the high efficiency region, and demands for the remaining output to the rear motor, which is less efficient at those conditions, but having to provide less power, causes also smaller losses. As the power split gets closed to even distribution between front and rear axle, the consumptions rise again, due to the decreasing efficiency of the smaller motor which gets more and more capable as the middle point of the plot is reached. After the minimum, in fact, the torque allocation strategy prefers once again only one axle for high power levels, since it is enough to fulfill the torque demand, and the consumption is purely related to the increase in dimensions and power. As the even distribution is reached, the trend is inverted, and the motor that before was smaller becomes the bigger, and the other becomes the dominant.

Another trend to highlight is the motion of the minima as the power drops. Those, in fact, get near the even distribution as the power drops. In the 300 kW level, the minima are found at 15:85 front to rear distribution, or vice versa, while lowering the power they shift to 20:80 and 30:70 for 200 kW and 100 kW respectively. This behavior can be explained by the decrease of power, since for the highest power level, the smallest motor has a nominal power of 45 kW, 40kW for the second bigger power level and 30 kW for the lowest level. Those are very similar in specification, and due to the lower weight of the low power level, it is realistic to have a decrease of motor power as well for the best configurations consumption-wise. The key point here is that the lowest energetic demand is reached when the smallest motor is able to provide the most of torque requested, and the other motor does seldomly has to provide torque with very low efficiency, which would result in an increase of the consumption.

Looking at the vehicle efficiency plot (Figure 6.11), evaluated as the efficiency between the electric power delivery and the mechanical power transmitted to the wheel, it is clearly visible the relation with the previous graph.

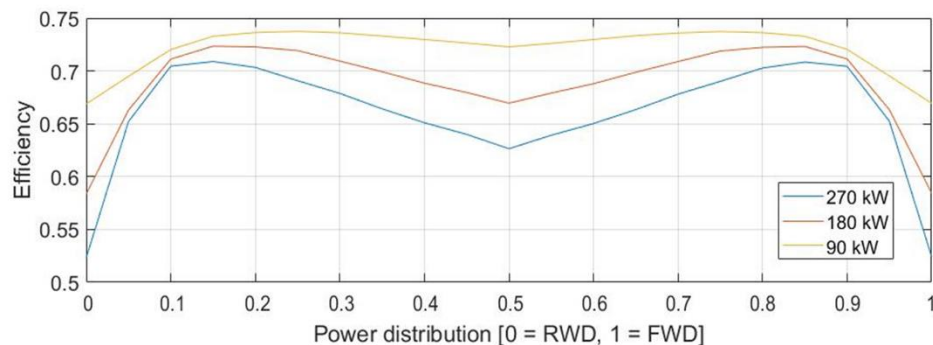


Figure 6.11: Vehicle efficiency results with Tschochner model

Since efficiency is inversely proportional to the consumption, it is maximum when the latter is at its minimum. The FWD and RWD layouts show a very low efficiency, especially for the highest power level. However, compared with the previous engine model, the consumption and the efficiency are more optimistic, hence the results are qualitatively better but not quantitatively. This has to be taken into account since the comparison results are still valid but the consumptions and efficiency themselves are overrated for the WLTP cycle on which they have been tested.

More information is given if the average electric efficiencies of the front and rear axle power-trains are compared, as in Figure 6.12.

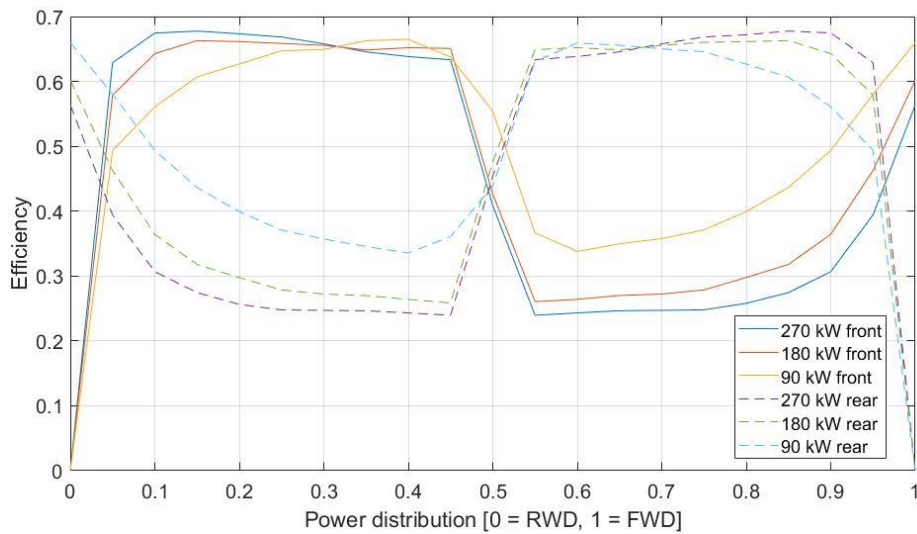


Figure 6.12: Electric efficiency of front and rear axles

The average efficiency plots of front and rear axles give, as a matter of facts, a wider prospective on the operating conditions of the motors during the cycle. As clearly visible, as the power starts to be provided by an AWD configuration, the efficiency of the small motors immediately increases to high figures. This is caused by the high torque demand, compared to the motors capabilities, which makes them operate in the high efficiency region, where torque is almost at the maximum providable. Certainly, the curves do not reach a peak immediately since the bigger motors still operate with significant losses and have to provide a relevant amount of the total power, given the limits of small, low power motors. Hence, the maximum is reached as the smaller motors are able to supply most of the traction and braking power, as explained above. This is especially true for the medium and high levels of power, where the lowest consumption is reached as the smaller motor efficiency has its peak, meaning that they are predominant in the cycle, while for lower power, as found in the literature analysis [27] in state of the art (Chapter 2.3), the lowest consumption is provided by the cooperation of front and rear motors. This behavior is mostly symmetric, especially for the high-power level configurations, where at 50:50 allocation the exchange of roles of the motors is clear, as visible. The front electric machines, which were smaller for low distribution ratios, becomes the larger and the rear motors are preferred for the operation of the vehicle. This trend, however, is not similar for all the tested configurations. The more the power level is decreased, the lesser is the efficiency of smaller motors for very front or rear biased layouts. This is due to the incapacity of small electric machines to supply all the required torque to propel the vehicle, hence the most efficient mix of the twos is adopted, with lower efficiency of the smaller but better overall. Especially for the 100 kW level, when the distribution gets close to even, a gradual change in efficiency is present, compared to the abrupt turnaround of higher power levels. Differently to those, both the axles cooperate to provide the required torque, since both of them are more efficient, being smaller and less capable. At 50:50 distribution they are not evenly used, but the front is more requested to operate, given the higher efficiency compared to the rear figure. The reason is that a mix of the two motors operates during traction, while for braking, due to different efficiency maps, the front only is selected, while for former configurations with same distribution one axle at a time was operating, giving similar results for front and rear efficiency (See appendix).

Concerning the costs of the powertrain, the Figure 6.13 illustrates the variation with and without the battery, for all the selected configurations.

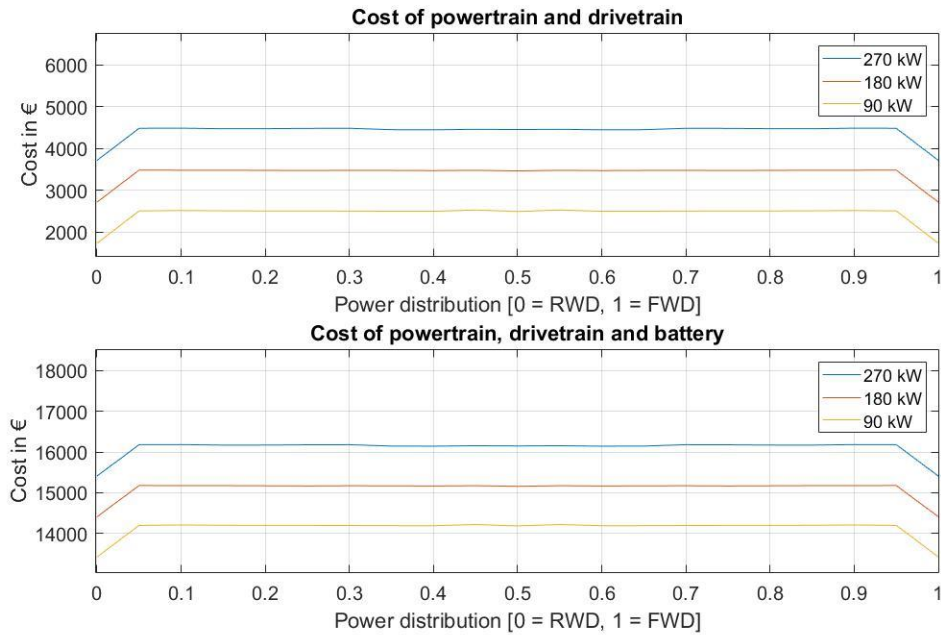


Figure 6.13: Cost of powertrain and drivetrain with and without battery with the Tschochner model

As predictable, the 2WD costs are inferior with respect to the AWD layouts. However, the introduction of a smaller powertrain, for the 0.05 and 0.95 distribution ratios, results in an increase of price of 773 € (45 % compared to the powertrain and drivetrain costs) in case of the 100 kW level and as low as 764 € (25 %) for the 300 kW one. If the battery price is also included, the ratio to the overall cost is significantly smaller, since the total costs of 16200 € for the higher power level and 14200 € for the lower one mitigates the increase of price to a small 5%, which is still significant but negligible compared to the advantages available. Considering the AWD layouts only, in all the different allocations, the cost curve is quite stable, keeping an almost constant value for all the lines. This behavior is mainly due to the cost of the motors, which is not anymore related to the selection of certain components and discrete amount of raw material, as in Horlbeck's model, but is purely proportional to the nominal power. The minimum variations which are still hardly visible are due to the gearbox and power electronics. As explained in chapter 6.1.2, those are dependent on the torque of the motor. There are not infinite configurations, but rather a defined number, among which the model is set, according to the specifications. This may cause the price to oscillate when the power of the two motors requires a bigger and costlier component, where in other configurations the increase of the price of one axle is fully balanced by the decrease of the second.

This is the limit of the Tschochner's model, which lacks a precise cost model to correlate the price of the components to the adopted motor. Nevertheless, when the plots of costs obtained with the two models are compared (refers to Figure 6.5 and Figure 6.13), it is clearly visible that the behaviors are quite similar, and that the Horlbeck's model shows a slightly increasing cost as the distribution approaches even figures. Hence, it is still valid to consider the results obtained with the Tschochner's model, but the small increase for AWD must be accounted for.

Considering the weight of the vehicles, the oscillating trend of the all-wheel drive configurations is also present, always for the same reasons as previously explained (Figure 6.14).

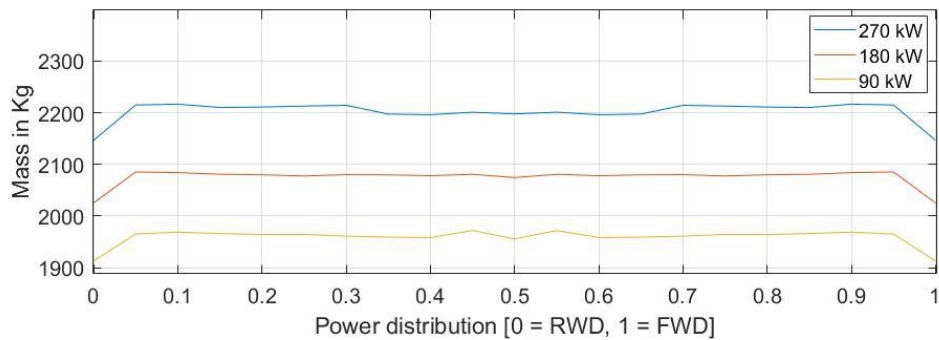


Figure 6.14: Mass results

Similarly to the already seen the trend of costs, the FWD and RWD configurations show a lower value, being lighter with respect to the rest, from 70 Kg to 50 Kg for the 300 kW and 100 kW power levels respectively. Despite the oscillations present, due to the steps of gearbox and electronics design, the trend of AWD layout is generally descending as the middle is reached, even if by a small margin, for the three curves. Due to the introduction of the motors, axles, gearboxes, differentials and power electronics for low power motors such as the ones present on 5:95 and 95:5 power distribution, the weight increases more than the decrease of the bigger motor from lowering the power of 5%. This behavior becomes less relevant as the power difference between the two axles decreases, since the increase of mass is more in line with the increase of power, hence the total mass lowers. Speaking of the overall mass, given as the curb weight plus driver mass, it changes significantly between the power levels, since none of the mass figures of each level gets into the range of lower or higher levels, but not with the same ratio as the power does. The change between each level is approximately of 130 Kg each (around 6-7 %), while the nominal power doubles or triples. This low influence is given not only by the mass of the chassis, internal components and all the mechanical systems not included in the powertrain and drivetrain, but also by the battery weight, which sets its mass to 410 Kg, as the heaviest component of the vehicle, if compared to the 100-200 Kg of the powertrain and drivetrain per each axle.

The effect of mass variation is also visible in the acceleration and elasticity test results, as noticeable in the Figure 6.15.

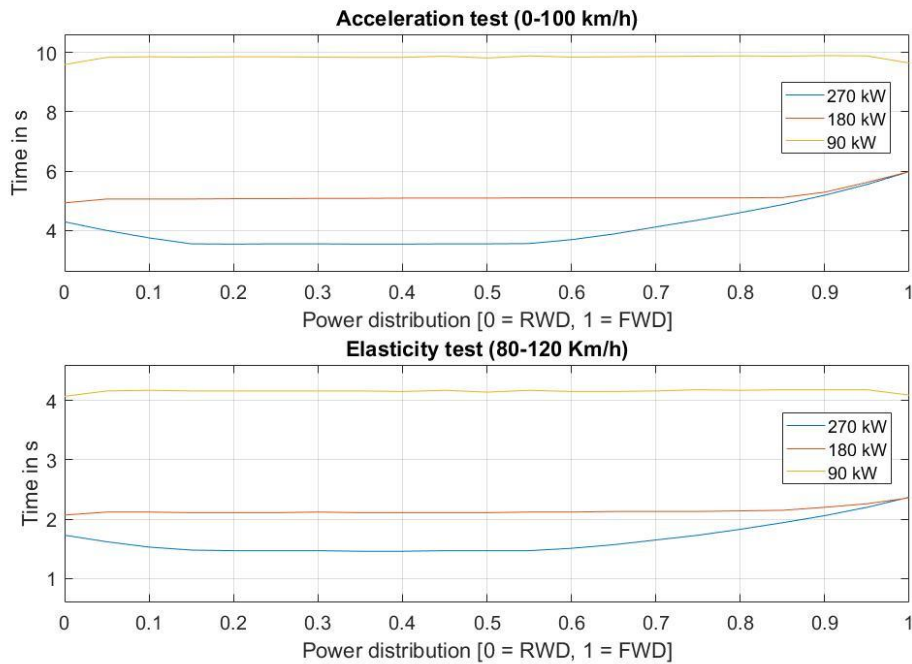


Figure 6.15: Acceleration and elasticity tests with Tschochner model

In this figure three different trends are visible. The first trend is given by the low power level configurations, which show a totally symmetric curve. Further analysis proved that the time reduction present in the 2WD configurations of the 90 kW level is given by the decrease of the overall mass of the vehicle, which plays an important role for the results. The rest of the curve is completely flat since the mass is constant and the overall power as well, causing constant acceleration and elasticity times. The mass distribution, in fact, does not give any advantage in this case, since the tires never reach their limits, not even in FWD configuration, which is the most problematic layout in acceleration tests. This can be understood by observing the Figure 6.16.

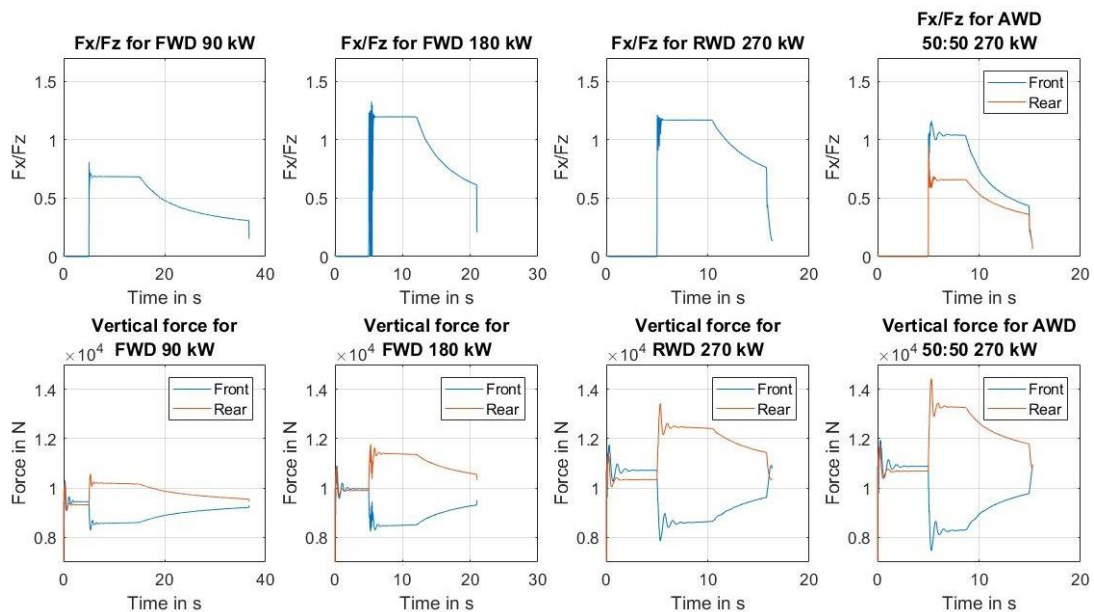


Figure 6.16: Acceleration forces

The ratio  $F_x/F_z$  is called the longitudinal force coefficient [23, pp. 93-97] and describes how much force the tire is able to transmit on x-axis according to the vertical load. In this case, it never gets

close to one, which is a reasonable limit of a street tire. This means that the tires are able to transmit all the provided torque without showing any kind of longitudinal slip. In case of RWD with same power, the ratio would only lower, since the force transmitted in x-direction does not vary, given the limit of the motor, but the vertical forces increase due to pitch motion which loads the rear tires. Obviously, splitting the force between two axles, rather than one, even lowers this value. The acceleration figures are not so positive for an electric vehicle, setting its 0-100 Km/h time around 9.8 seconds and 80-120 Km/h around 4.2 seconds, given that an electric vehicle, with significant more torque of an endothermic engine at low rotational speed, is normally capable of better results. Moreover, the different power configurations do not play any role, the times are only influenced by the mass.

Different case is visible for the 180 kW curve. From full RWD up to a value of 0.85 of power distribution coefficient, the curve has the same behavior of the previously analyzed one. But from that point on, the times start to increase, due to the stability controller which limits the torque output to avoid slip. The ratio  $F_x/F_z$ , in FWD combination, reaches values as high as 1.2, which actually is even a bit optimistic, but does not overcome it. The force transmitted to the front axle is only 1.2 times the vertical force, which also decreases during acceleration due to pitch and motor torque limits, as visible in the plots. In this case, however the times are significantly better for the AWD configurations, with a 0-100 Km/h time around 5 seconds and 80-120 Km/h around 2.1 seconds. The influence of AWD is, nevertheless, not particularly significant, since the best time has been set by the RWD configuration (4.93 seconds and 2.11 seconds respectively), thanks to the lower weight and better traction of this configuration, due to the increased vertical load on rear tires during acceleration.

For the 270 kW curve, the behavior is even more influenced by the tire limit. In fact, both the FWD and RWD configurations show an increase of acceleration and elasticity time compared to the AWD topology. The rear-wheel drive, still, thanks to the better traction, is able to set lower times when compared to front-wheel drive, respectively of 4.29 seconds and 6 seconds for the 0-100 Km/h test or 1.73 seconds and 2.37 seconds for the 80-120 Km/h. The limit of traction becomes evident at 15:85 and 55:55 distribution ratios, since the main motors reach their maximum potential without slip (rear in the first case and the front motor in the second case), and the secondary motors are not able to produce more power due to design limits, while the tires could still cope with more torque. The all-wheel drive layout with power distribution within those ratios are able to transmit all the whole power to the ground, as visible from the constant acceleration and elasticity times. The 50:50 distribution 270 kW plots, in Figure 6.16, show how the tires would be still capable of handling more force, given their vertical load, but the limit is now set by the motors. In this case a clear advantage has been given thanks to the AWD configuration, which permits to divide the torque between the axles, hence increasing the traction capabilities of the vehicle.

By further analysis it is safe to assume that, increasing the power even more, the best configuration would result between 30:70 and 40:60, for the selected vehicle. However, the center of gravity, together with the pitch center and the suspension stiffnesses would influence the results for other vehicles, shifting the ratio more towards the front or towards the rear. Lowering the COG height would reduce the arm length of the moment on y-axis, so the pitch angle, and increasing the stiffness would reduce the compliance of the springs, limiting the motion. In both cases, it would lead to a decrease of load shift to the rear axle during acceleration, favoring a more even front to rear distribution. In addition, a clear advantage has been given from the rear-wheel drive over the front-wheel drive, despite the limits set by the tires. It is clear, even in AWD

topologies, how the rear predominant vehicles showed better results compared to their counterparts, due to the better traction and additional weight on the driven axle.

It can also be noticed that the acceleration and elasticity times are not linear with the power levels, even for cases in which the slip is not present but halving the power leads to a more severe effect on the times for low power.

The trends in acceleration and elasticity times do not show any difference. Since the motor torque is constant up to 8600 1/min, which correspond to a speed of 105 Km/h with the give transmission ratio and wheel radius, the decrease in performance in the remaining 15 Km/h is not so different to influence the results of the elasticity times, so the perfect correlation in trends can be explained.

To sum up, it is worth comparing the obtained results with the other publication which has been conducted on a former version of this model, with similar investigation and objectives. Considering the Figure 2.18, it is clearly visible how the trend of the three plots coincide with the results of the investigation done in this thesis. The consumption plot shows the same behavior with the change of power distribution, and same attitude when the overall power is diminished. Concerning the costs, the results are qualitatively and quantitatively similar and in line. The trend of cost increase as the even distribution is reached, behavior present also in the obtained results, further proving the validity of the Horlbeck's motor model for this investigation. For the performances instead, since a more complete test, which included the weighted average score of several maneuvers, has been conducted, a different trend is observable. Nevertheless, the rear prevailing AWD configuration has been identified as the most advantaged, as it has been done in the present research for high power levels.

As the quantitative results are analyzed, instead, the effect of a shorter duration cycle with a lower average speed is balanced by the higher accelerations ( $1.9 \text{ m/s}^2$  [40, p. 2] for the custom cycle of the publication and  $1.04 \text{ m/s}^2$  for the WLTP [42, p. 143]). The values are different for consumption, if compared to the results obtained with Tschochner's motor model since. As it has been said, the latter has more optimistic efficiency maps, while figures are averagely similar for the Horlbeck's results. For costs, the outputs are closely related, while the performance values cannot be compared.



# 7 Summary and conclusions

## 7.1 Summary

The initial task tackled has been the optimization and fastening of the simulation of driving cycles. By removing the parts of the Simulink model which were not fundamental for the operation, a first improvement has been achieved. The second gain comes from the simplification from a double track to single track model, guaranteed by the absence of lateral forces and steering input for the selected maneuver. The results showed a global 25 % reduction in the required time.

Successively the operation strategy of the model and of the efficient torque allocation controller has been optimized. It operates by analyzing the consumption of hundred possible front-to-rear torque distributions and selecting, with some limits to ensure stability of the simulation, the one which permits the highest reduction for the creation of traction force or the highest production of regenerated energy from braking conditions. Additionally, the tool for computing correctly the axles and vehicle electric efficiency has been designed and implemented.

Prior to the comparison, a validation process has been conducted based on graphical comparison of the results between the model and the selected vehicle as reference on the same driving cycle. Successively, a sensitivity analysis has been carried on. The outcome of the first proved a sufficiently validated model for the intended research but highlighted some form of inconsistencies of the results. The figures for the torque transmitted at the wheel turned out to be lower than the reference measurements, pointing out a probable overestimation of the mechanical efficiency of the model, given by several influences among which the transmission through the tires and the losses in the drivetrain or, an imprecision of the measured data and the cycle created successively to the physical test of the vehicle. The motor and power electronics efficiency also proved to be reliable in average, but with lower excursion compared to the tested sample. The sensitivity analysis, however, confirmed the correct influence on the results of the variation of input parameters within the tested ranges.

Lastly, the comparison with different powertrain topologies has been conducted with the intention to study the effect on consumption, costs and performances. The vehicle model has been configured as the validated one, excluding the parameters changed for investigation purposes, as the torque distribution and the overall power. After an analysis of the literature in the state of the art and a brief benchmarking of the alternatives offered in the actual market, the WLTP cycle, an acceleration and an elasticity tests have been conducted as study maneuvers for this research.

## 7.2 Conclusions

From the results obtained in the comparison and the analysis of the so gathered data, it is possible to collect some relevant information. In the case the minimum consumption in the WLTP cycle is the main objective, a low nominal power configuration of approximately 90 kW must be chosen, with an all-wheel drive powertrain and a 25:75 power distribution among the axles. This ensures the maximum efficiency since, as the overall power increases, the consumption rises for all the distributions. Nevertheless, the shape of the motor efficiency map which leads to significantly small efficiency values for low power and low speed (as seen in validation, chapter 5.2) could not be as accurate as expected, hence decreasing the losses of the bigger motor and shifting the ideal repartition towards a more even ratio. Analyzing the effect of other power distributions on the consumption, it has been noted that the trend is symmetric front to rear, and that the general behavior shows steeply decreasing figures as the power distribution ratio passes from 2WD (both FWD and RWD) to 20:80, and slightly increases after the minimum has been reached. The reduction in demanded energy is related to the rise of efficiency in the operating area of the smaller motor, while the increment is caused by the increase in capabilities of the latter, which is proportional to the power losses for the demanded mechanical power. By diminishing the power level, the optimal distribution shifts towards the even repartition since the smaller motor becomes powerless and not able to provide enough torque, hence forcing the bigger one to operate under low efficiency and increasing consumption for the distribution ratio which was ideal for higher power values.

If a comparison with another driving cycle has to be done, it is possible to forecast, based on the obtained data, that for a given overall power, the more the requested average power of the cycle is, the more the optimal distribution shifts towards the even repartition, with a global increase of consumptions for all the configurations.

As the costs are selected as the reference objective, the ideal choice has to be the 2WD layout, either front-wheel drive if the oversteering behavior wants to be avoided or rear-wheel drive if the traction advantage wants to be exploited. Obviously, the lower the power, the lower the final price will be. The analysis of the other power distribution shows that the price steeply increases as vehicle configuration passes from 2WD to AWD, to then raise slightly when the allocation ratio moves to a 50:50 distribution in all-wheel drive vehicles. The cost of the powertrain and drivetrain also grows as the overall power rises. However, the criticalities of this analysis are that the economy of scale due to the production of the same powertrain twice in the 50:50 power distribution case has not been considered, hence its value should be lower than the forecasted one. Additionally, the price increase due to the complication in the chassis and suspension design is not considered as well, hence the increase in between 2WD and AWD could be even greater.

For performance purposes, the selection of the optimal distribution depends on the power level and on the target of the designed vehicle. For EVs with low capabilities in terms of power, the results are suggesting a 2WD layout, due to the advantage given by the lower weight. Nevertheless, the tire limit of the investigation is optimistic, and the result may greatly change if a low friction terrain is the normal operation environment. In this case, the ideal configuration can be assumed to be the same as for high power vehicles. Increasing the vehicle power, the preference is a rear biased all-wheel drive layout, which achieves the best performances in terms of acceleration and elasticity for every situation. The analysis of the rest of the results highlights that the times are quite constant for low power vehicles despite the configuration since the limit is given by the motor and not the tires. Increasing the torque, the times increase for the 2WD topology

due to lack of traction, especially for front-wheel drive, since the dynamic load shifts causes a decrease in vertical force, hence the longitudinal is diminished as well to avoid slip. The ideal repartition for high power levels can be assumed to be between 30:70 and 40:60: an all-wheel drive layout more biased towards the rear axle.

Among the relevant configurations and trends which must be highlighted, a significant decrease of consumption can be achieved for high powers if a small engine is introduced in the 2WD vehicles on the non-driven axle. Despite the increase of cost which, as reported is not significant when the overall price is considered (less than 5%), the performance and efficiency of the vehicle would only have an advantage from this situation. This layout could guarantee the advantages in terms of driving behavior of a 2WD vehicle with an added reduction in energetic demand.

A configuration which does not lead to any benefit, at least for this investigation, is the four-wheel drive layout with even repartition of power between front and rear axle. The consumption figures only worsen with respect to uneven allocations and the costs, even if by a small margin, show an increase. The performances are not enhanced by this repartition. Nevertheless, it must be said that the analysis did not consider the economy of scale of a car company. The simplification of the production line and purchase of parts given by the presence of a single typology of powertrains to be produced may lead to an economic advantage which is not considered in the former research. A proof is the Tesla Model S itself, which has the same powertrain at both the axles.

Considering the limits of the work which has been done in this thesis, it is necessary to mention that, despite having made a validation sufficient for the comparison which had to be performed, the model has not still achieved a total reliability, since the mechanical losses are different from the measurements done on the reference vehicle. An analysis specifically designed between a real vehicle and the model still has to be conducted in the future, to fortify the reliability of the results and to investigate the causes of the diversity which were not possible to be understood with the tools and data given for this thesis.

A second consideration is the ideal behavior of the efficient torque allocation controller, which behaves only according to a reduction in consumption. However, for the private and public mobility, this objective is obtained as a compromise between the different targets set by the car manufacturer during the design and planning phase. The controller does not consider if the torque shift weakens or interacts with the stability of the vehicle which, being related to the safety of the occupants, is a major concern. Moreover, the comfort issue has not been analyzed as well, since the change in torque distribution may cause undesirable disturbances in terms of noise, vibrations and harshness. The last point to be added to this topic is that the controller works by comparing the actual and future situation of the vehicle. In real driving, even though some algorithm may offer a form of prediction based on measurements of driver inputs and vehicle conditions, the vehicle cannot forecast exactly what the driver will ask to the vehicle in terms of steering, acceleration and braking and the vehicle parameters change. This is an optimistic environment, in which the exact speed is known first and reached later but does not represent the exact reality.

Finally, the investigation is relevant and in line with the results of the state of the art analysis, but under the performance point of view, only one maneuver has been studied, while some publications considered a multitude of test to evaluate and score the behavior of each configuration.

## 7.3 Outline

A future development of this research can be done in the improvement of the Horlbeck's motor model, by analyzing the operation and specifying more intervals, so that the motor characteristics would be more distributed and not aggregated in clusters as it is at the moment. A further tool could be developed to select the motors not based on the nominal value, but on the actual capabilities, so that a more reliable and realistic comparison could be achieved. More profound validation of the model is also a priority since it is necessary to further investigate and verify the exact and precise operation of the model. Finally, a more detailed comparison could be conducted once the limits have been overcome, with several more power levels to study the precise influence on the three research objectives and with a more detailed and integrated evaluation for the performance of the vehicles, which could also consider some of the lateral dynamic maneuvers which the model is capable to simulate.

# List of figures

Figure 1.1: Thesis diagram .....	3
Figure 2.1 Model scheme for electric vehicles [9, p. 1771].....	6
Figure 2.2 Force balance in simplified model [10, p. 2] .....	6
Figure 2.3: Section of cycle to represent regenerative energy stored into batteries [12, p. 263] 7	
Figure 2.4 Model scheme .....	9
Figure 2.5 WLTP Class 3 Cycle [20].....	10
Figure 2.6 Double track model.....	10
Figure 2.7 Monotrack or bicycle model .....	11
Figure 2.8 Examples of vehicle layouts with one to four electric powertrains [24, p. 2].....	12
Figure 2.9 Results for longitudinal behavior of the research from the University of Surrey [24, p. 11].....	13
Figure 2.10 The iCOMPOSE EV at Lommel test center (Belgium) [28, p. 2].....	14
Figure 2.11 Power consumption varying torque split for different weighted vehicles and different maneuvers [31, p 7] .....	15
Figure 2.12 Average energy efficiency [31, p. 7] .....	16
Figure 2.13: Results from the Dynamometer test at 200 N m for different torque distributions under acceleration conditions (a) Battery Output Power (b) Drive System Efficiency [32, S 15].....	17
Figure 2.14: Results from the Dynamometer test at 120 N m for different torque distributions (a) Battery Output Power (b) Drive System Efficiency [32, S 14].....	17
Figure 2.15: Demanded power for three different allocation strategy [34, S 8] .....	18
Figure 2.16: Experimental results of different allocation ratio [38, S 696].....	19
Figure 2.17: Power transmitted at ground at a speed of 50 Km/h on loamy terrain [39, p. 11].	19
Figure 2.18: Performance, consumption and cost results of the comparison [40, p. 3] .....	20
Figure 3.1: Time division of the simulation.....	24
Figure 3.2: Time division according to functions .....	25
Figure 3.3: Vehicle model scheme .....	26
Figure 3.4: Tire Calculation structure.....	27
Figure 3.5: Body calculation structure.....	27
Figure 3.6: Rotation around pitch center.....	28
Figure 3.7: Driving dynamic calculation .....	28

Figure 3.8: Time analysis after optimization .....	30
Figure 4.1: Power evaluation of the combinations .....	34
Figure 4.2: Torque combination. (a) reference axle torque, (b) secondary axle torque .....	35
Figure 4.3: Torque allocator without reference axle. (a) Rear, (b) Front.....	35
Figure 4.4: Efficiency curve for electric motors .....	36
Figure 4.5: Electric power evaluation diagram.....	37
Figure 4.6: Torque allocation and distribution .....	37
Figure 4.7: Effect of controller on torque distribution .....	38
Figure 4.8: Torque limiter operation .....	39
Figure 4.9: Results of power prediction .....	40
Figure 4.10: Possible powertrain and drivetrain layout configurations [46, p. 4].....	41
Figure 4.11: Layout of components for the efficiency calculation .....	42
Figure 5.1: Validation cycle speed profile .....	44
Figure 5.2: Altitude profile .....	44
Figure 5.3 Speed and altitude profile magnification .....	45
Figure 5.4: Road inclination angle evaluation .....	45
Figure 5.5: Wheel altitude calculation .....	46
Figure 5.6: Altitude variation for front and rear axles .....	46
Figure 5.7: Torque data from Tesla Model S .....	47
Figure 5.8: Torque curves result based on nominal speed.....	47
Figure 5.9: Estimated Tesla Model S torque curve.....	48
Figure 5.10: Driving losses and forces.....	49
Figure 5.11: Speed result.....	51
Figure 5.12: Acceleration results .....	51
Figure 5.13: Speed and acceleration analysis of the relevant interval.....	51
Figure 5.14: Torque delivered to front and rear axle.....	52
Figure 5.15: Vertical force and wheel radius of the simulation .....	52
Figure 5.16: Motor efficiency map.....	53
Figure 5.17: Consumption based on torque distribution .....	53
Figure 5.18: Overall torque .....	54
Figure 5.19: Road inclination of the simulated cycle.....	54
Figure 5.20: Power of driving losses in a section of cycle.....	55
Figure 5.21: Steering angle of the Tesla Model S.....	55
Figure 5.22: Power at the battery and at the motor .....	56
Figure 5.23: Efficiency map of the model.....	57

---

Figure 5.24: Power losses in electric components.....	57
Figure 6.1: Renault Twizy. Motor and battery position [63].....	61
Figure 6.2: WLTP cycle speed profile .....	63
Figure 6.3: Consumption results .....	66
Figure 6.4: Vehicle efficiency results .....	66
Figure 6.5: Cost of the powertrain and the battery.....	67
Figure 6.6: Acceleration and elasticity tests.....	67
Figure 6.7: Comparison torque curves for 160 kW configuration.....	68
Figure 6.8: Maximum torque and weight of the configurations .....	69
Figure 6.9: Acceleration difference with real and ideal tire .....	69
Figure 6.10: Consumption results with Tschochner model.....	70
Figure 6.11: Vehicle efficiency results with Tschochner model .....	71
Figure 6.12: Electric efficiency of front and rear axles .....	72
Figure 6.13: Cost of powertrain and drivetrain with and without battery with the Tschochner model.....	73
Figure 6.14: Mass results.....	74
Figure 6.15: Acceleration and elasticity tests with Tschochner model.....	75
Figure 6.16: Acceleration forces .....	75



# List of tables

Table 2.1: Test results in driving conditions [33, p. 770] ..... 17

Table 3.1: Parameters input for the reference simulation ..... 23

Table 3.2: Modification to vehicle model ..... 29

Table 3.3: Time reduction achievements ..... 30

Table 5.1: Summary validation parameters ..... 50

Table 5.2: Sensitivity analysis consumptions ..... 59

Table 6.1: Input parameters summary ..... 65



# References

- [1] T. DiChristopher, *Electric vehicles will grow from 3 million to 125 million by 2030, International Energy Agency forecasts*. [Online] Available: <https://www.cnn.com/2018/05/30/electric-vehicles-will-grow-from-3-million-to-125-million-by-2030-iaa.html>. Accessed on: Aug. 27 2018.
- [2] J. Gu, M. Ouyang, D. Lu, J. Li, and L. Lu, "Energy efficiency optimization of electric vehicle driven by in-wheel motors," *Int. J. Automot. Technol.*, vol. 14, no. 5, pp. 763–772, 2013.
- [3] S. Clarke, *How green are electric cars?* [Online] Available: <https://www.theguardian.com/football/ng-interactive/2017/dec/25/how-green-are-electric-cars>. Accessed on: Aug. 27 2018.
- [4] A. Khaligh and Z. Li, "Battery, Ultracapacitor, Fuel Cell, and Hybrid Energy Storage Systems for Electric, Hybrid Electric, Fuel Cell, and Plug-In Hybrid Electric Vehicles: State of the Art," *IEEE Trans. Veh. Technol.*, vol. 59, no. 6, pp. 2806–2814, 2010.
- [5] N. Qin, "Electric Vehicle Architecture," 2016.
- [6] Lubrizol Additives 360, *Forecasts Show Global AWD Volumes Rising but FWD SUVs Growing*. [Online] Available: <https://passenger.lubrizoladditives360.com/forecasts-show-global-awd-volumes-rising-but-fwd-suvs-growing/>. Accessed on: Aug. 27 2018.
- [7] R. Kranz, *All-Wheel-Drive Vehicles Grow in Popularity With Car Shoppers*. [Online] Available: <https://www.edmunds.com/car-news/all-wheel-drive-vehicles-grow-in-popularity-with-car-shoppers.html>. Accessed on: Aug. 27 2018.
- [8] X. Zhang, D. Gohlich, and J. Li, "Energy-Efficient Torque Allocation Design of Traction and Regenerative Braking for Distributed Drive Electric Vehicles," *IEEE Trans. Veh. Technol.*, vol. 67, no. 1, pp. 285–295, 2018.
- [9] K. L. Butler, M. Ehsani, and P. Kamath, "A Matlab-based modeling and simulation package for electric and hybrid electric vehicle design," *IEEE Trans. Veh. Technol.*, vol. 48, no. 6, pp. 1770–1778, 1999.
- [10] Anuja R. Jadhav, "Drive Cycle Analysis for Electric Vehicle using MATLAB," *International Journal of Engineering Science and Computing*, pp. 14007–14011, 2017.
- [11] Vyas Singh Chauhan, "Simulation of Electric Vehicle Including Different Power Train Components," Master Thesis, Czech Technical University, Prague, 2017.
- [12] C. Fiori, K. Ahn, and H. A. Rakha, "Power-based electric vehicle energy consumption model: Model development and validation," *Applied Energy*, vol. 168, pp. 257–268, 2016.
- [13] D. W. Gao, C. Mi, and A. Emadi, "Modeling and Simulation of Electric and Hybrid Vehicles," *Proc. IEEE*, vol. 95, no. 4, pp. 729–745, 2007.
- [14] A. Schultze and M. Lienkamp, "Potential of an improved energy efficiency in the chassis," *Automot. Engine Technol.*, vol. 1, no. 1-4, pp. 15–25, 2016.

- [15] A. Heilmeier, "Minimierung der Energieverluste durch Optimierung des Fahrwerkskonzeptes unter Berücksichtigung von Fahrdynamik und Fahrkomfort," Master Thesis, Technische Universität München, 2016.
- [16] I. Eroglu, "Fertigungstechnische Beurteilung, Kostenmodellierung und Analyse der Topologie elektrischer Antriebsstrangsysteme unter Berücksichtigung fahrdynamischer Eigenschaften," Master Thesis, Technische Universität München, München, 2017.
- [17] *What is WLTP and how does it work*. [Online] Available: <http://wltpfacts.eu/what-is-wltp-how-will-it-work/>. Accessed on: Aug. 16 2018.
- [18] Peter Mock, Jörg Kühlwein, Uwe Tietge, Vicente Franco, Anup Bandivadekar, John German, *The WLTP: How a new test procedure for cars will affect fuel consumption values in the EU*: The International Council on Clean Transportation, 2014.
- [19] Peter Mock, Uwe Tietge, Vicente Franco, John German, Anup Bandivadekar (ICCT) Norbert Ligterink (TNO), "From laboratory to road: A 2014 update of official and "real-world" fuel consumption and CO<sub>2</sub> values for passenger cars in Europe," *White Paper*, 2014.
- [20] Dr. Jakob Seiler, *Exhaust emissions*. [Online] Available: <https://www.vda.de/en/topics/environment-and-climate/exhaust-emissions/wltp-worldwide-harmonized-light-vehicles-test-procedure.html>.
- [21] M. Tutuianu *et al.*, "Development of a worldwide harmonized Light duty driving Test Cycle," 2013.
- [22] G. Genta and L. Morello, *The Automotive Chassis: Volume 2: System design*: Springer, 2009.
- [23] G. Genta and L. Morello, *The Automotive Chassis: Volume 1: Components design*: Springer, 2009.
- [24] L. de Novellis, A. Sorniotti, and P. Gruber, "Design and comparison of the handling performance of different electric vehicle layouts," *Proceedings of the Institution of Mechanical Engineers, Part D: Journal of Automobile Engineering*, vol. 228, no. 2, pp. 218–232, 2014.
- [25] A. Pennycott, L. de Novellis, A. Sabbatini, P. Gruber, and A. Sorniotti, "Reducing the motor power losses of a four-wheel drive, fully electric vehicle via wheel torque allocation," *Proceedings of the Institution of Mechanical Engineers, Part D: Journal of Automobile Engineering*, vol. 228, no. 7, pp. 830–839, 2014.
- [26] G. de Filippis, B. Lenzo, A. Sorniotti, P. Gruber, and W. de Nijs, "Energy-Efficient Torque-Vectoring Control of Electric Vehicles With Multiple Drivetrains," *IEEE Trans. Veh. Technol.*, vol. 67, no. 6, pp. 4702–4715, 2018.
- [27] A. M. Dizqah *et al.*, "A Fast and Parametric Torque Distribution Strategy for Four-Wheel-Drive Energy-Efficient Electric Vehicles," *IEEE Trans. Ind. Electron.*, vol. 63, no. 7, pp. 4367–4376, 2016.
- [28] F. Bucchi, Lenzo, Basilio: frendo, Francesco, W. de Nijs, and A. Sorniotti, "The effect of the front-to-rear wheel torque distribution on vehicle handling: an experimental assessment," *Sheffield Hallam University Research Archive*, 2017.
- [29] M. Croft-White and M. Harrison, "Study of torque vectoring for all-wheel-drive vehicles," *Vehicle System Dynamics*, vol. 44, no. sup1, pp. 313–320, 2006.

- 
- [30] G. Parker, J. Griffin, and A. Popov, "The effect on power consumption & handling of efficiency-driven active torque distribution in a four wheeled vehicle," *The Dynamics of Vehicle on Road and Tracks*, 2016.
- [31] J. Tobol'á'r, R. de Castro, U. Bleck, C. Satzger, J. Brembeck, Y. Hirano, "Comparative evaluation of energy efficiency of electrical vehicle powertrain configurations,"
- [32] D. Wu, Y. Li, J. Zhang, and C. Du, "Torque distribution of a four in-wheel motors electric vehicle based on a PMSM system model," *Proceedings of the Institution of Mechanical Engineers, Part D: Journal of Automobile Engineering*, vol. 33, 095440701773476, 2017.
- [33] J. Gu, M. Ouyang, D. Lu, J. Li, and L. Lu, "Energy efficiency optimization of electric vehicle driven by in-wheel motors," *Int.J Automot. Technol.*, vol. 14, no. 5, pp. 763–772, 2013.
- [34] X. Jiang *et al.*, "Analysis and optimization of energy efficiency for an electric vehicle with four independent drive in-wheel motors," *Advances in Mechanical Engineering*, vol. 10, no. 3, 168781401876554, 2018.
- [35] Sang-Jae Lee, Yong-Gi Kim, Tal-Chol Kim, and Ki-Nam Kim, "Fuel Economy Improvement of an Electric All Wheel System (eAWD)," *EVS28 International Electric Vehicle Symposium and Exhibition*, 2015.
- [36] Ziqi Ye, Dr. Michael Stapelbroek, Dr. Jan Pfluger, Thomas Reckeweg, and Rene Savelsberg, "Smart Torque Vectoring Functionality for AWD Electric Vehicles," *EVS30 International Battery, Hybrid and Fuel Cell Electric Vehicle Symposium*, 2017.
- [37] J. Lee, D. J. Nelson, *Rotating Inertia Impact on Propulsion and Regenerative Braking for Electric Motor Driven Vehicles*. Piscataway, NJ: IEEE Operations Center, 2005.
- [38] Y. Zhao, W. Deng, J. Wu, and R. He, "Torque Control allocation based on constrained optimization with regenerative braking for electric vehicles," *Int.J Automot. Technol.*, vol. 18, no. 4, pp. 685–698, 2017.
- [39] C. Senatore and C. Sandu, "Torque distribution influence on tractive efficiency and mobility of off-road wheeled vehicles," *Journal of Terramechanics*, vol. 48, no. 5, pp. 372–383, 2011.
- [40] C. Angerer, N. Holjevac, G. Sethuraman, and M. Lienkamp, "AWD for Electric Vehicles, A Revolution for Vehicle Efficiency?," pp. 1–6, 2018.
- [41] MathWorks, *How profiler captures performance data*. [Online] Available: <https://www.mathworks.com/help/simulink/ug/how-profiler-captures-performance-data.html>. Accessed on: Aug. 01 2018.
- [42] J. Pavlovic, B. Ciuffo, G. Fontaras, V. Valverde, and A. Marotta, "How much difference in type-approval CO<sub>2</sub> emissions from passenger cars in Europe can be expected from changing to the new test procedure (NEDC vs. WLTP)?," *Transportation Research Part A: Policy and Practice*, vol. 111, pp. 136–147, 2018.
- [43] T. Zuchriegel, "Drehmomentenverteilung und Betriebsstrategien für mehrmotorige Elektrofahrzeuge," Technische Universität München, 2017.
- [44] T. Lübbers, "Modellierung der optimalen Momentenverteilung bei elektrischen Allradantriebssträngen," Master thesis, Technische Universität München, 2017.
- [45] T. Pesce, "Ein Werkzeug zur Spezifikation von effizienten Antriebstopologien für Elektrofahrzeuge," Technische Universität München, 2014.

- [46] F. Seeger, “Energetische Modellierung verschiedener Systeme zur Momentenverteilung für ein adaptives Antriebsstrangmodell,” Semester thesis, Technische Universität München, 2017.
- [47] L. Horlbeck, “Auslegung elektrischer Maschinen für Automobile Antriebsstränge unter Berücksichtigung des Überlastpotentials,” Disertation, Lehrstuhl für Fahrzeugtechnik, Technische Universität München, Munich, 2018.
- [48] P. Crnošija, R. Krishnan and T. Bjažić, “Transient Performance Based Design Optimization of PM Brushless DC Motor Drive Speed Controller,” *IEEE Trans. Ind. Electron.*
- [49] T. Ara, T. Akima, and S. Oda, “A method of predicting transient constants of synchronous machines,” *Elect. Eng. Jpn.*, vol. 116, no. 1, pp. 132–143, 1996.
- [50] R. Sintatra, *Macchine e meccanismi: Rendimento di una macchina*. [Online] Available: [http://www.diim.unict.it/users/rsinatra/corsi/allegati\\_modellistica/05%20-%20Rendimeno%20\(efficiency\).pdf](http://www.diim.unict.it/users/rsinatra/corsi/allegati_modellistica/05%20-%20Rendimeno%20(efficiency).pdf). Accessed on: Sep. 20 2018.
- [51] O. Balci, “Golden Rules of Verification, Validation, Testing, and Certification of Modeling and Simulation Applications,” *SCS M&S Magazine*, 2010.
- [52] E.A. MacNair, K.J. Musselman, P. Heidelberger, “How To Assess The Acceptability And Credibility Of Simulation Results - Simulation Conference Proceedings, 1989. Winter,” pp. 62–71, 1989.
- [53] O. Balci, “Validation, verification, and testing techniques throughout the life cycle of a simulation study,” *Ann Oper Res*, vol. 53, no. 1, pp. 121–173, 1994.
- [54] A. Holtz, “Fahrversuchsbasierte Validierung und Optimierung eines modularen Gesamtfahrzeugmodells mit adaptiver Parametrierung,” Technische Universität München, Garching bei München, 2018.
- [55] MathWorks, *Spline*. [Online] Available: <https://it.mathworks.com/help/matlab/ref/spline.html>.
- [56] Tesla Inc, *Model S Specifications*. [Online] Available: <https://www.tesla.com/support/model-s-specifications>. Accessed on: Sep. 04 2018.
- [57] S. Karmakar, S. Chattopadhyay, M. Mitra, and S. Sengupta, “Induction Motor and Faults,” in *Power Systems, Induction Motor Fault Diagnosis: Approach through Current Signature Analysis*, S. Karmakar, S. Chattopadhyay, M. Mitra, and S. Sengupta, Eds., Singapore: Springer Singapore, 2016, pp. 7–28.
- [58] B. Jansen, “Brake-by-steer concept,” Master Thesis, TUDelft, 2010.
- [59] Ford Motor Company, *2018 Focus Electric*. [Online] Available: <https://www.ford.com/cars/focus/models/focus-electric/>. Accessed on: Sep. 21 2018.
- [60] Opel, *Ampera-e*. [Online] Available: <https://www.opel.ch/it/veicoli/ampera-e/ampera-e.html#trim-excellence>. Accessed on: Sep. 21 2018.
- [61] VW AG, *e\_Golf*. [Online] Available: <http://www.vw.com/models/e-golf.61000.m/section/masthead/>. Accessed on: Sep. 21 2018.
- [62] Daimler AG, *Smart ForTwo and ForFour electric*. [Online] Available: <https://www.smart.com/en/en/index/smart-electric-drive/engine.html>. Accessed on: 21/9/18.

- 
- [63] Andrea Silvuni, *Renault: Twizy test in anteprima*. [Online] Available: <http://aimcircolare.blogspot.com/2011/04/renault-twizy-test-in-anteprima.html>. Accessed on: Sep. 14 2018.
- [64] BMW AG, *BMW i3*. [Online] Available: <https://www.bmw.de/de/neufahrzeuge/bmw-i/i3/2017/auf-einen-blick.html?bmw=sea:1434652045:59052874747:bmw%20i3>. Accessed on: Sep. 21 2018.
- [65] Tesla Motors Inc, *Tesla Roadster*. [Online] Available: [https://web.archive.org/web/20071024192721/http://www.teslamotors.com/performance/perf\\_specs.php](https://web.archive.org/web/20071024192721/http://www.teslamotors.com/performance/perf_specs.php). Accessed on: Sep. 21 2018.
- [66] F. Lambert, *Tesla Roadster 3.0: the electric car that sparked a revolution, revisited*. [Online] Available: <https://electrek.co/2017/06/25/tesla-roadster-3-0-review/>. Accessed on: Sep. 21 2018.
- [67] Tesla Motors Inc, *Model S, Model X and Model 3*. [Online] Available: <https://www.tesla.com/models>. Accessed on: Sep. 21 2018.
- [68] Daimler AG, *Mercedes-Benz SLS AMG Coupé Electric Drive: Electrifying – the world's most powerful electric super sports car*. [Online] Available: <https://media.daimler.com/marsMediaSite/en/instance/ko/Mercedes-Benz-SLS-AMG-Coup-Electric-Drive-Electrifying--the-worlds-most-powerful-electric-super-sports-car.xhtml?oid=9904727>. Accessed on: Sep. 21 2018.
- [69] Porsche Cars North America, Inc, *A sports car that covers over 300 miles with superb performance—but without a drop of gasoline? Welcome to the future: the Mission E electric concept car*. [Online] Available: <https://www.porsche.com/usa/aboutporsche/christophorusmagazine/archive/374/articleoverview/article01/>. Accessed on: Sep. 21 2018.
- [70] J. McAulay, “Technology, Challenges, and the Future of Electric Drive,” 2008.
- [71] BP, *Renewable energy*. [Online] Available: <https://www.bp.com/en/global/corporate/energy-economics/statistical-review-of-world-energy/renewable-energy.html>. Accessed on: Sep. 21 2018.
- [72] P. A. Eisenstein, *Luxury electric cars promoting performance over planet-saving*. [Online] Available: <https://www.nbcnews.com/business/autos/luxury-electric-cars-lure-buyers-performance-not-planet-n889851>. Accessed on: Sep. 21 2018.
- [73] EV Database, *Audi e-tron*. [Online] Available: <https://ev-database.uk/car/1092/Audi-e-tron>. Accessed on: Sep. 21 2018.
- [74] G Rizzo, L Glielmo, C Pianese, F Vasca, Ed., *Advances in Automotive Control*. (2-volume Set), 2004.
- [75] G. Lestoille, “Fahrdynamische Potentialanalyse unterschiedlicher elektrischer Antriebskonzepte mithilfe einer automatisierten Eigenschaftsbewertung,” Technische Universität München, München, 2018.
- [76] VTT Technical Research Centre of Finland, “Vehicle energy efficiencies,”
- [77] M. Tschochner, “Comparative Assessment of Early Development Phase Powertrain Concepts,” Dissertation, Institute of Automotive Technologies, Technische Universität München, Munich, 2018.



# Appendix

Figure 1: Torque plot for a 50:50 front to rear distribution with 90 kW configuration in WLTP cycle .....xiii

Figure 2: Torque plot for a 10:90 front to rear distribution with 90 kW configuration in WLTP cycle .....xiv

Figure 3: Torque plot for a 75:25 front to rear distribution with 90 kW configuration in WLTP cycle .....xiv

Figure 4: Torque plot for a 50:50 front to rear distribution with 180 kW configuration in WLTP cycle .....xiv

Figure 5: Torque plot for a 85:15 front to rear distribution with 180 kW configuration in WLTP cycle .....xv

Figure 6: Torque plot for a 95:5 front to rear distribution with 180 kW configuration in WLTP cycle .....xv

Figure 7: Acceleration forces for a front, rear and 50:50 all-wheel drive 90 kW configuration...xv

Figure 8: Acceleration forces for a front, rear and 50:50 all-wheel drive 180 kW configuration xvi

Figure 9: Acceleration forces for a front, rear and 50:50 all-wheel drive 270 kW configuration xvi

Here, the most relevant plots of the various configurations of the comparison have been reported. They either describe the torque allocation strategy, by highlighting which of the axle oversees delivering the torque, or the tire limits and vertical forces for the acceleration tests.

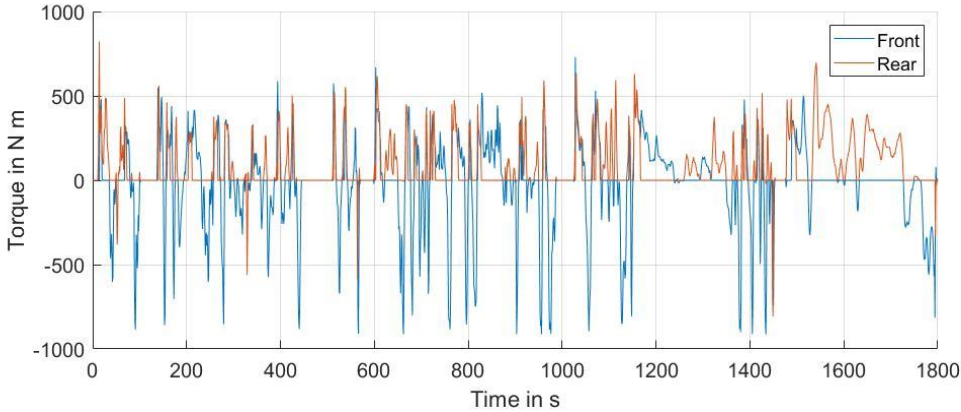


Figure 1: Torque plot for a 50:50 front to rear distribution with 90 kW configuration in WLTP cycle

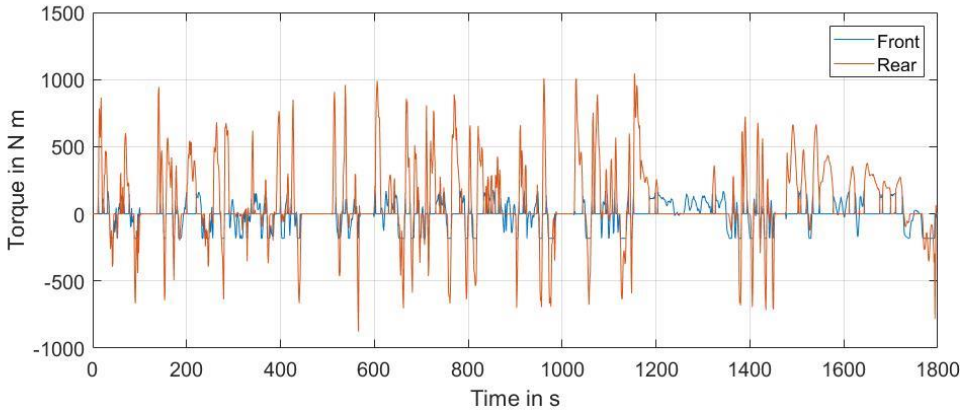


Figure 2: Torque plot for a 10:90 front to rear distribution with 90 kW configuration in WLTP cycle

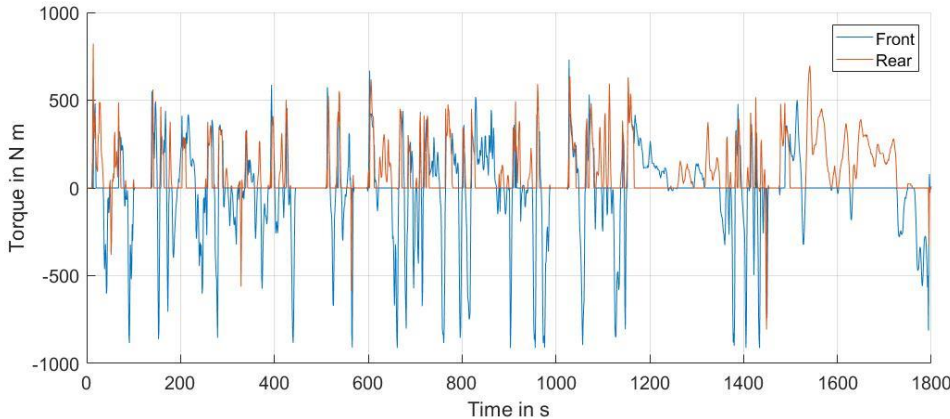


Figure 3: Torque plot for a 75:25 front to rear distribution with 90 kW configuration in WLTP cycle

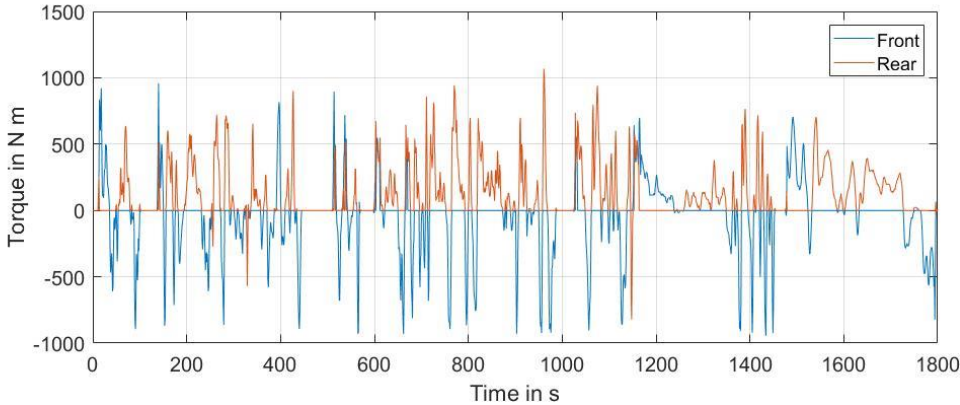


Figure 4: Torque plot for a 50:50 front to rear distribution with 180 kW configuration in WLTP cycle

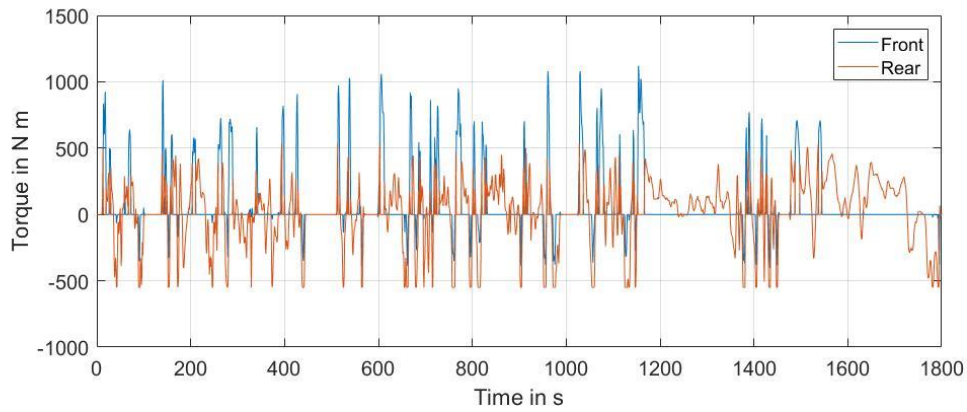


Figure 5: Torque plot for a 85:15 front to rear distribution with 180 kW configuration in WLTP cycle

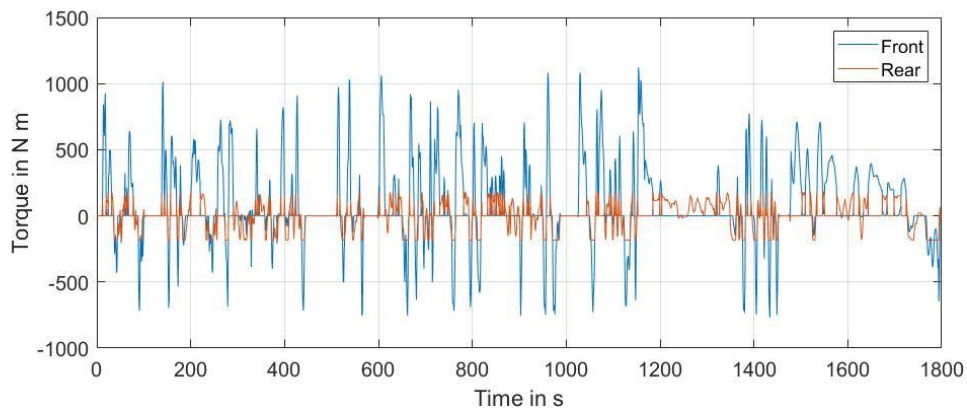


Figure 6: Torque plot for a 95:5 front to rear distribution with 180 kW configuration in WLTP cycle

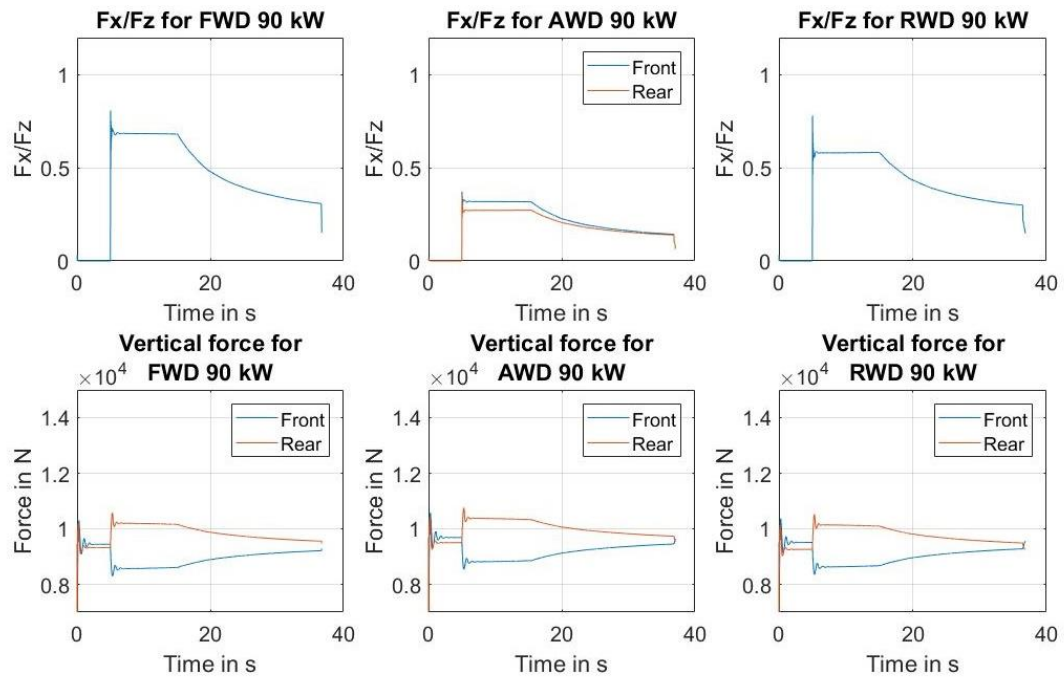


Figure 7: Acceleration forces for a front, rear and 50:50 all-wheel drive 90 kW configuration

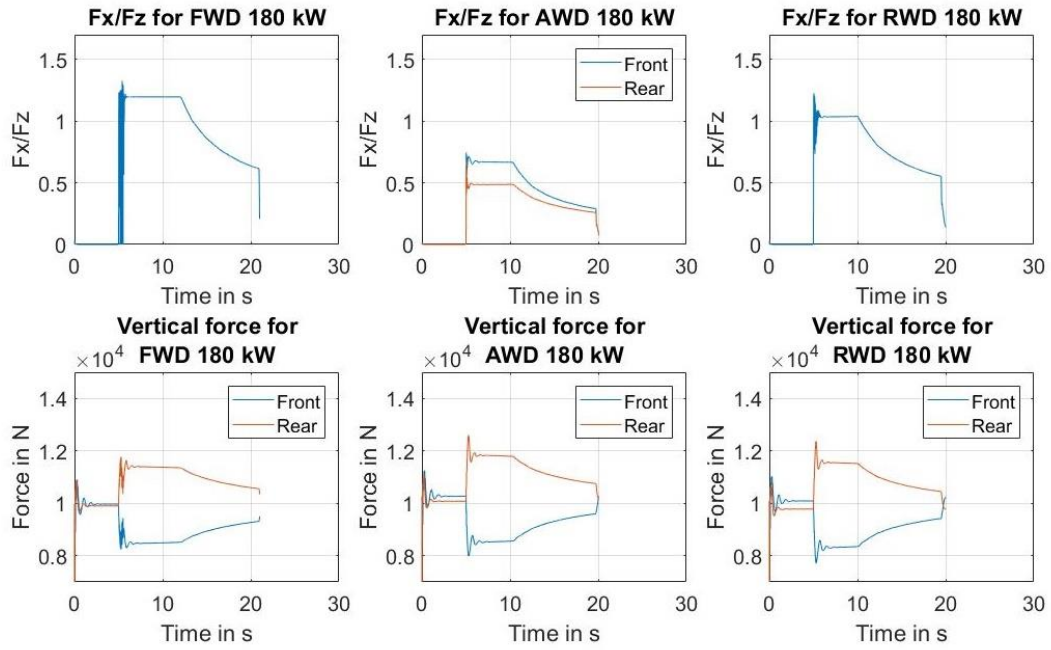


Figure 8: Acceleration forces for a front, rear and 50:50 all-wheel drive 180 kW configuration

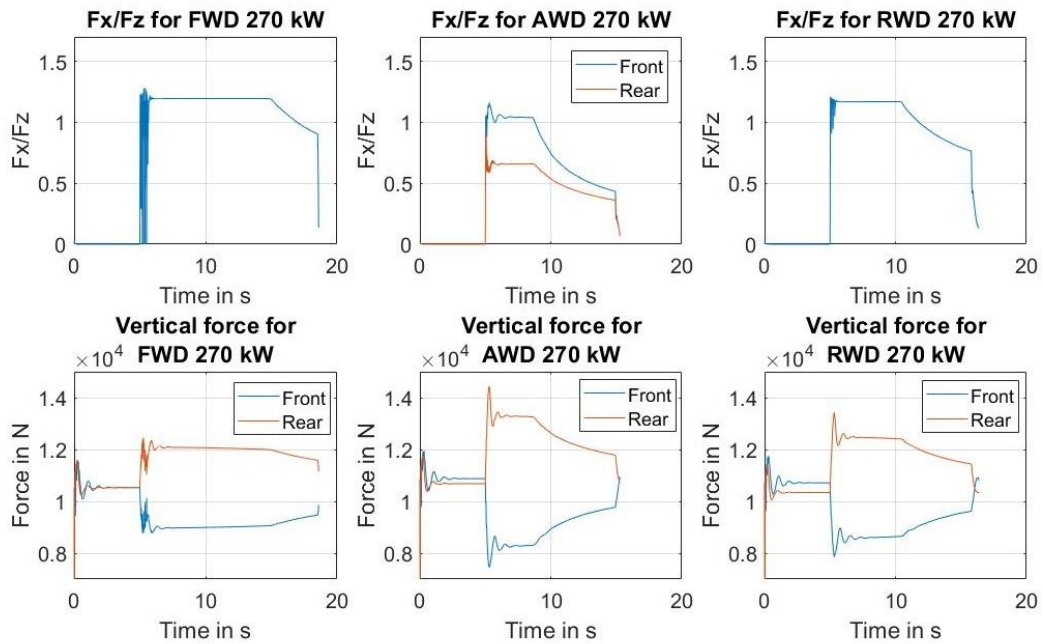


Figure 9: Acceleration forces for a front, rear and 50:50 all-wheel drive 270 kW configuration